Coordinating and supramolecular prospects of unsymmetrically substituted carbohydrazides

Edi Topić,[a] Ivana Landripet,[b] Maëlle Duguin,[c,d] Jana Pisk,[a] Ivica Đilović,[a] Višnja Vrdoljak[a] and Mirta Rubčić[a]*

a. University of Zagreb, Faculty of Science, Department of Chemistry, Horvatovac 102a, 10000 Zagreb, Croatia

b. Ruđer Bošković Institute, Division of Materials Chemistry, Bijenička 54, 10000 Zagreb, Croatia

c. INP-ENSIACET, 4 Allëe Emile Monso, 31030 Toulouse, France

d. Sleever Technologies, ZA Gabor, 81370 Saint-Sulpice

* E-mail: mirta©chem.pmf.hr

Electronic Supplementary Information

Table of Contents

Synthesis

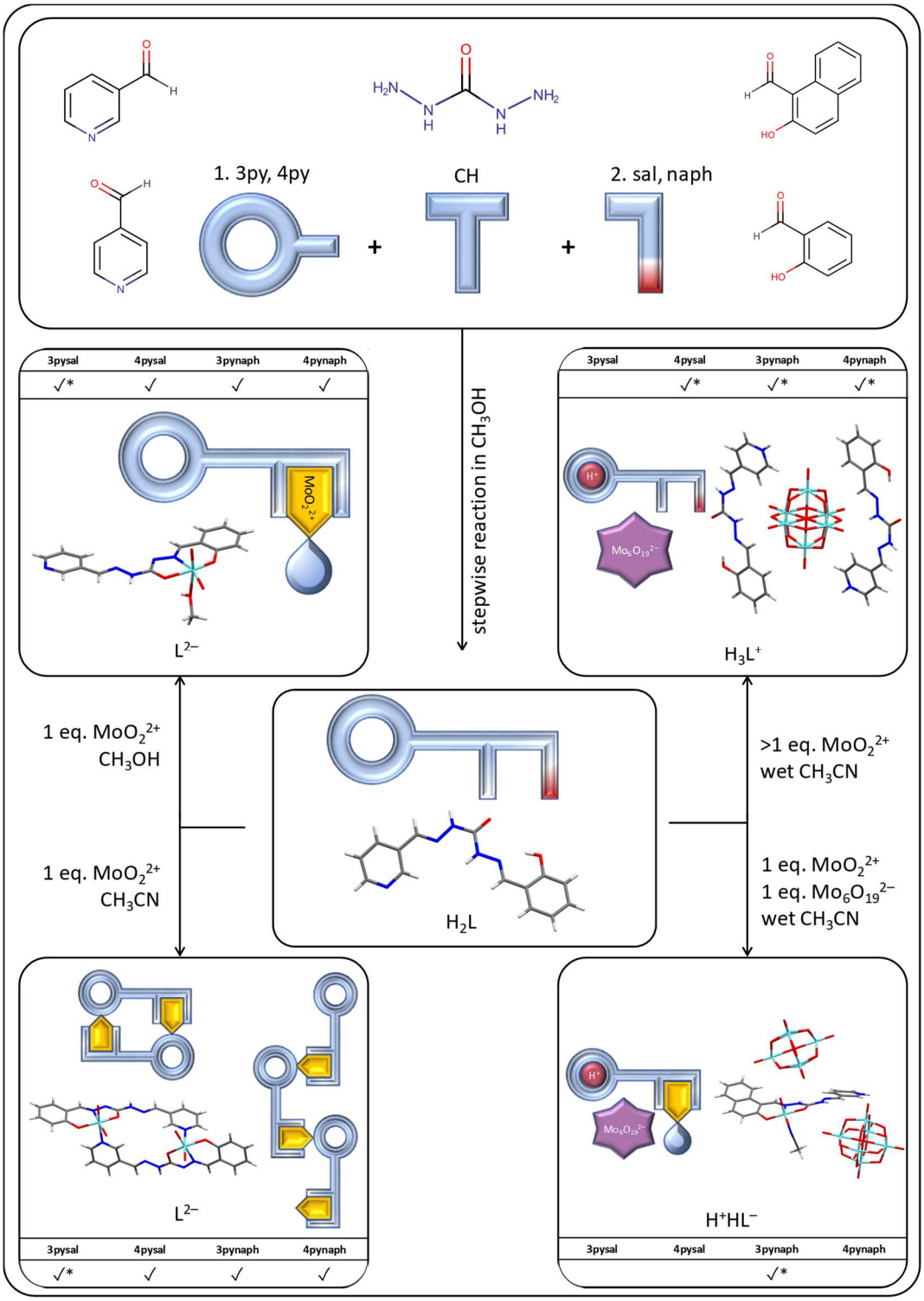

Scheme S1. Synthetic routes to unsymmetrical carbohydrazides and their Mo(VI) derivatives. Tick mark (✓) represents an isolated product, and asterisk (*) represents a product for which SC-XRD experiment was successfully performed.

(a) Monomeric complex of $\{MoO_2\}^{2+}$

General formula, with MeOH as solvent.

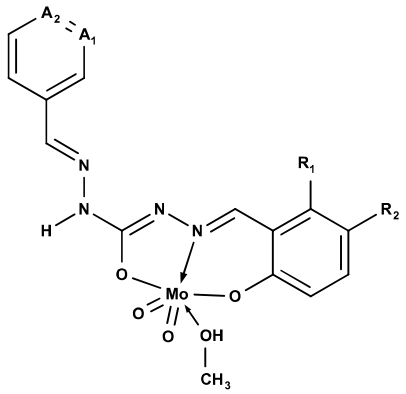

	A_1	A_2	R_1	R_2
H_2L^{3pysal}	CH	N	H	H
H_2L^{4pysal}	N	CH	H	H
$H_2L^{3pynaph}$	CH	N	-CH=CH-CH=CH-	
$H_2L^{4pynaph}$	N	CH	-CH=CH-CH=CH-	

(b) Dimeric complex of $\{MoO_2\}^{2+}$

General formula, with ligands derived from 3-pyridinecarboxaldehyde

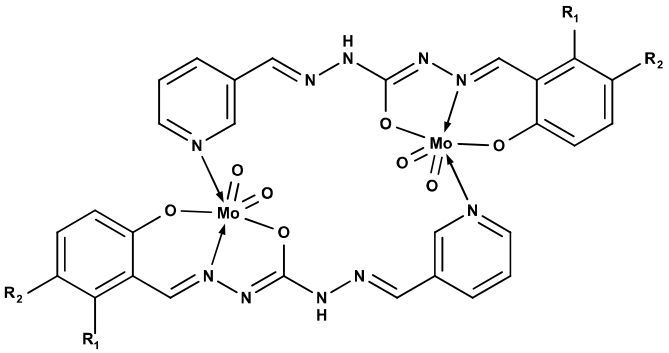

	R_1	R_2
H_2L^{3pysal}	H	H
$H_2L^{3pynaph}$	-CH=CH-CH=CH-	

Scheme S2. General formulae of (a) monomeric $\{MoO_2\}^{2+}$ complexes and (b) dimeric $\{MoO_2\}^{2+}$ complexes characterized in this work.

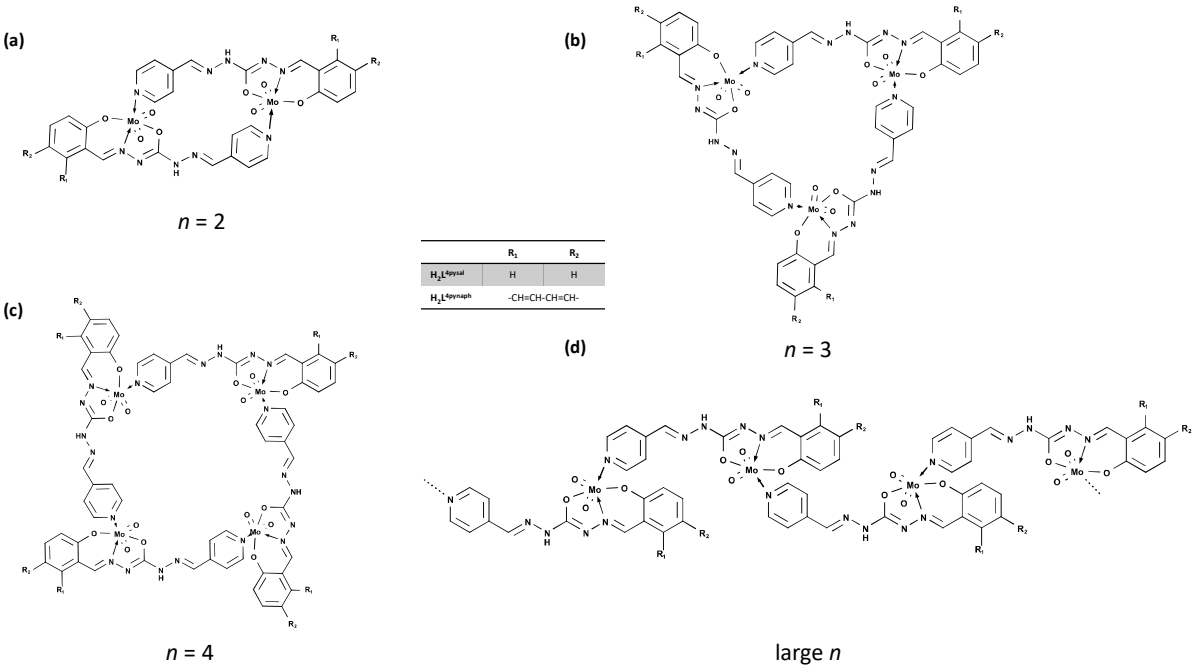

	R_1	R_2
H_2L^{4pysal}	H	H
$H_2L^{4pynaph}$	-CH=CH-CH=CH-	

Scheme S3. General formulae of (a) dimeric, (b) trimeric, (c) tetrameric and (d) polymeric ensembles that could be present alone or in a mixture in $[MoO_2(L^{4pysal})]_n$ and $[MoO_2(L^{4pynaph})]_n \cdot xnCH_3CN$. However, structures of type (a) and (b) are not yet observed, while structures of type (c) and (d) are known in the literature.

Molecular and crystal structure description

Carbohydrazide ligands

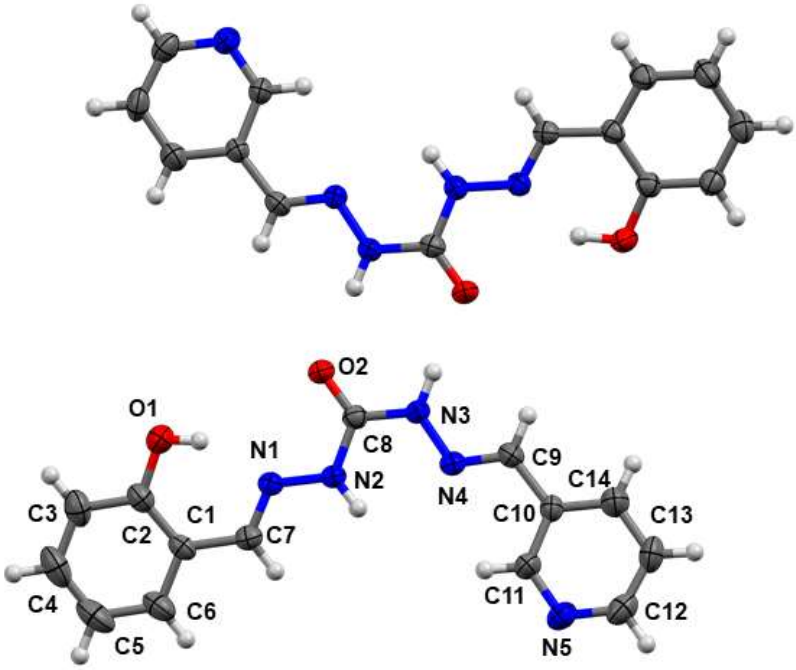

(a)

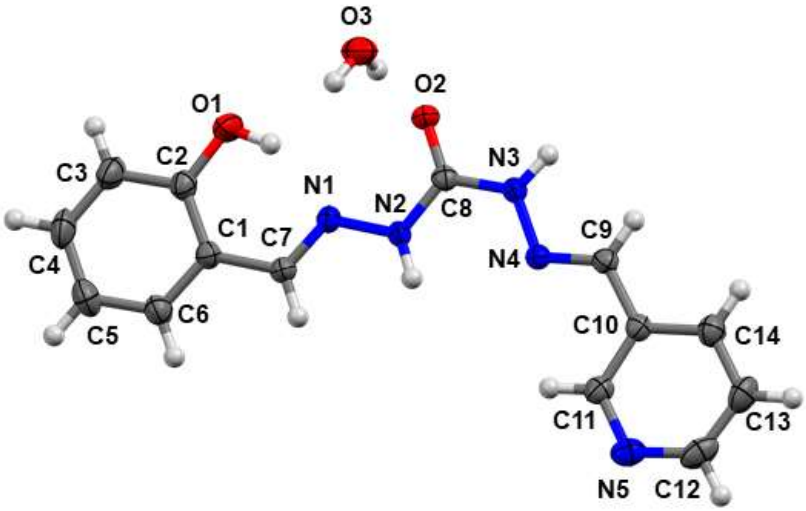

(b)

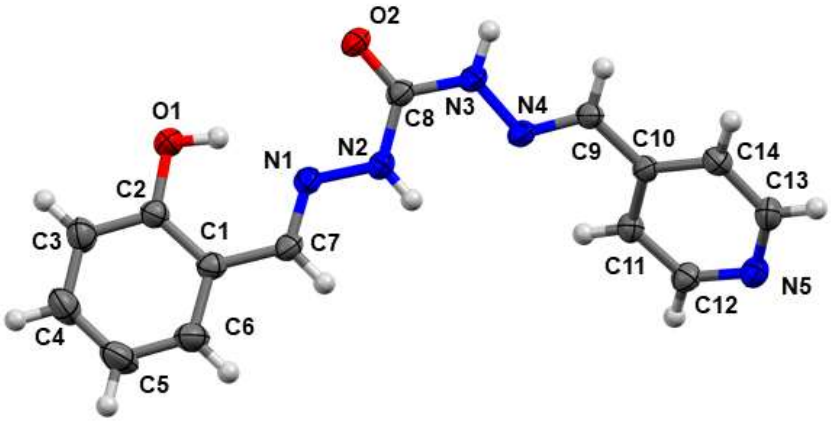
O2
O1
C8
N3
N4
N2
N1
C9
C10
C14
C13
C2
C1
C7
C3
C11
N5
C12
C4
C6
C5

(c)

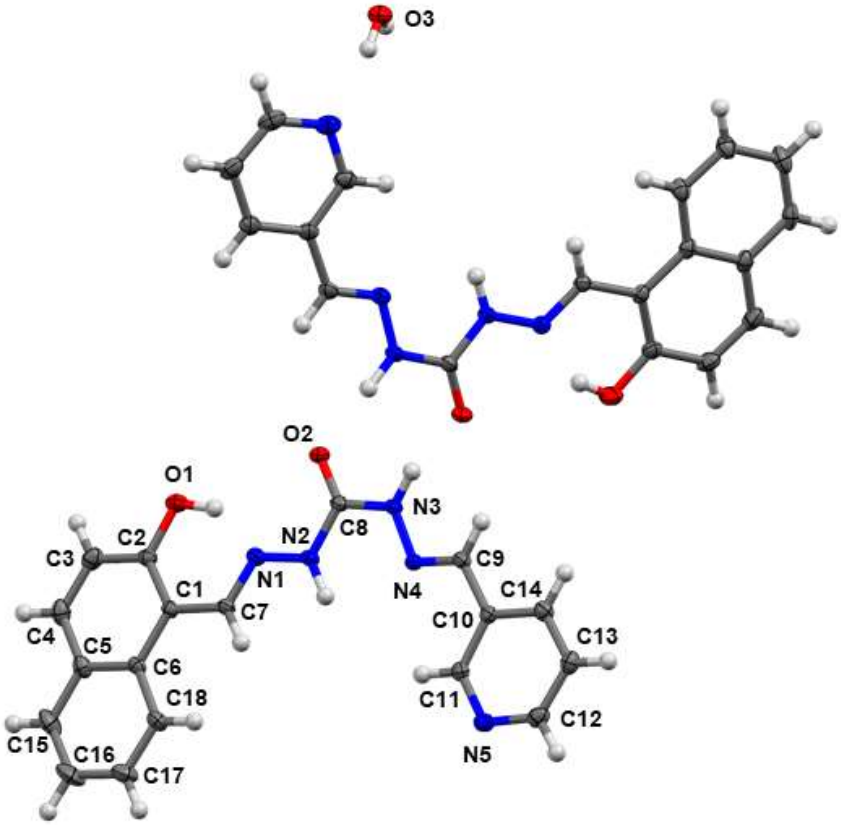
O3
O2
O1
N3
C8
N2
C2
C3
C9
N1
C1
N4
C14
C7
C10
C4
C13
C5
C6
C18
C11
C12
C15
C16
C17
N5

(d)

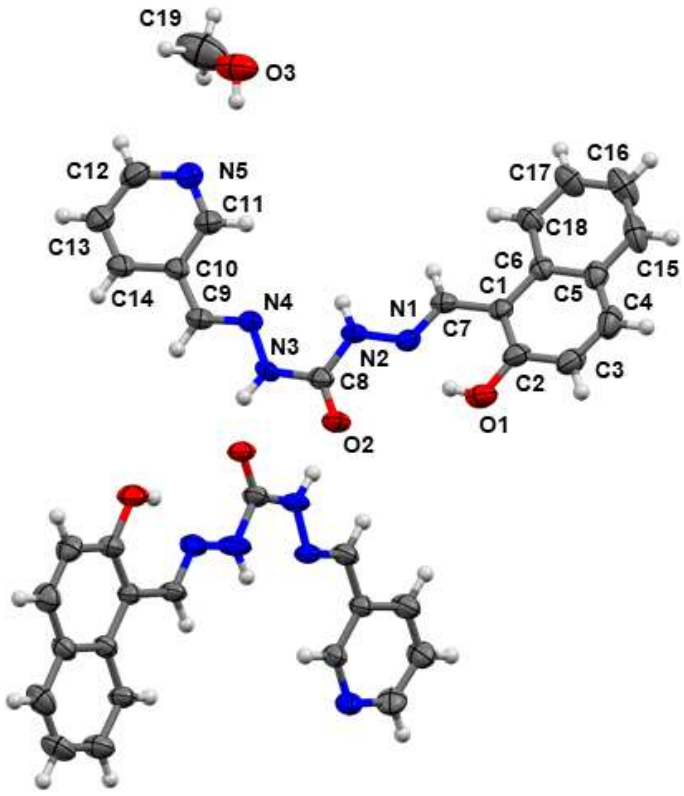

(e)

Figure S1. Mercury-ORTEP view of the asymmetric unit of (a) $\mathbf{H_2L^{3pysal}}$, (b) $\mathbf{H_2L^{3pysal}\cdot H_2O}$, (c) $\mathbf{H_2L^{4pysal}}$, (d) $\mathbf{H_2L^{3pynaph}\cdot 0.5H_2O}$ and (e) $\mathbf{H_2L^{3pynaph}\cdot 0.5CH_3OH}$. The displacement ellipsoids are drawn at 30% probability level. Hydrogen atoms are presented as spheres of arbitrary small radii.

Table S1. Selected bond lengths (in Å) for $\mathbf{H_2L^{3pysal}}$, $\mathbf{H_2L^{3pysal}\cdot H_2O}$, $\mathbf{H_2L^{4pysal}}$, $\mathbf{H_2L^{3pynaph}\cdot 0.5H_2O}$ and $\mathbf{H_2L^{3pynaph}\cdot 0.5CH_3OH}$. Atoms are numerated according to Figure S1. Two values per cell are given for crystal structures containing two symmetrically independent molecules.

Bond	$\mathbf{H_2L^{3pysal}}$	$\mathbf{H_2L^{3pysal}\cdot H_2O}$	$\mathbf{H_2L^{4pysal}}$	$\mathbf{H_2L^{3pynaph}\cdot 0.5H_2O}$	$\mathbf{H_2L^{3pynaph}\cdot 0.5CH_3OH}$
N1–N2	1.365(5), 1.369(5)	1.377(3)	1.3740(19)	1.372(3), 1.378(3)	1.376(5), 1.362(6)
N1–C7	1.279(5), 1.275(5)	1.277(3)	1.280(2)	1.282(3), 1.283(3)	1.289(6), 1.281(6)
N2–C8	1.364(5), 1.365(5)	1.348(3)	1.355(2)	1.358(3), 1.369(3)	1.370(6), 1.373(6)
N3–N4	1.374(5), 1.367(5)	1.380(2)	1.3719(19)	1.374(3), 1.375(3)	1.371(5), 1.376(5)
N3–C8	1.361(6), 1.359(6)	1.357(3)	1.363(2)	1.358(3), 1.364(3)	1.374(6), 1.363(6)
N4–C9	1.262(5), 1.279(5)	1.281(3)	1.276(2)	1.280(4), 1.284(3)	1.278(7), 1.271(6)
O2–C8	1.229(5), 1.234(5)	1.246(2)	1.2319(19)	1.231(3), 1.229(3)	1.220(6), 1.216(6)

Table S2. Selected bond angles (in °) for **H_2L^{3pysal}, $H_2L^{3pysal}\cdot H_2O$, H_2L^{4pysal}, $H_2L^{3pynaph}\cdot 0.5H_2O$** and **$H_2L^{3pynaph}\cdot 0.5CH_3OH$**. Atoms are numerated according to Figure S1. Two values per cell are given for crystal structures containing two symmetrically independent molecules.

Angle	H_2L^{3pysal}	$H_2L^{3pysal}\cdot H_2O$	H_2L^{4pysal}	$H_2L^{3pynaph}\cdot 0.5H_2O$	$H_2L^{3pynaph}\cdot 0.5CH_3OH$
N1–C7–C1	119.2(3), 120.3(4)	119.84(18)	120.42(14)	119.6(2), 120.1(2)	119.9(4), 120.6(4)
N2–C8–N3	115.6(4), 115.1(4)	117.36(18)	116.16(14)	116.0(2), 114.8(2)	114.0(4), 113.4(4)
O2–C8–N2	122.5(4), 123.4(4)	123.2(2)	123.61(15)	123.0(2), 123.4(2)	124.3(4), 123.5(4)
O2–C8–N3	121.9(4), 121.5(4)	119.4(2)	120.19(14)	121.0(2), 121.8(2)	121.8(5), 123.1(4)
N4–C9–C10	120.5(4), 119.9(4)	121.70(19)	120.24(14)	120.7(2), 121.9(2)	121.2(4), 121.1(4)
N2–N1–C7	121.3(3), 118.9(3)	119.38(18)	118.67(13)	119.2(2), 116.9(2)	118.6(3), 118.0(4)
N1–N2–C8	115.4(3), 116.7(3)	115.46(18)	116.99(13)	116.1(2), 116.2(2)	114.5(4), 119.0(4)
N4–N3–C8	120.0(3), 119.1(3)	121.06(17)	120.90(14)	119.8(2), 119.9(2)	121.1(4), 121.2(4)
N3–N4–C9	116.5(3), 116.5(3)	114.74(16)	115.50(13)	115.6(2), 115.7(2)	116.0(4), 116.0(4)

Table S3. Selected interplanar angles (in °) for **H_2L^{3pysal}, $H_2L^{3pysal}\cdot H_2O$, H_2L^{4pysal}, $H_2L^{3pynaph}\cdot 0.5H_2O$** and **$H_2L^{3pynaph}\cdot 0.5CH_3OH$**. *ar* represents LS plane passing through hydroxyaryl subunit, while *py* represents LS plane passing through pyridyl subunit. Associated indices represent the indices of symmetrically independent molecules.

Interplanar angle	H_2L^{3pysal}	$H_2L^{3pysal}\cdot H_2O$	H_2L^{4pysal}	$H_2L^{3pynaph}\cdot 0.5H_2O$	$H_2L^{3pynaph}\cdot 0.5CH_3OH$
ar_1–py_1	14.5(2)	6.43(12)	49.85(8)	8.22(12)	9.4(2)
ar_2–py_2	19.2(2)			3.99(12)	7.4(2)
ar_1–ar_2	5.0(2)			63.71(12)	67.8(2)
py_1–py_2	9.9(2)			55.49(13)	60.1(2)
ar_1–py_2	23.7(2)			59.74(12)	66.0(2)
ar_2–py_1	10.6(2)			59.48(13)	62.9(2)

Table S4. The geometry of hydrogen bonds (Å, °) for **H_2L^{3pysal}**, **$H_2L^{3pysal}\cdot H_2O$**, **H_2L^{4pysal}**, **$H_2L^{3pynaph}\cdot 0.5H_2O$** and **$H_2L^{3pynaph}\cdot 0.5CH_3OH$**. Atoms are numerated according to Figure SX.

D–H···A	D–H	H···A	D···A	∠D–H···A	Symmetry code
H_2L^{3pysal}					
O1–H1···N1	0.98(5)	1.73(5)	2.587(4)	144(4)	
O1A–H1···N1A	0.85(4)	1.81(4)	2.582(4)	151(5)	·
N2–H2···N4	0.90(5)	2.29(5)	2.638(5)	103(3)	
N2–H2···N5A	0.90(5)	2.51(4)	3.265(5)	142(4)	–0.5+*x*,–*y*,z
N2A–H2···N4A	0.88(5)	2.27(5)	2.604(5)	103(3)	
N2A–H2···N5	0.88(5)	2.54(4)	3.306(5)	147(4)	0.5+*x*,1–*y*,z
N3···O2A	0.89(4)	1.97(4)	2.856(5)	179(5)	
N3A–H3···O2	0.92(4)	1.88(4)	2.797(5)	178(5)	
$H_2L^{3pysal}\cdot H_2O$					
O1–H1···N1	0.86(2)	1.83(2)	2.602(3)	149(2)	
N2–H2···O3	0.90(2)	2.02(2)	2.886(3)	161(2)	–1+*x*,y,z
N3–H3···O2	0.92(2)	1.93(2)	2.845(2)	173(2)	2–*x*,–*y*,1–*z*
O3–H3B···O2	0.85(2)	2.00(2)	2.842(2)	175(2)	
O3–H3C···N5	0.84(2)	2.06(2)	2.893(3)	169(3)	1–*x*,1–*y*,1–*z*
H_2L^{4pysal}					
O1–H1···N1	0.89(2)	1.81(2)	2.6164(19)	149(2)	
N2–H2···N5	0.84(2)	2.27(2)	3.098(2)	167(2)	–*x*,1–*y*,1–*z*
N3–H3···O2	0.92(2)	1.95(2)	2.8686(19)	173.3(18)	1–*x*,1–*y*,–*z*
$H_2L^{3pynaph}\cdot 0.5H_2O$					
O1–H1···N1	0.86(3)	1.75(3)	2.527(3)	150(3)	
O1A–H1A···N1A	0.93(2)	1.74(2)	2.554(3)	144(2)	
N2–H2···N4	0.91(3)	2.32(3)	2.637(3)	100.2(19)	
N2–H2···O2A	0.91(3)	2.02(3)	2.866(3)	153(2)	1–*x*,1–*y*,1–*z*
N3A–H3AA···O2	0.93(3)	1.90(3)	2.804(3)	164(3)	
N2A–H2A···O3	0.976(19)	2.086(19)	2.989(3)	153(2)	1+*x*,1+*y*,z
N2A–H2A···N4A	0.976(19)	2.27(3)	2.623(3)	100.0(15)	
N3–H3···N5A	0.99(3)	1.99(3)	2.972(3)	171(2)	1–*x*,2–*y*,1–*z*

O3–H3B···N5	0.91(3)	1.95(3)	2.832(3)	162(2)	
O3–H3C···N4A	0.84(3)	2.40(3)	3.229(3)	168(2)	1–*x*,1–*y*,1–*z*
$H_2L^{3pynaph}\cdot 0.5CH_3OH$					
O1–H1···N1	0.82	1.81	2.531(5)	146	
O1A–H1A···N1A	0.82	1.84	2.558(5)	145	
N2–H2···N4	0.86	2.31	2.640(5)	103	
N2–H2···O2A	0.86	2.24	3.009(4)	149	1–*x*,1–*y*,1–*z*
N2A–H2A···O3	0.86	2.52	3.294(5)	151	1+*x*,–1+*y*,z
N2A–H2A···N4A	0.86	2.26	2.625(6)	106	
N3–H3···N5A	0.86	2.13	2.979(6)	169	1–*x*,–*y*,1–*z*
N3A–H3A···O2	0.86	2.07	2.857(5)	151	
O3–H3C···N5	0.82	2.13	2.856(6)	148	

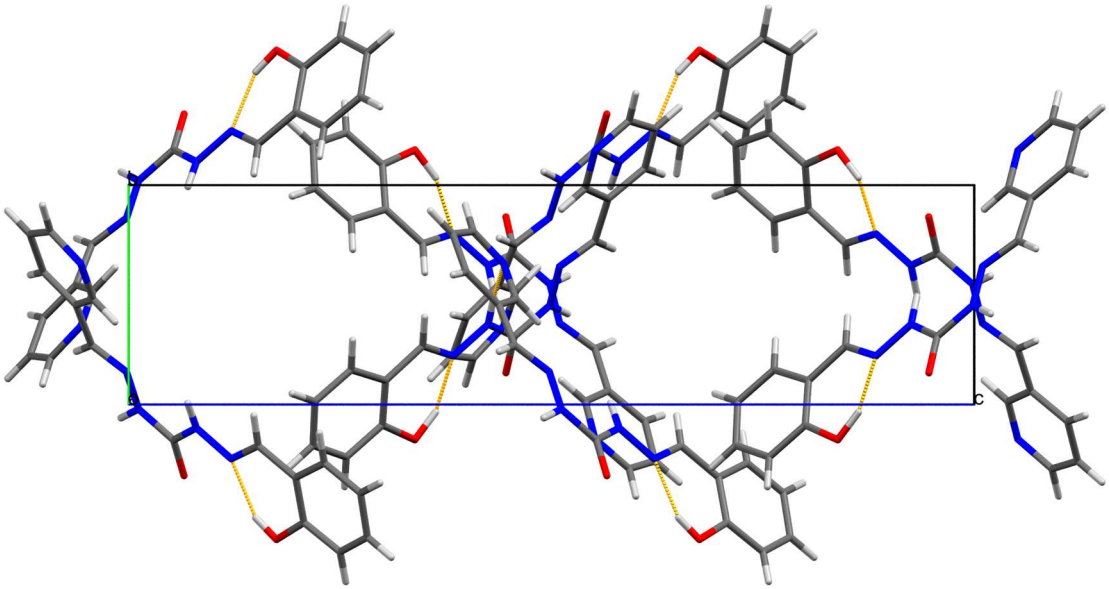

(a)

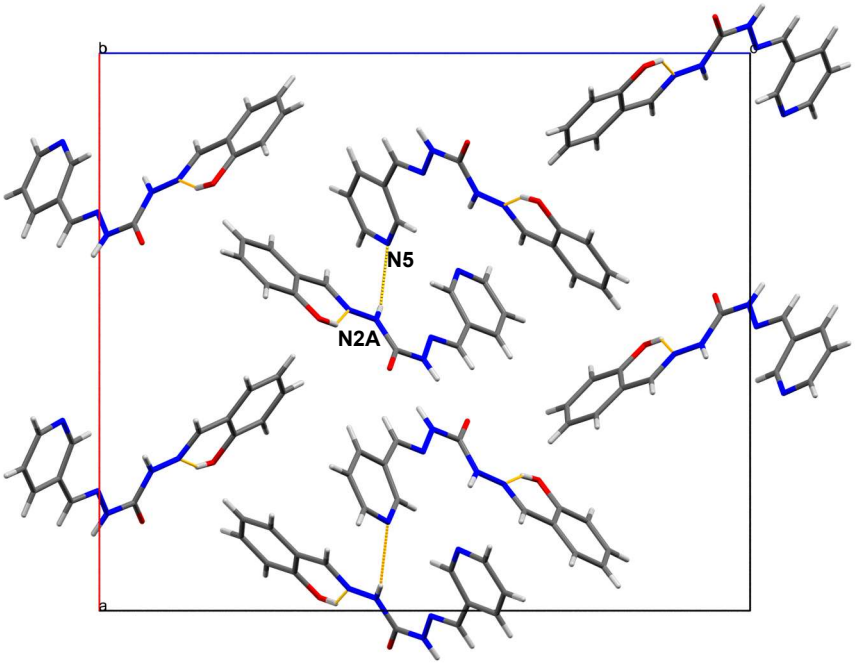

(b)

Figure S2. Crystal packing in $\mathbf{H_2L^{3pysal}}$ shown down the: (a) *a*-axis; (b) *b*-axis. Hydrogen bonds are presented by orange dashed lines. Symmetrically independent molecules are connected through N2A-H2A...N5 and N2-H2...N5A hydrogen bonds.

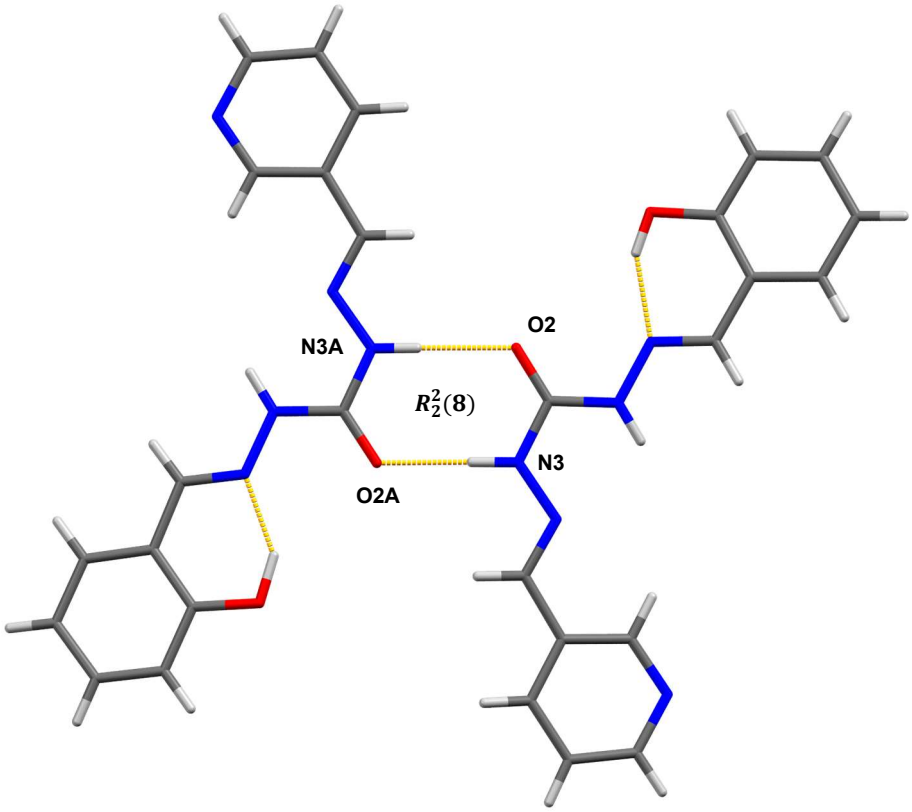

Figure S3. Supramolecular dimer in $\mathbf{H_2L^{3pysal}}$ achieved through amide homosynthon $R_2^2(8)$.

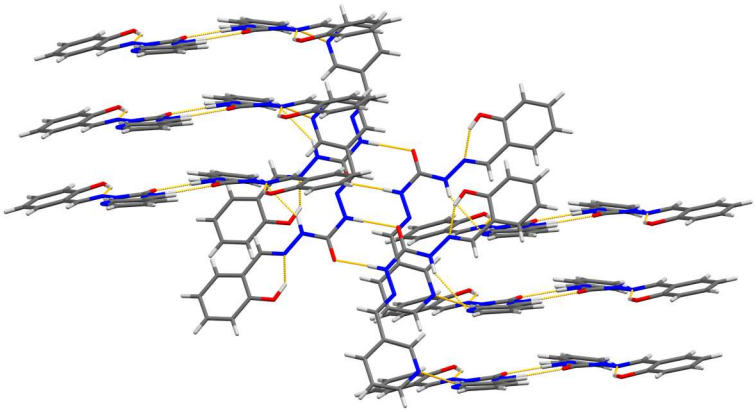

Figure S4. Supramolecular dimers of $\mathbf{H_2L^{3pysal}}$ stack in layers 2.457 Å apart. The expanded set of molecules again form layers misaligned for about 10°, while layers of original fragment close the angle of about 60° with expanded layers.

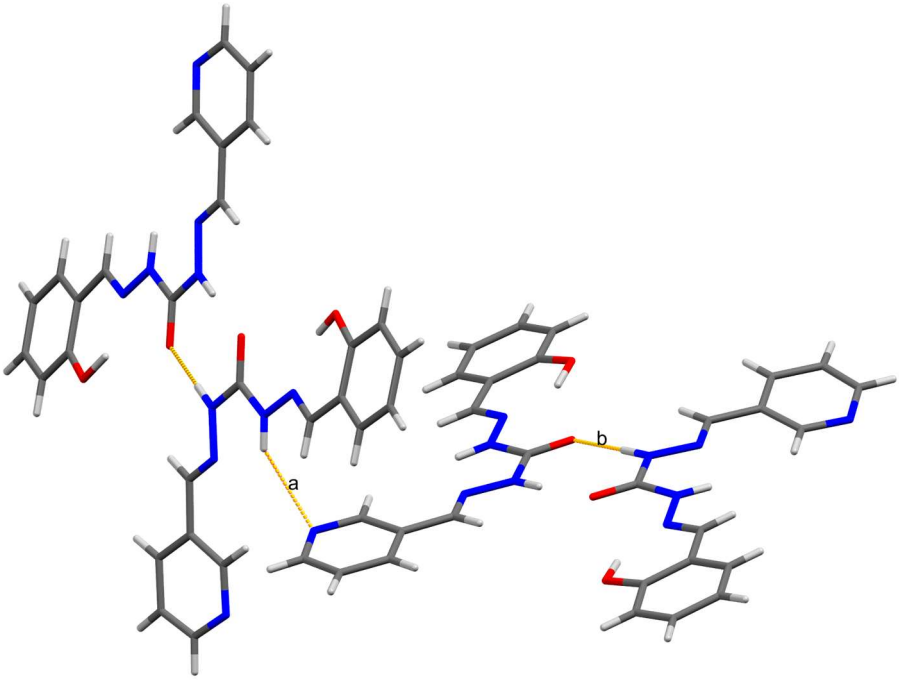

Figure S5. $C_2^2(13)$ supramolecular chain motif formed by combining N2-H2...N5 and N3-H3...O2 hydrogen bonds in the structure of $\mathbf{H_2L^{3pysal}}$.

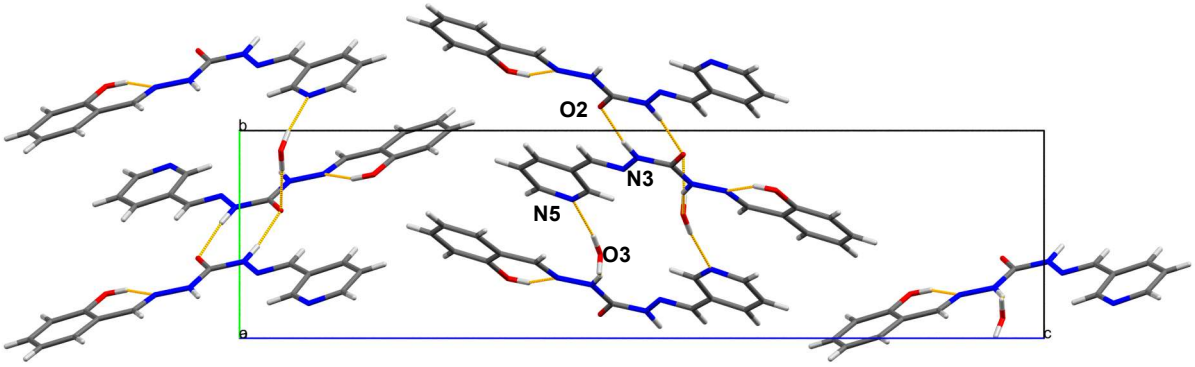

(a)

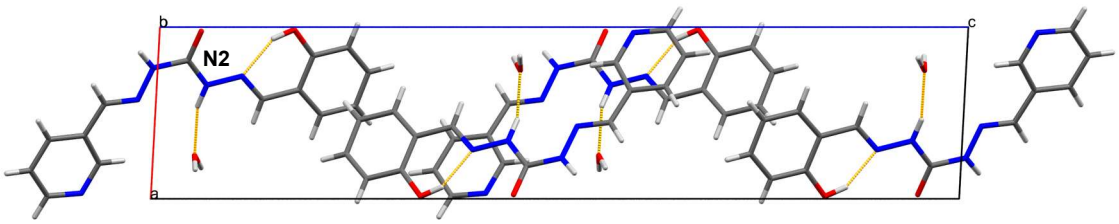

(b)

Figure S6. Crystal packing in $\mathbf{H_2L^{3pysal}{\cdot}H_2O}$ shown down the: (a) *a*-axis; (b) *b*-axis. Hydrogen bonds are presented by orange dashed lines. Supramolecular interactions are achieved through O2, O3 and N5 hydrogen bond acceptors, and N2-H2, N3-H3, O3-H3A and O3-H3B hydrogen bond donors.

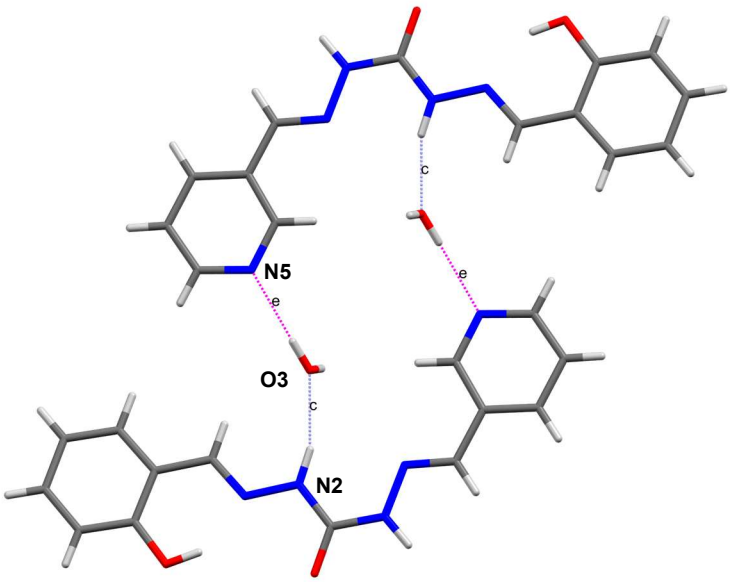

Figure S7. $R_4^4(22)$ supramolecular ring motif formed by combining N2-H2...O3 and O3-H3B...N5 hydrogen bonds in the structure of $\mathbf{H_2L^{3pysal}{\cdot}H_2O}$.

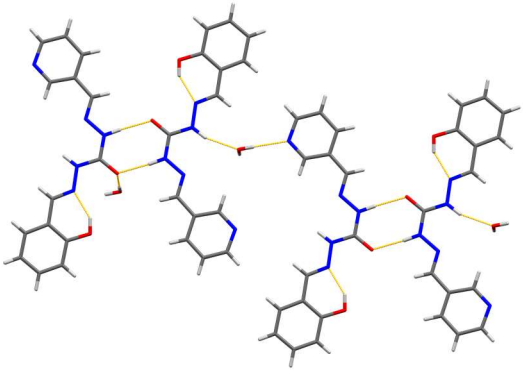

(a)

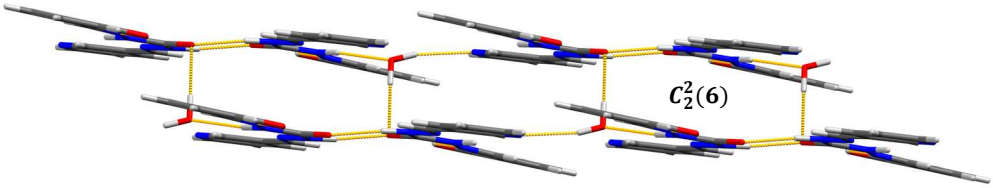

(b)

Figure S8. (a) Supramolecular dimers connecting through water molecule into layers and (b) layers bridged by remaining hydrogen bond donor from water molecule in the structure of $\mathbf{H_2L^{3pysal}{\cdot}H_2O}$. Hydrogen bond O3-H3B...O2 connecting adjacent layers forms a supramolecular $C_2^2(6)$ chain motif.

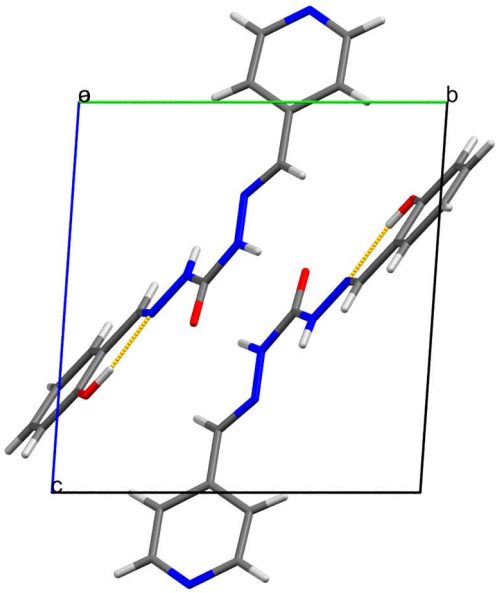

(a)

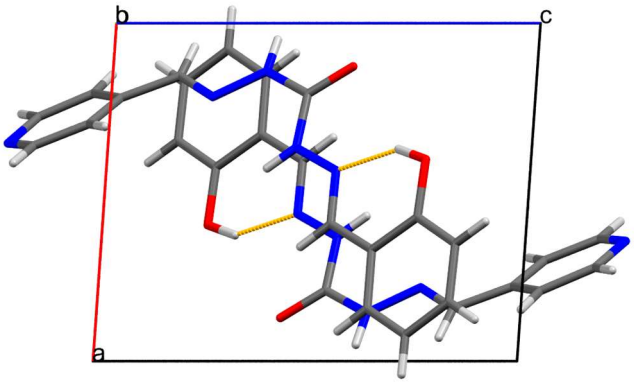

(b)

Figure S9. Crystal packing in $\mathbf{H_2L^{4pysal}}$ shown down the: (a) *a*-axis; (b) *b*-axis. Hydrogen bonds are presented by orange dashed lines.

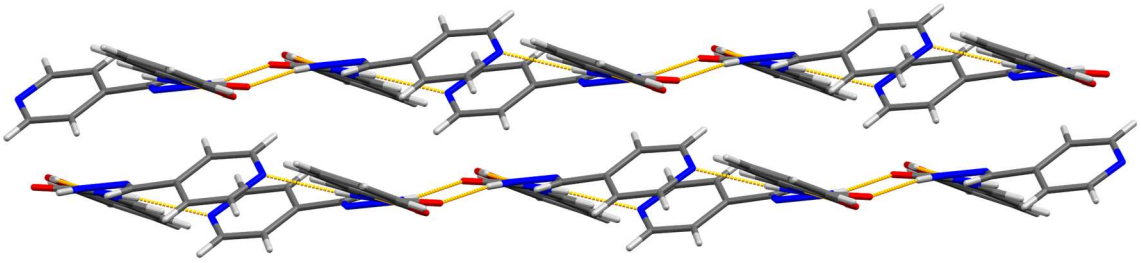

Figure S10. Supramolecular dimers of $\mathbf{H_2L^{4pysal}}$ stack in layers 4.605 Å apart. Layers are interacting mainly by C-H...O and C-H...N contacts (not shown for clarity).

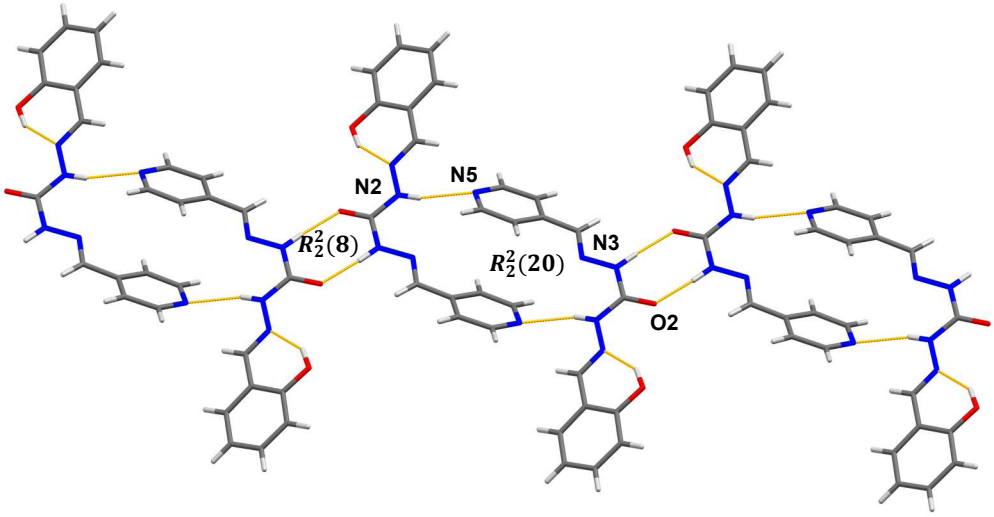

Figure S11. Two types of supramolecular dimers in $\mathbf{H_2L^{4pysal}}$, one achieved through amide homosynthon $R_2^2(8)$ and the other through N2-H2...N5 homosynthon $R_2^2(20)$.

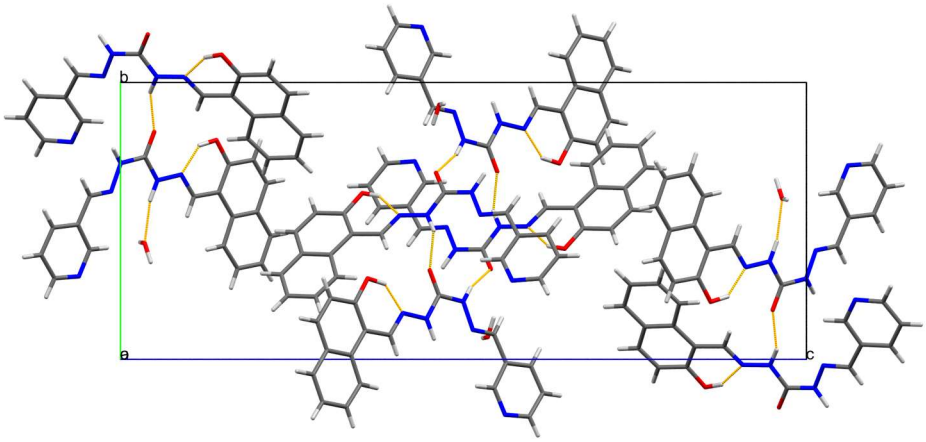

(a)

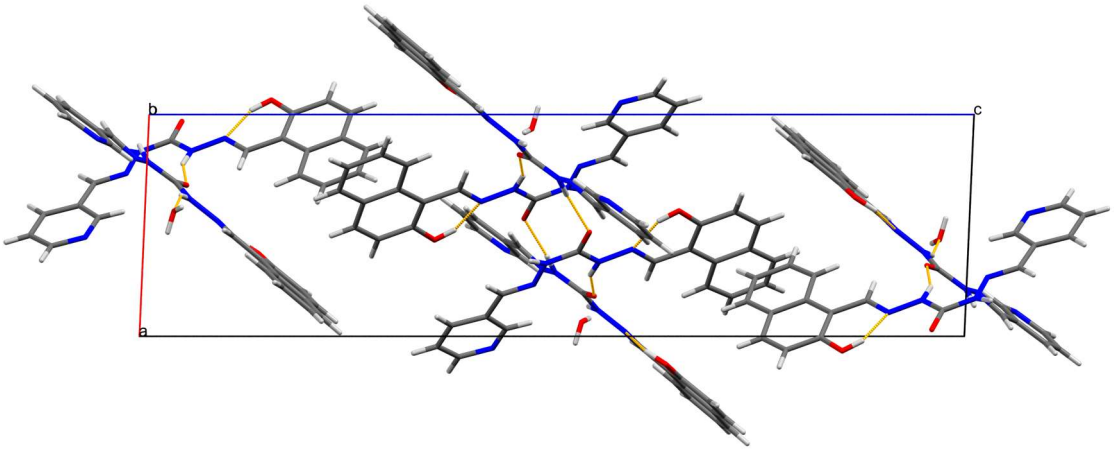

(b)

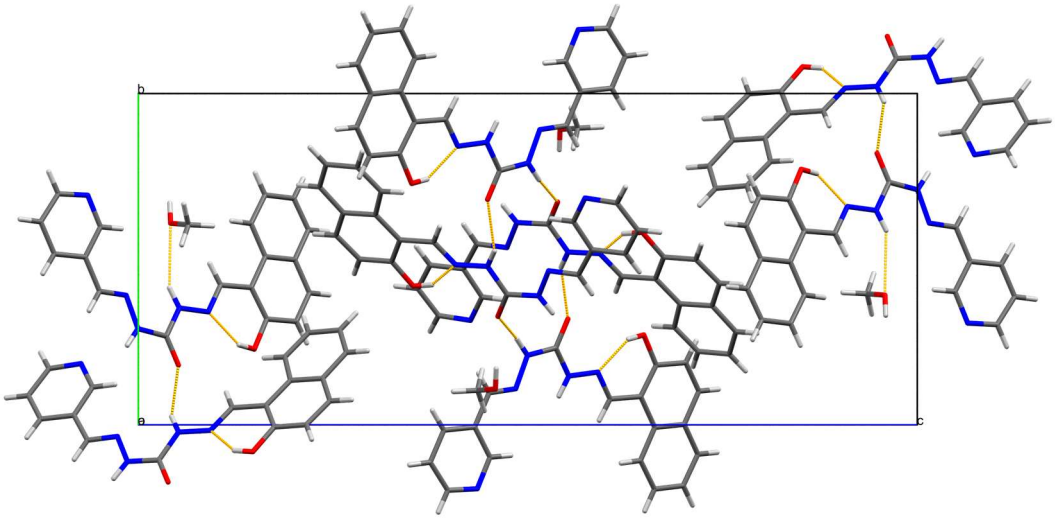

(c)

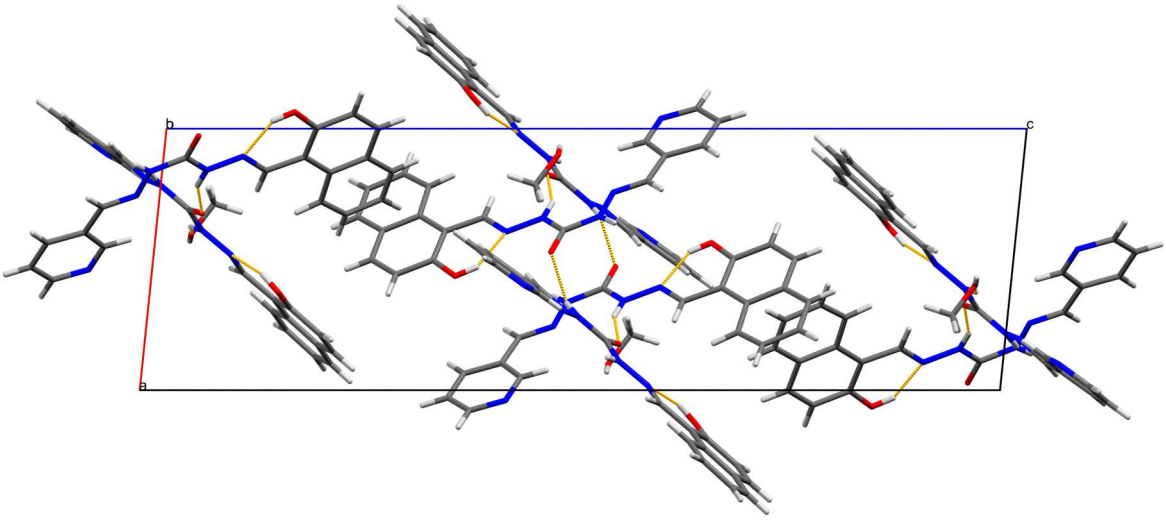

(d)

Figure S12. Crystal packing in $\mathbf{H_2L^{3pynaph}\cdot 0.5H_2O}$ shown down the: (a) *a*-axis; (b) *b*-axis, and crystal packing in $\mathbf{H_2L^{3pynaph}\cdot 0.5CH_3OH}$ shown down the: (c) *a*-axis, (d) *b*-axis. Hydrogen bonds are presented by orange dashed lines.

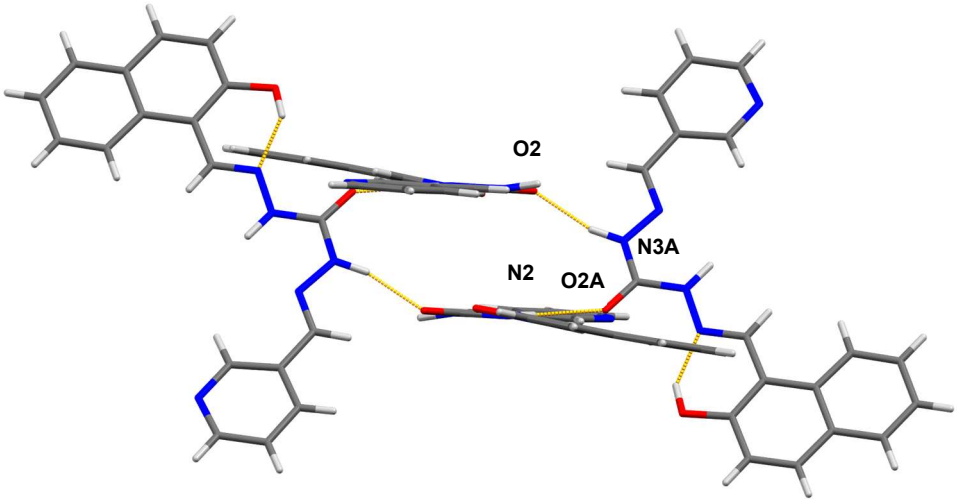

(a)

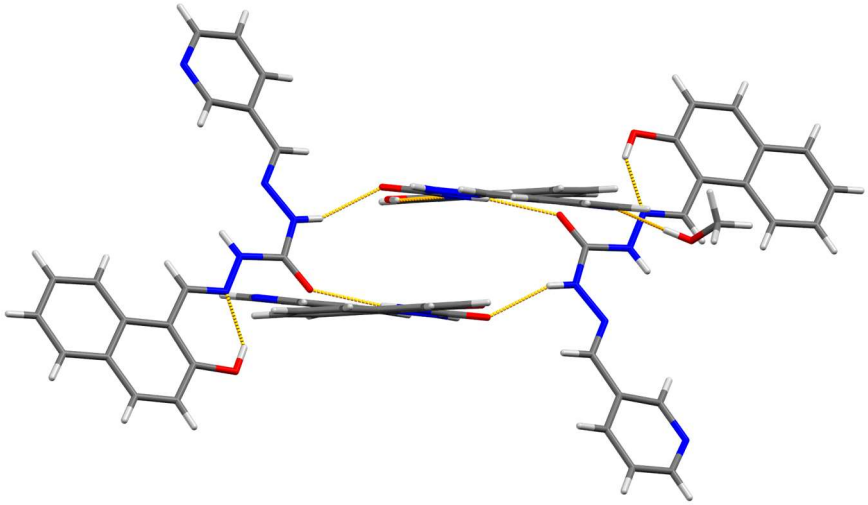

(b)

Figure S13. Supramolecular tetramer in (a) **$H_2L^{3pynaph}$·0.5H_2O** and (b) **$H_2L^{3pynaph}$·0.5CH_3OH** containing two pairs of symmetry independent molecules, forming $R_4^4(16)$ ring motif.

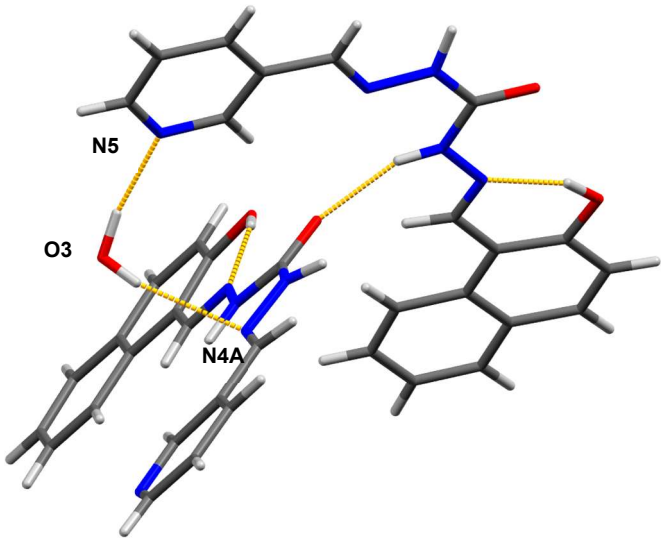

Figure S14. The role of the water molecule in the supramolecular linkage between symmetrically independent molecules in **$H_2L^{3pynaph}$·0.5H_2O.**

Dioxomolybdenum(VI) complexes

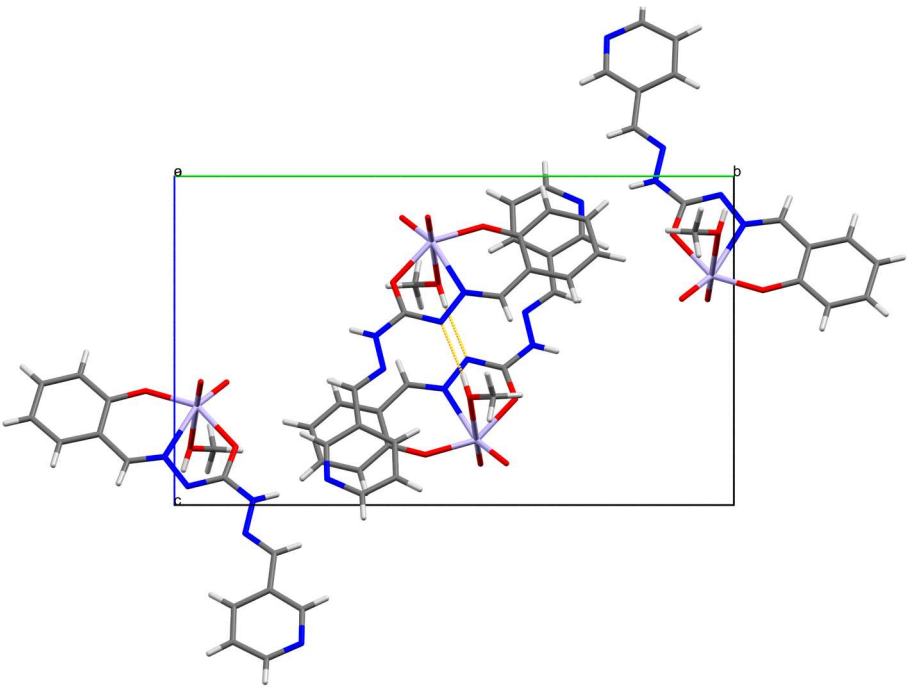

(a)

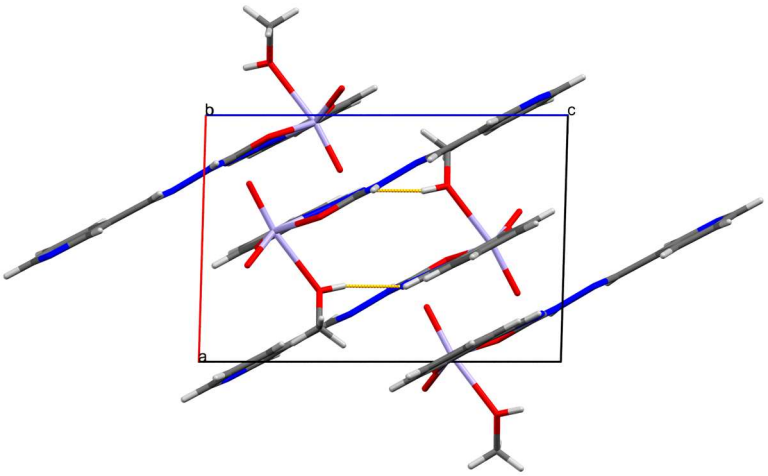

(b)

Figure S15. Crystal packing in **[$MoO_2(L^{3pysal})$(MeOH)]** shown down the: (a) *a*-axis; (b) *b*-axis. Hydrogen bonds are presented by orange dashed lines.

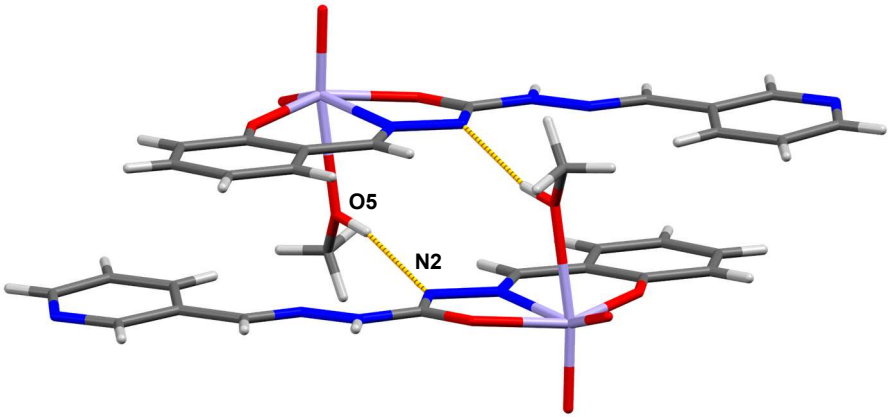

(a)

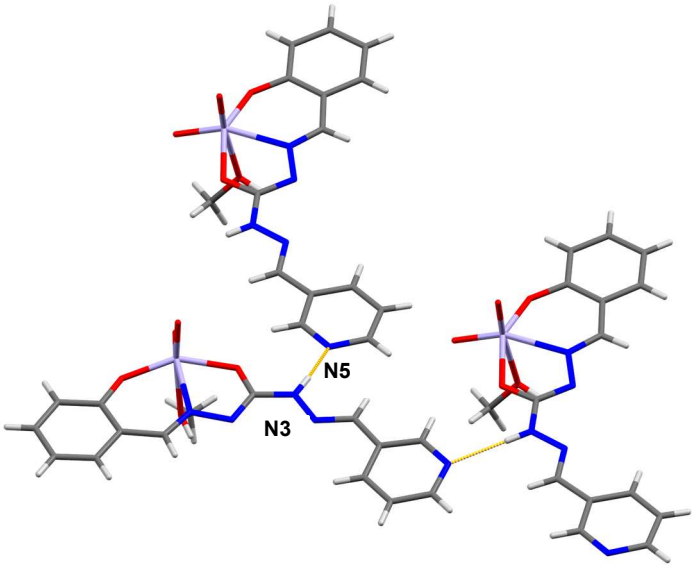

(b)

Figure S16. (a) the $R_2^2(10)$ supramolecular ring formed by O5-H5...N2 hydrogen bond and (b) $C_1^1(7)$ supramolecular chain formed by N3-H3...N5 hydrogen bond in the crystal structure of **[$MoO_2(L^{3pysal})(MeOH)$].**

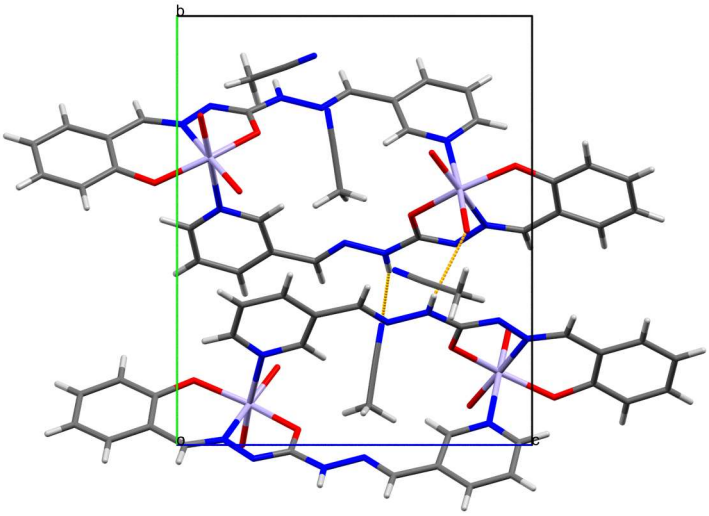

(a)

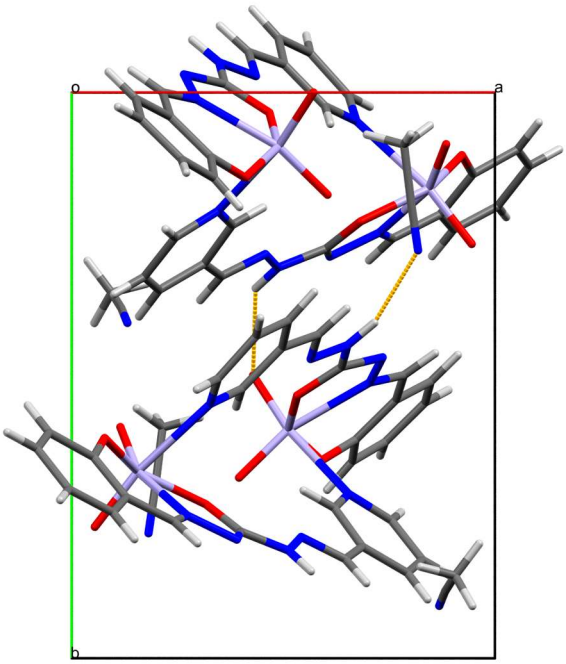

(b)

Figure S17. Crystal packing in **[$MoO_2(L^{3pysal})]_2$·xCH_3CN** shown down the: (a) *a*-axis; (b) *b*-axis. Hydrogen bonds are presented by orange dashed lines.

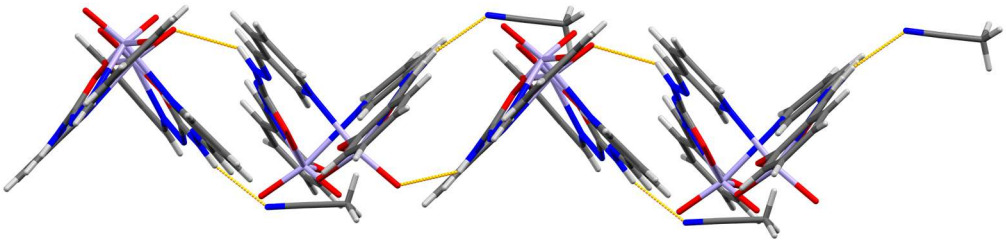

Figure S18. The chain-like structure formed by molecules in **[$MoO_2(L^{3pysal})]_2 \cdot xCH_3CN$** by N3-H3...O4=Mo hydrogen bond. Non-bonded acetonitrile molecules are omitted for clarity.

Table S5. Selected bond lengths (in Å) for **[$MoO_2(L^{3pysal})(MeOH)$]** and**[$MoO_2(L^{3pysal})]_2 \cdot xCH_3CN$**. Atoms are numerated according to Figure 3. Two values per cell are given for crystal structures containing two symmetrically independent molecules.

Bond	**[$MoO_2(L^{3pysal})(MeOH)$]**	**[$MoO_2(L^{3pysal})]_2 \cdot xCH_3CN$**
Mo1–O1	1.912(3)	1.920(6), 1.927(6)
Mo1–A6	2.368(3)	2.427(9), 2.436(9)
Mo1–O2	2.026(2)	2.015(7), 2.028(7)
Mo1–N1	2.259(3)	2.264(9), 2.231(9)
Mo1–O3	1.684(3)	1.708(7), 1.695(7)
Mo1–O4	1.699(3)	1.689(8), 1.695(8)
N1–N2	1.402(4)	1.387(13), 1.393(13)
N1–C7	1.287(4)	1.286(13), 1.294(13)
N2–C8	1.315(5)	1.304(14), 1.317(14)
N3–N4	1.369(4)	1.367(11), 1.370(11)
N3–C8	1.343(4)	1.366(14), 1.374(14)
N4–C9	1.275(5)	1.284(13), 1.276(13)
O2–C8	1.306(4)	1.301(15), 1.291(15)

Table S6. Selected bond angles (in °) for **[$MoO_2(L^{3pysal})(MeOH)$]** and **[$MoO_2(L^{3pysal})]_2 \cdot xCH_3CN$**. Atoms are numerated according to Figure 3. Two values per cell are given for crystal structures containing two symmetrically independent molecules.

Angle	**[$MoO_2(L^{3pysal})(MeOH)$]**	**[$MoO_2(L^{3pysal})]_2 \cdot xCH_3CN$**
N1–C7–C1	124.9(3)	123.0(10), 125.2(11)
O2–C8–N2	124.5(3)	117.9(9), 118.4(9)
O2–C8–N3	113.9(3)	115.8(11), 115.0(11)
N2–C8–N3	121.7(3)	126.4(10), 126.5(10)
N4–C9–C10	121.4(3)	120.1(10), 119.5(10)
O1–Mo1–O2	150.24(10)	149.2(3), 148.3(3)
O1–Mo1–A6	82.07(11)	84.0(3), 81.5(3)
O2–Mo1–O4	95.04(11)	95.7(3), 98.1(3)
O3–Mo1–O4	106.11(13)	105.7(4), 105.8(4)
O4–Mo1–A6	81.94(11)	169.4(3), 169.1(3)
O1–Mo1–O3	100.86(13)	102.5(3), 103.4(3)
O1–Mo1–N1	81.56(10)	81.7(3), 81.5(3)
O2–Mo1–A6	79.13(9)	76.0(3), 76.5(3)
O3–Mo1–A6	170.18(11)	82.3(3), 84.5(3)
O4–Mo1–N1	155.45(12)	93.4(3), 91.3(4)
O1–Mo1–O4	104.94(13)	100.7(3), 99.3(3)
O2–Mo1–O3	94.33(11)	97.8(3), 97.1(3)
O2–Mo1–N1	71.55(10)	71.5(3), 71.7(3)
O3–Mo1–N1	95.58(12)	159.1(3), 160.9(3)
A6–Mo1–N1	75.47(10)	77.7(3), 78.0(3)
Mo1–N1–N2	115.4(2)	115.8(6), 116.9(6)
Mo1–N1–C7	127.6(3)	127.3(8), 126.7(8)
N2–N1–C7	117.0(3)	116.8(9), 116.5(9)
N1–N2–C8	108.5(3)	107.5(9), 106.7(9)
N4–N3–C8	120.2(3)	120.3(9), 120.3(9)
N3–N4–C9	115.9(3)	115.5(9), 115.6(9)
Mo1–O2–C8	119.4(2)	118.9(6), 118.2(6)

Table S7. Selected interplanar angles (in °) for **[$MoO_2(L^{3pysal})(MeOH)$]** and **[$MoO_2(L^{3pysal})]_2 \cdot xCH_3CN$**. *ar* represents LS plane passing through hydroxyaryl subunit, while *py* represents LS plane passing through pyridyl subunit. L1 represents plane passing through O1, N1 and O2 (chelating atoms). Associated indices represent the indices of symmetrically independent molecules. Atoms are numerated according to Figure 3.

Interplanar angle	**[$MoO_2(L^{3pysal})(MeOH)$]**	**[$MoO_2(L^{3pysal})]_2 \cdot xCH_3CN$**
ar_1–py_1	5.12(19)	3.7(6)
ar_2–py_2		0.3(5)
ar_1–ar_2		87.9(6)
py_1–py_2		88.8(5)
ar_1–py_2		87.8(6)
ar_2–py_1		88.7(5)
L_1–*ar*	6.3(3)	14.1(5), 13.8(5)
L_1–*py*	2.3(3)	15.9(5), 13.6(5)
d(Mo–L_1)	0.27(2)	0.36(4), 0.31(4)

Table S8. Geometry of hydrogen bonds (Å, °) for **[$MoO_2(L^{3pysal})(MeOH)$]** and **[$MoO_2(L^{3pysal})]_2 \cdot 2CH_3CN$**. Atoms are numerated according to Figure 3.

D–H···A	D–H	H···A	D···A	∠D–H···A	Symmetry code
[$MoO_2(L^{3pysal})(MeOH)$]					
N3–H3···N5	0.86	2.08	2.912(4)	163	–1/2+*x*,3/2–*y*,1/2+*z*
O5–H5···N2	0.80(3)	2.02(3)	2.798(4)	167(5)	1–*x*,1–*y*,1–*z*
[$MoO_2(L^{3pysal})]_2 \cdot 2CH_3CN$					
N3–H3···N6	0.86	2.19	3.006(14)	159	
N3A–H3A···O4	0.86	2.42	3.137(11)	141	1–*x*,1/2+*y*,1–*z*

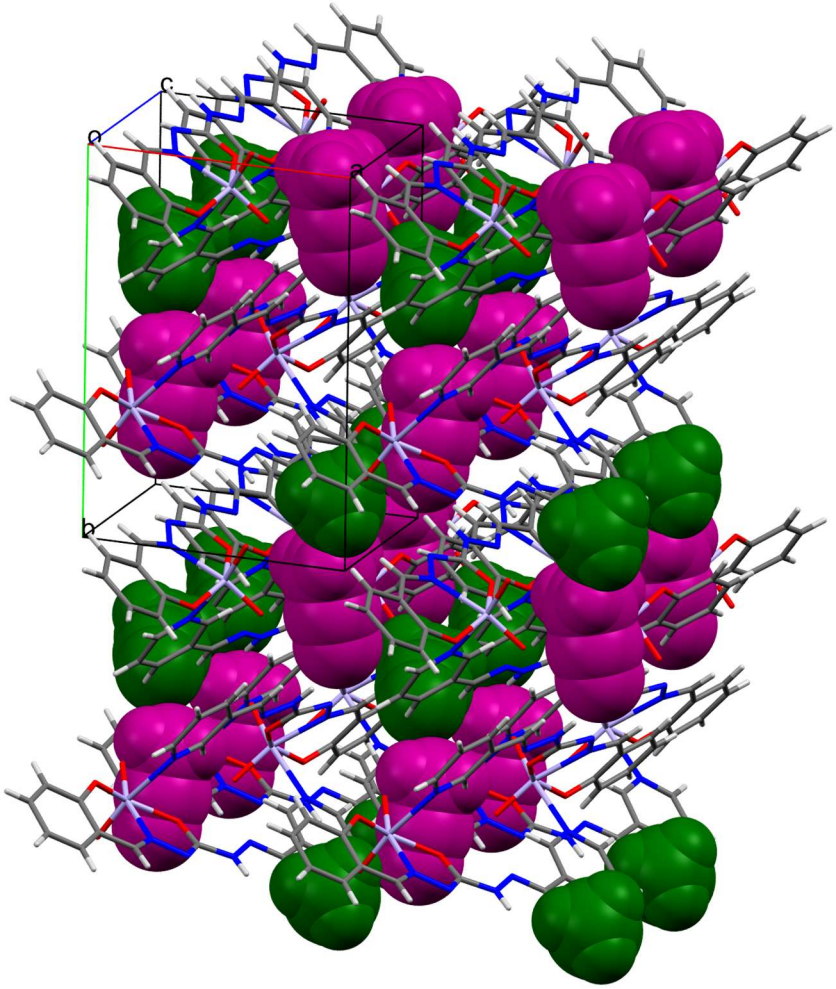

Figure S19. Crystal packing in **[$MoO_2(L^{3pysal})]_2$·xCH_3CN** shown with acetonitrile molecules drawn in spacefill style. Hydrogen-bonded acetonitrile molecules are shown in violet, while non-bonded acetonitrile molecules are shown in green colour.

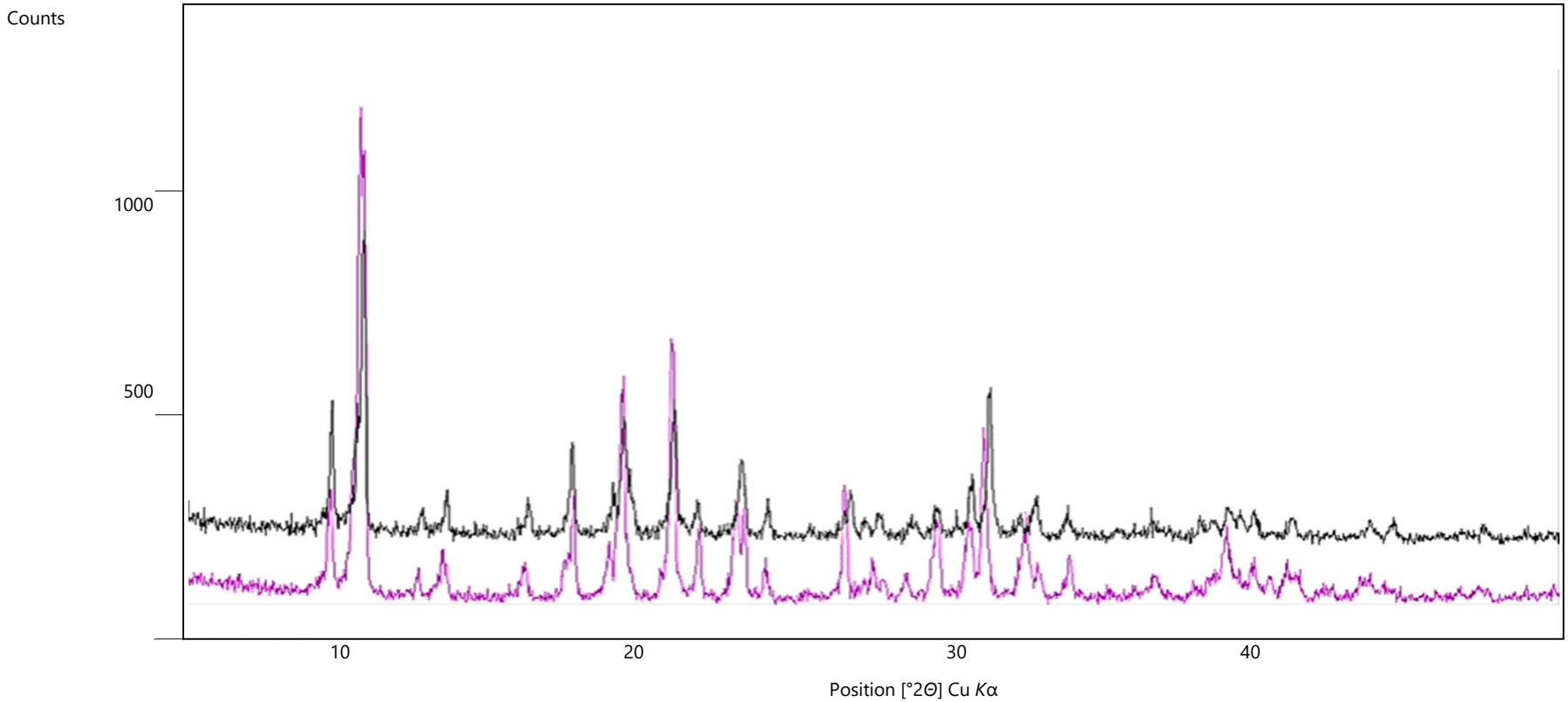

Figure S20. PXRD patterns of **[MoO$_2$(L^{3pysal})]$_2$·xCH$_3$CN** (magenta) and the sample obtained from **[MoO$_2$(L^{3pysal})]$_2$·xCH$_3$CN** heated from the ambient temperature up to 215°C (black). It can be concluded that the crystal structure of **[MoO$_2$(L^{3pysal})]$_2$** remains preserved even after removal of acetonitrile molecules.

Hexamolybdate salts

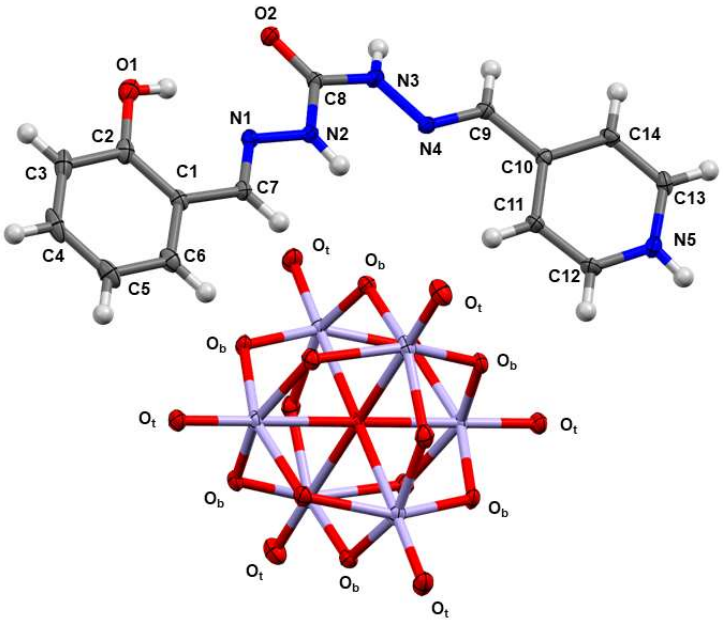

(a)

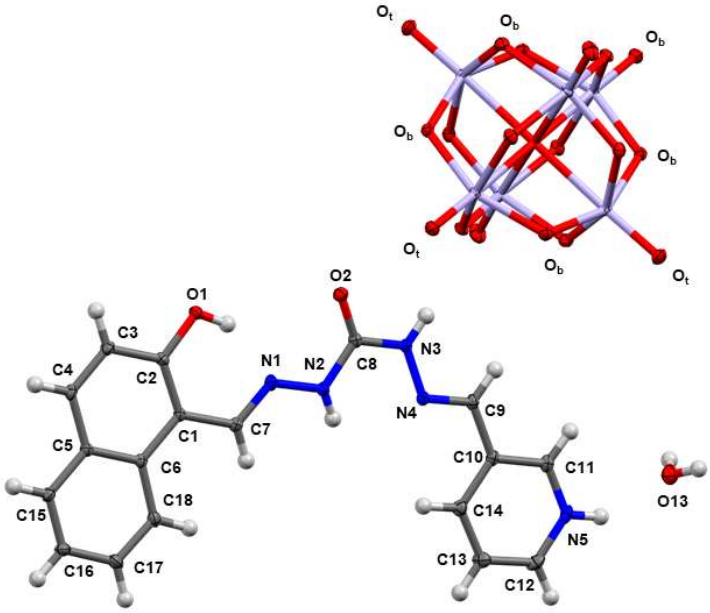

(b)

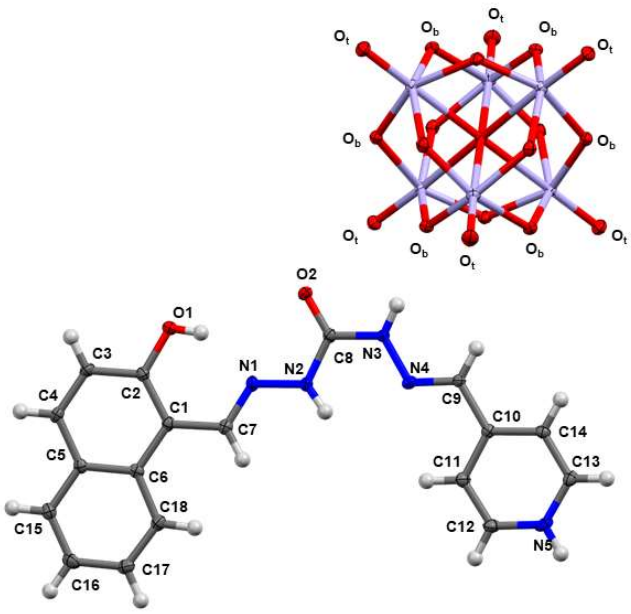

(c)

Figure S21. Mercury-ORTEP view of the asymmetric unit of (a) **$(H_3L^{4pysal})_2Mo_6O_{19}$**, (b) **$(H_3L^{3pynaph})_2Mo_6O_{19}\cdot 2H_2O$** and (c) **$(H_3L^{4pynaph})_2Mo_6O_{19}$**. The displacement ellipsoids are drawn at 30% probability level. Hydrogen atoms are presented as spheres of arbitrary small radii.

Table S9. Selected bond lengths (in Å) for **$(H_3L^{4pysal})_2Mo_6O_{19}$, $(H_3L^{3pynaph})_2Mo_6O_{19}\cdot 2H_2O$** and **$(H_3L^{4pynaph})_2Mo_6O_{19}$**. Atoms are numerated according to Figure S21.

Bond	$(H_3L^{4pysal})_2Mo_6O_{19}$	$(H_3L^{3pynaph})_2Mo_6O_{19}\cdot 2H_2O$	$(H_3L^{4pynaph})_2Mo_6O_{19}$
N1–C7	1.282(5)	1.284(3)	1.281(5)
N1–N2	1.372(4)	1.362(3)	1.370(5)
N2–C8	1.357(5)	1.371(4)	1.360(5)
N3–N4	1.371(4)	1.361(3)	1.355(4)
N3–C8	1.360(4)	1.367(3)	1.368(5)
N4–C9	1.276(4)	1.279(3)	1.280(5)
O2–C8	1.230(5)	1.222(4)	1.229(5)

Table S10. Selected bond angles (in °) for **$(H_3L^{4pysal})_2Mo_6O_{19}$, $(H_3L^{3pynaph})_2Mo_6O_{19}\cdot 2H_2O$** and **$(H_3L^{4pynaph})_2Mo_6O_{19}$.** Atoms are numerated according to Figure S22.

Angle	$(H_3L^{4pysal})_2Mo_6O_{19}$	$(H_3L^{3pynaph})_2Mo_6O_{19}\cdot 2H_2O$	$(H_3L^{4pynaph})_2Mo_6O_{19}$
N1–C7–C1	120.1(3)	118.3(3)	118.9(4)
N2–C8–N3	115.3(3)	115.1(2)	116.1(4)
O2–C8–N2	123.4(3)	123.5(2)	123.7(3)
O2–C8–N3	121.3(3)	121.3(2)	120.2(3)
N4–C9–C10	119.8(3)	118.7(2)	118.3(3)
N2–N1–C7	117.8(3)	120.9(3)	121.2(4)
N1–N2–C8	116.9(3)	115.2(3)	115.6(4)
N4–N3–C8	121.0(3)	119.6(2)	119.8(3)
N3–N4–C9	116.0(3)	117.5(2)	117.9(3)
ar_1–py_1	13.75(14)	3.3(5)	4.84(10)

Table S11. The geometry of hydrogen bonds (Å, °) for **$(H_3L^{4pysal})_2Mo_6O_{19}$, $(H_3L^{3pynaph})_2Mo_6O_{19}\cdot 2H_2O$** and **$(H_3L^{4pynaph})_2Mo_6O_{19}$**. Atoms are numerated according to Figure S22.

D–H···A	D–H	H···A	D···A	∠D–H···A	Symmetry code
$(H_3L^{4pysal})_2Mo_6O_{19}$					
O1–H1···N1	0.81(5)	1.93(5)	2.637(4)	145(5)	
N2–H2···O_b	0.84(5)	2.38(4)	3.132(4)	150(4)	
N3–H3···O_t	0.82(4)	2.36(4)	3.154(4)	166(3)	1/2+*x*,3/2–*y*,–1/2+*z*
N5–H5···O2	0.83(4)	1.92(4)	2.738(4)	172(4)	–1/2+*x*,3/2–*y*,1/2+*z*
$(H_3L^{3pynaph})_2Mo_6O_{19}\cdot 2H_2O$					
O1–H1···N1	0.83(3)	1.78(3)	2.524(3)	148(2)	
N2–H2···O_t	0.83(2)	2.66(3)	3.402(3)	149(2)	
N3–H3···O_b	0.85(3)	2.21(3)	3.038(3)	166(3)	
N5–H5···O13	0.86	1.96	2.716(3)	146	
O13–H13A···O_b2	0.80(3)	2.51(3)	3.044(3)	125(2)	1–*x*,2–*y*,1–*z*
O13–H13B···O2	0.82(3)	1.99(3)	2.810(3)	174(4)	1–*x*,1/2+*y*,3/2–*z*
$(H_3L^{4pynaph})_2Mo_6O_{19}$					
O1–H1···N1	0.79(3)	1.83(4)	2.508(4)	144(4)	
N2–H2···N4	0.85(3)	2.27(3)	2.640(5)	106(3)	
N2–H2···O_t	0.85(3)	2.53(4)	3.265(5)	146(3)	1–*x*,1/2+*y*,1/2–*z*
N3–H3···O_b	0.88(4)	2.12(4)	2.956(4)	159(4)	
N5–H5···O2	0.85(3)	2.00(4)	2.739(5)	145(5)	–1+*x*,1/2–*y*,–1/2+*z*

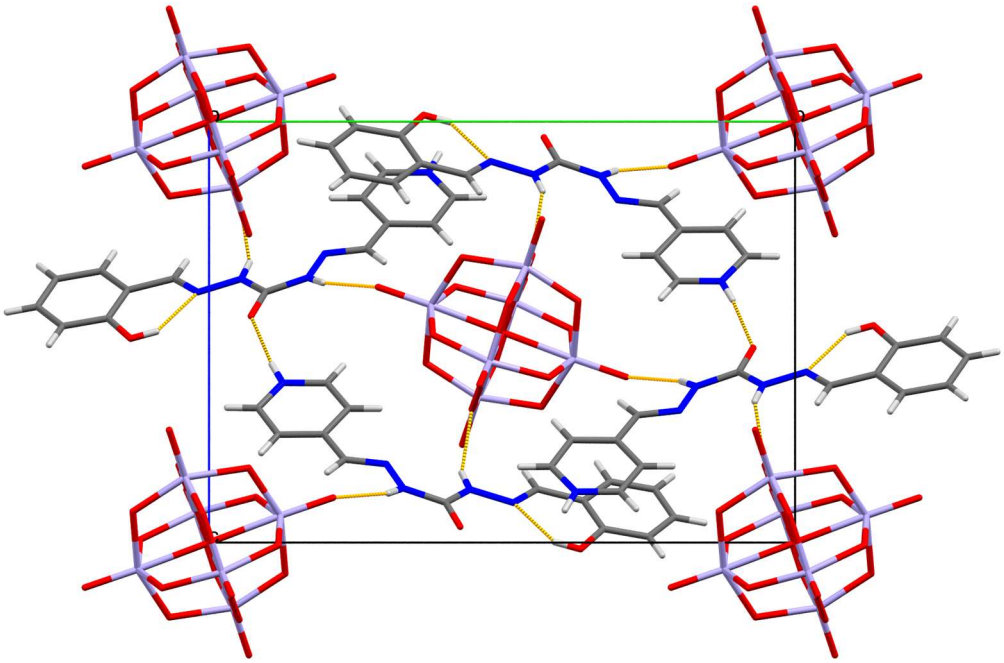

(a)

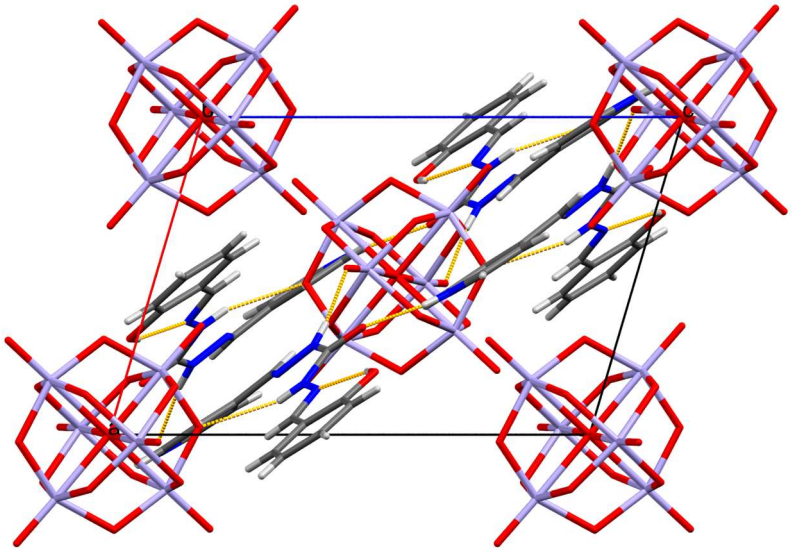

(b)

Figure S22. Crystal packing in **$(H_3L^{4pysal})_2Mo_6O_{19}$** shown down the: (a) *a*-axis; (b) *b*-axis. Hydrogen bonds are presented by orange dashed lines.

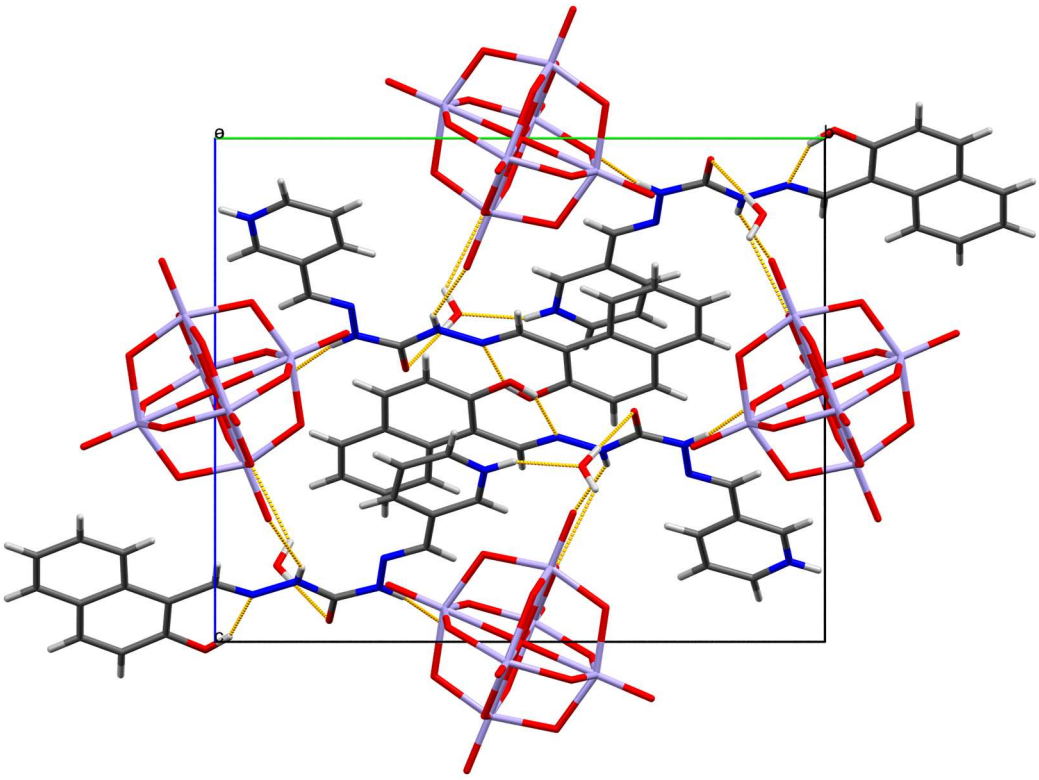

(a)

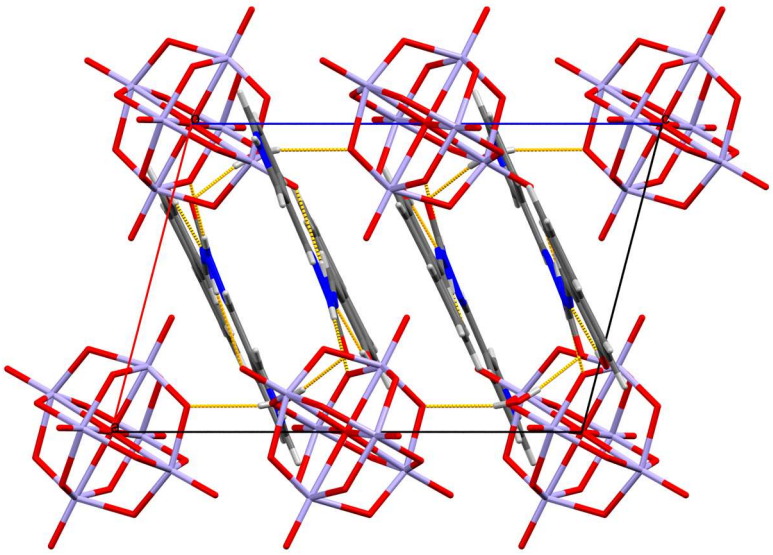

(b)

Figure S23. Crystal packing in **$(H_3L^{3pynaph})_2Mo_6O_{19}\cdot 2H_2O$** shown down the: (a) *a*-axis; (b) *b*-axis. Hydrogen bonds are presented by orange dashed lines.

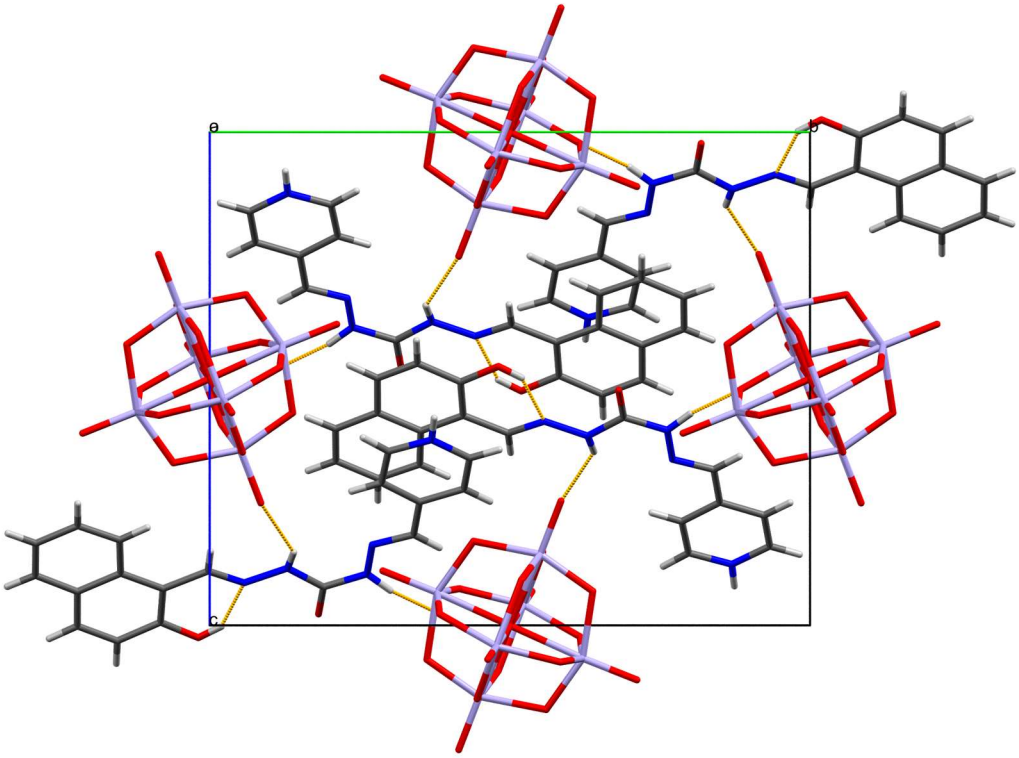

(a)

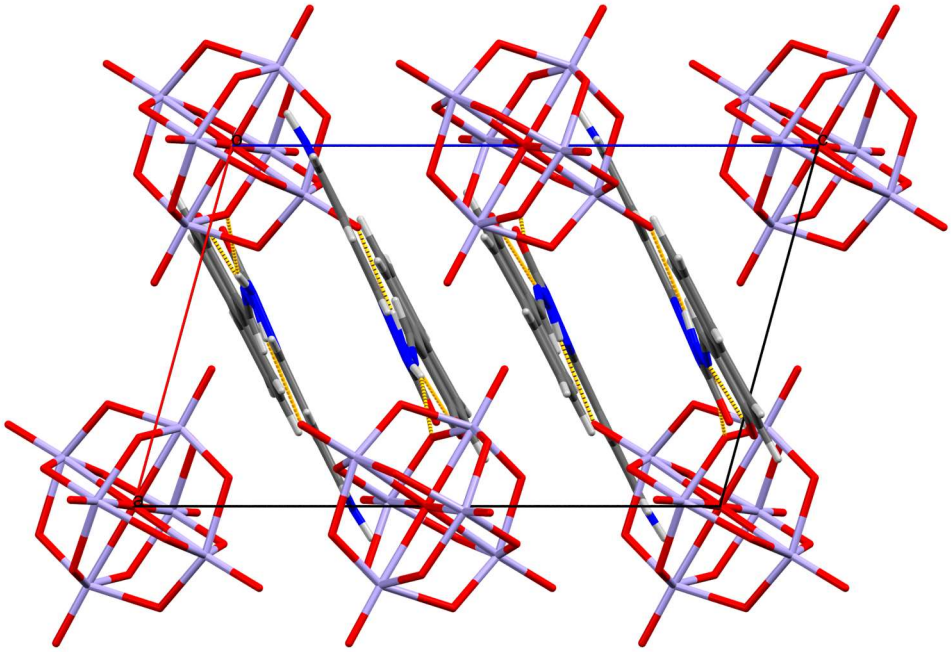

(b)

Figure S24. Crystal packing in $(H_3L^{4pynaph})_2Mo_6O_{19}$ shown down the: (a) *a*-axis; (b) *b*-axis. Hydrogen bonds are presented by orange dashed lines.

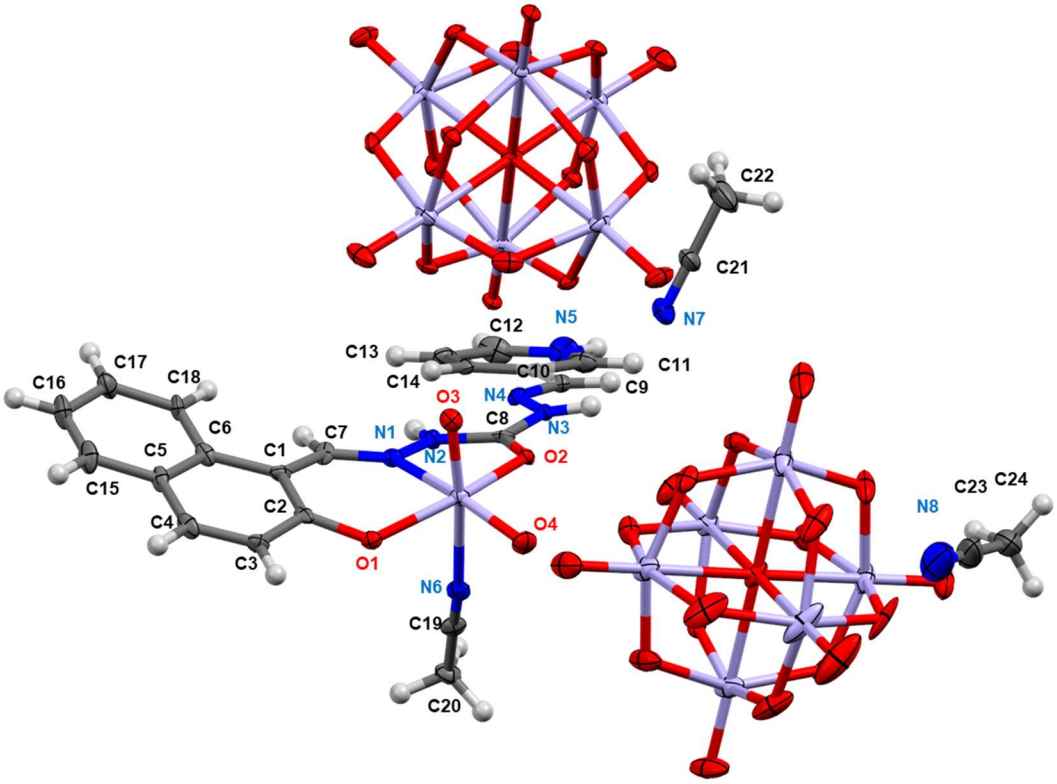
C22
C21
N7
N5
C12
C13
C11
C14
C10
C9
C17
C16
C18
O3
N4
C8
N3
C6
C7
N1
C5
C1
N2
O2
C15
C2
C4
O4
C3
O1
N6
C19
C20
N8
C23
C24

(a)

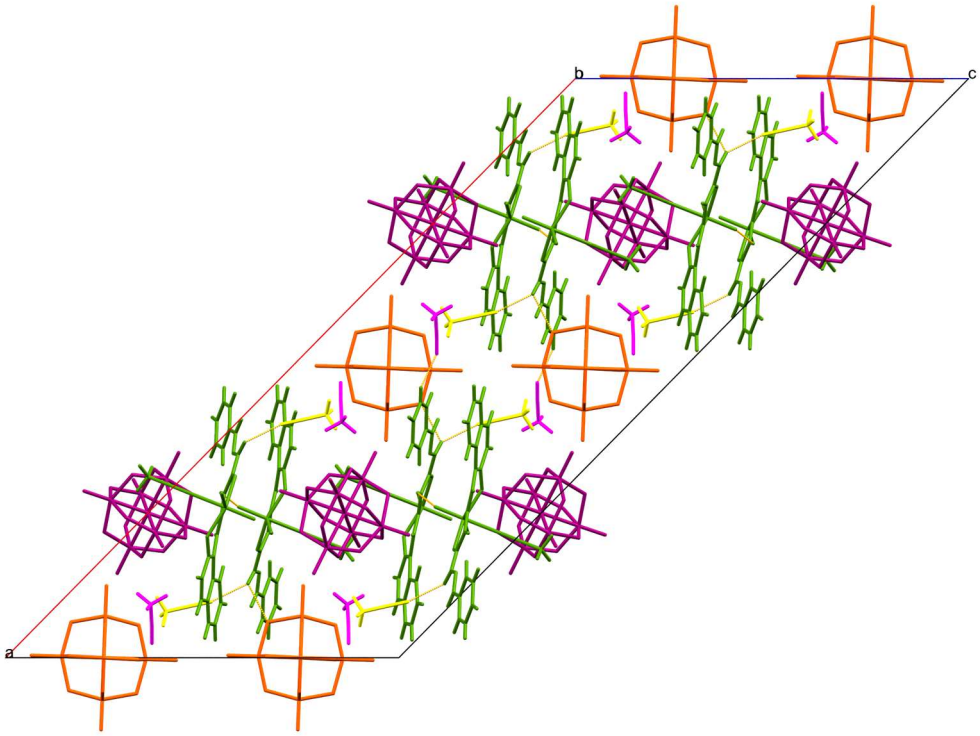
b
c
a

(b)

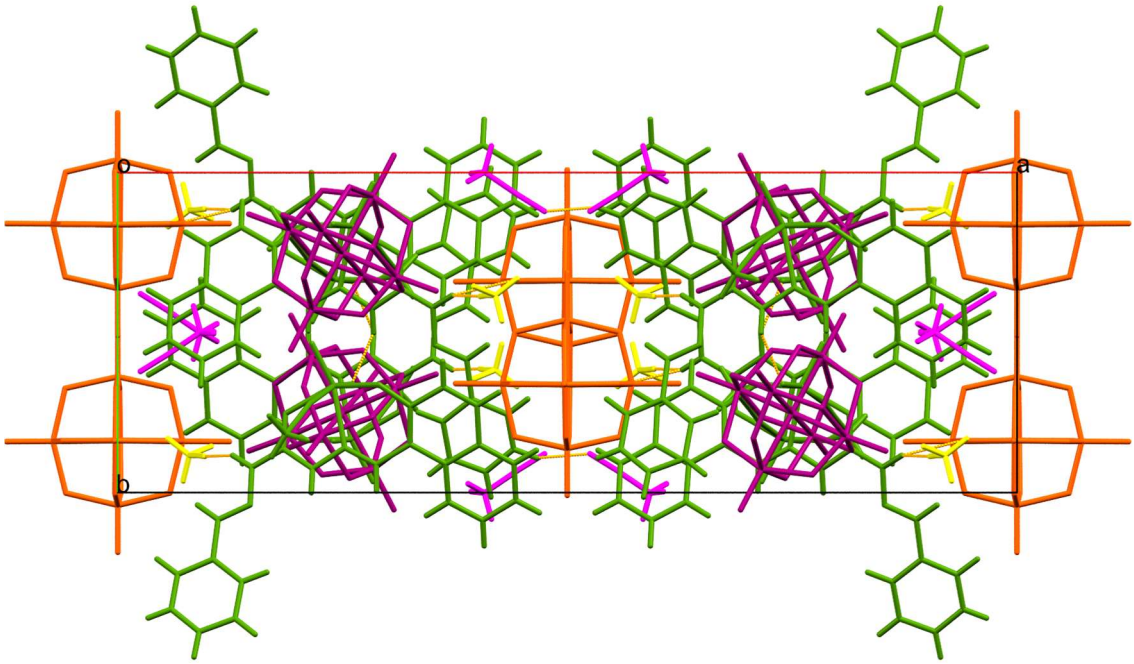

(c)

Figure S25. (a) Mercury-ORTEP view of the asymmetric unit of **[$MoO_2(H_2L^{3pynaph})(CH_3CN)]Mo_6O_{19}\cdot 2CH_3CN$**, along with crystal packing shown down the: (b) *a*-axis; (c) *b*-axis. Hydrogen bonds are presented by orange dashed lines. The species are coloured regarding their symmetry equivalence. Complex dication is coloured green, bonded hexamolybdate anion orange, non-bonded hexamolybdate anion violet, and two

Table S12. Selected bond lengths (in Å) **$[MoO_2(H_2L^{3pynaph})(CH_3CN)]Mo_6O_{19}\cdot 2CH_3CN$**. Atoms are numerated according to Figure S25(a).

Bond	$[MoO_2(H_2L^{3pynaph})(CH_3CN)]Mo_6O_{19}\cdot 2CH_3CN$
Mo1–O1	1.912(11)
Mo1–A6	2.397(11)
Mo1–O2	2.057(9)
Mo1–N1	2.252(8)
Mo1–O3	1.695(7)
Mo1–O4	1.705(7)
N1–N2	1.375(15)
N1–C7	1.294(19)
N2–C8	1.337(18)
N3–N4	1.368(11)
N3–C8	1.338(18)
N4–C9	1.260(19)
O2–C8	1.267(12)

Table S13. Selected bond angles (in °) for **$[MoO_2(H_2L^{3pynaph})(CH_3CN)]Mo_6O_{19}\cdot 2CH_3CN$**. Atoms are numerated according to Figure S25(a).

Angle	$[MoO_2(H_2L^{3pynaph})(CH_3CN)]Mo_6O_{19}\cdot 2CH_3CN$
N1–C7–C1	122.1(10)
O2–C8–N2	121.1(13)
O2–C8–N3	120.6(13)
N2–C8–N3	118.3(9)
N4–C9–C10	119.4(13)
O1–Mo1–O2	149.1(3)
O1–Mo1–A6	80.2(4)
O2–Mo1–O4	94.5(4)
O3–Mo1–O4	105.1(4)
O4–Mo1–A6	87.2(4)
O1–Mo1–O3	99.5(4)
O1–Mo1–N1	79.8(4)
O2–Mo1–A6	79.1(4)
O3–Mo1–A6	167.1(3)
O4–Mo1–N1	158.7(3)
O1–Mo1–O4	107.2(4)

O2–Mo1–O3	95.6(4)
O2–Mo1–N1	72.6(4)
O3–Mo1–N1	93.2(3)
A6–Mo1–N1	74.0(3)
Mo1–N1–N2	111.9(8)
Mo1–N1–C7	128.2(9)
N2–N1–C7	119.9(9)
N1–N2–C8	113.8(9)
N4–N3–C8	118.5(11)
N3–N4–C9	115.5(12)
Mo1–O2–C8	119.7(10)

Table S14. Selected interplanar angles (in °) for **$[MoO_2(H_2L^{3pynaph})(CH_3CN)]Mo_6O_{19}\cdot 2CH_3CN$**. *ar* represents LS plane passing through hydroxyaryl subunit, while *py* represents LS plane passing through pyridyl subunit. L1 represents plane passing through O1, N1 and O2 (chelating atoms). Atoms are numerated according to Figure S25(a).

Interplanar angle	**$[MoO_2(H_2L^{3pynaph})(CH_3CN)]Mo_6O_{19}\cdot 2CH_3CN$**
ar_1–py_1	29.4(6)
L_1–*ar*	15.4(6)
L_1–*py*	27.5(6)
d(Mo–L_1)	0.30(5)

Table S15. The geometry of hydrogen bonds (Å, °) for **$[MoO_2(H_2L^{3pynaph})(CH_3CN)]Mo_6O_{19}\cdot 2CH_3CN$**. Atoms are numerated according to Figure S25(a).

D–H···A	D–H	H···A	D···A	∠D–H···A	Symmetry code
$[MoO_2(H_2L^{3pynaph})(CH_3CN)]Mo_6O_{19}\cdot 2CH_3CN$					
N2–H2···N4	0.88	2.33	2.626(16)	100	
N2–H2···O3	0.88	2.22	2.905(10)	134	3/2–*x*,–1/2+*y*,3/2–*z*
N3–H3···O_b	0.88	2.46	3.060(12)	126	
N3–H3···N7	0.88	2.28	2.96(2)	135	
N5–H5···O_t	0.88	2.38	2.977(13)	125	x,–1+*y*,z
N5–H5···N8	0.88	2.1	2.88(3)	146	x,–1+*y*,z

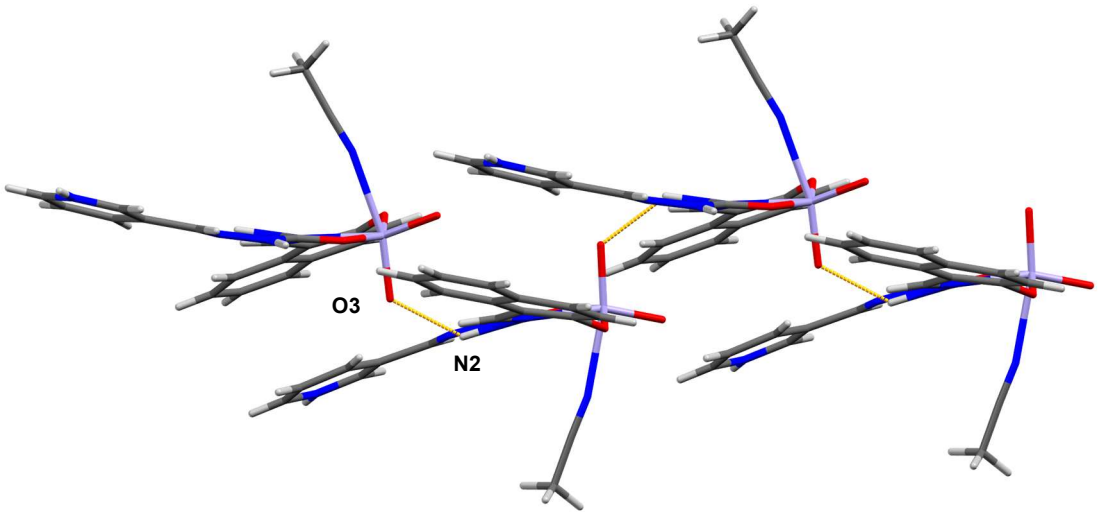

Figure S26. Supramolecular chain formed by dication moieties in the crystal structure of **[$MoO_2(H_2L^{3pynaph})(CH_3CN)]Mo_6O_{19}\cdot 2CH_3CN$**, formed by N2-H2...O3=Mo1 hydrogen bond.

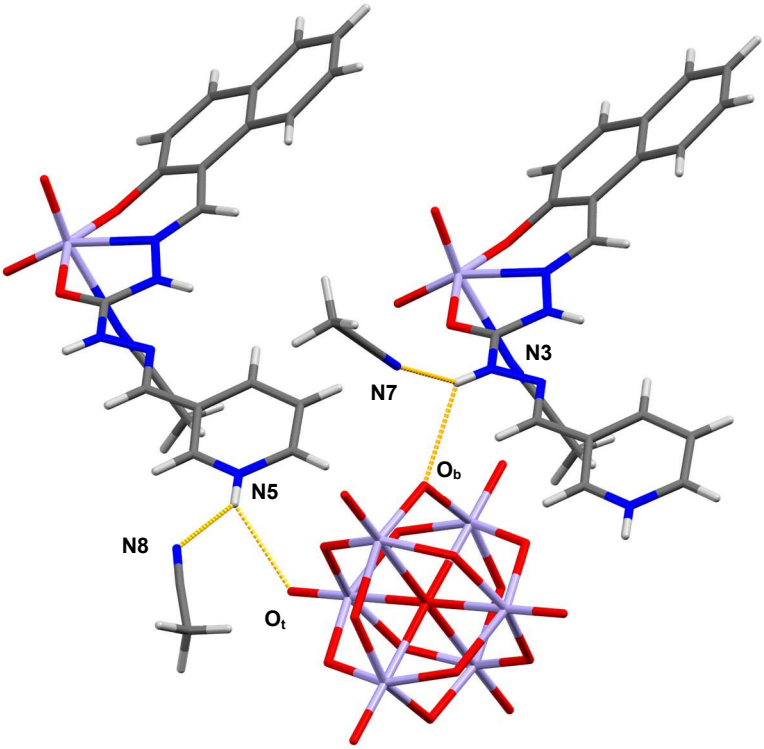

Figure S27. Two three-centred hydrogen bonds formed by acetonitrile nitrogen atoms and hexamolybdate oxygen atoms as hydrogen-bond acceptors, with pyridinium N5-H5 and amine N3-H3 as hydrogen bond donors in the crystal structure of **[$MoO_2(H_2L^{3pynaph})(CH_3CN)]Mo_6O_{19}\cdot 2CH_3CN$**.

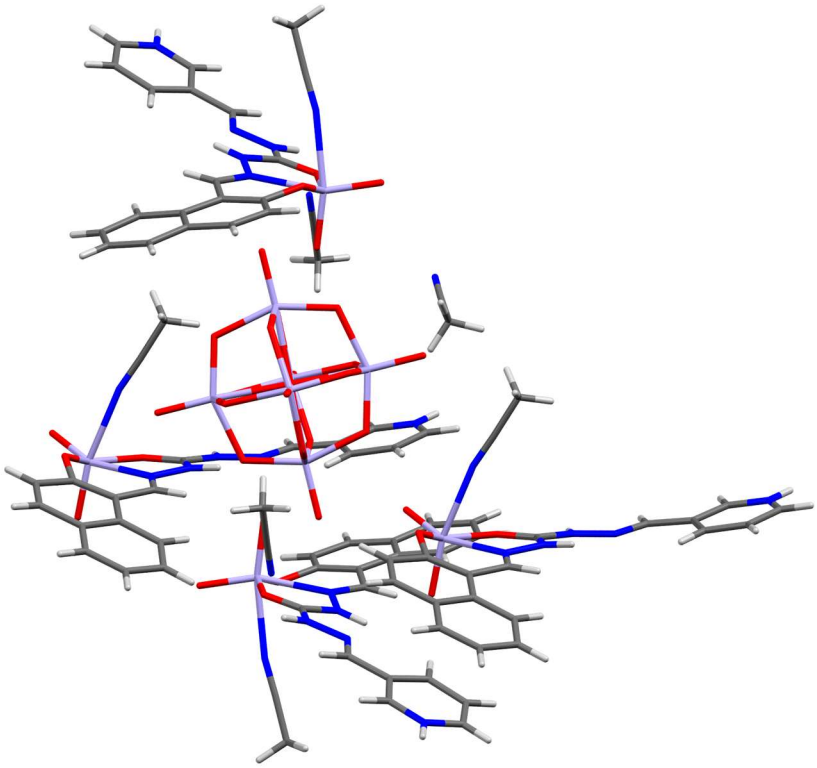

Figure S28. Surroundings of non-bonded hexamolybdate anion in the crystal structure of **$[MoO_2(H_2L^{3pynaph})(CH_3CN)]Mo_6O_{19}\cdot 2CH_3CN$.** Hexamolybdate anion participates only in weak C-H...O contacts.

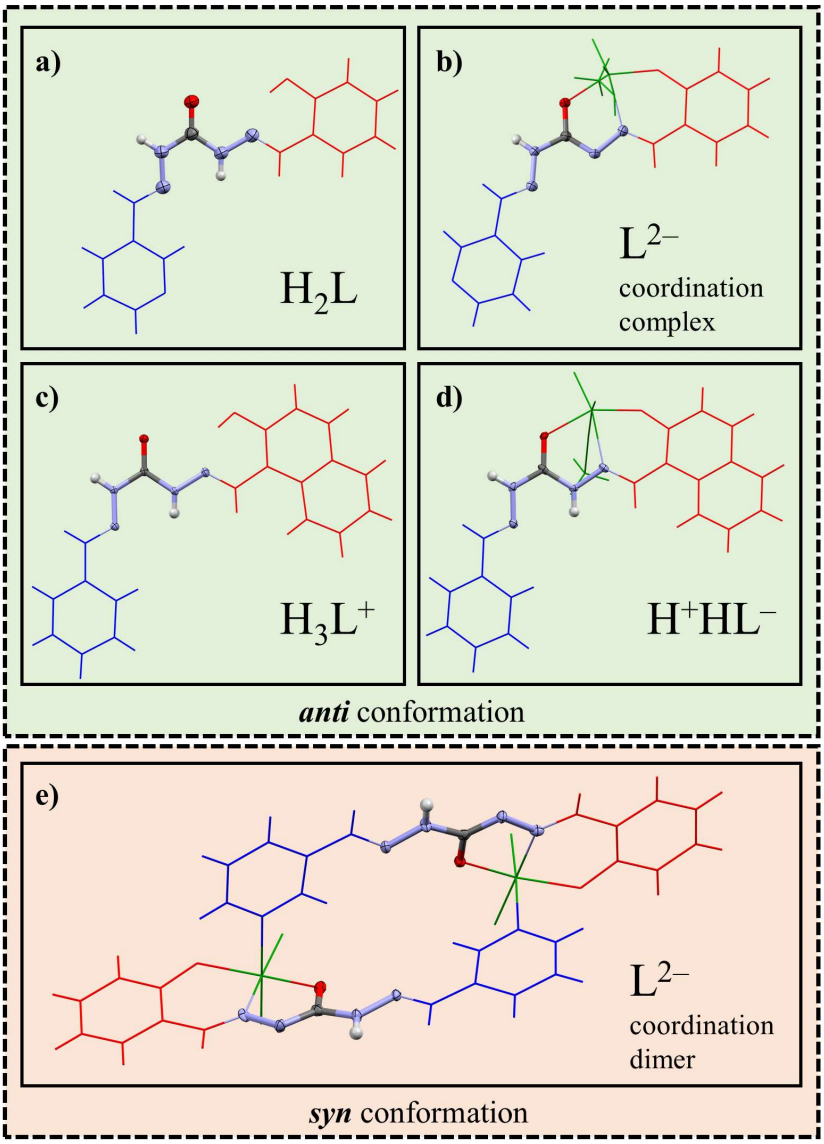

Figure S29. Conformation of the ligand in (a) neutral form (as found in **H_2L^{3pysal}**, **$H_2L^{3pysal}\cdot H_2O$**, **H_2L^{4pysal}**, **$H_2L^{3pynaph}\cdot 0.5H_2O$** and **$H_2L^{3pynaph}\cdot 0.5CH_3OH$**), (b) doubly deprotonated form as the part of monomeric coordination complex (as found in **$[MoO_2(L^{3pysal})(CH_3OH)]$**), (c) protonated form (as found in **$(H_3L^{4pysal})_2Mo_6O_{19}$**, **$(H_3L^{3pynaph})_2Mo_6O_{19}\cdot 2H_2O$** and **$(H_3L^{4pynaph})_2Mo_6O_{19}$**), (d) zwitterionic form as the part of monomeric coordination complex (as found in **$[MoO_2(H_2L^{3pynaph})(CH_3CN)][Mo_6O_{19}\cdot 2CH_3CN$**) and (e) doubly deprotonated form as the part of coordination dimer (as found in **$[MoO_2(L^{3pysal})]_2\cdot 2CH_3CN$**). It can be concluded that prepared ligands exist in predominately *anti* conformation, except where coordination imposes the *syn* conformation.

Table S16. Comparison of bond lengths in central carbohydrazide fragment for four distinct forms of the ligand. While neutral, protonated and zwitterionic form of ligand exhibit keto-amino tautomeric form, doubly deprotonated form expectedly takes the enol-imino form.

Bond length (Å)	**$[MoO_2(L^{3pysal})(MeOH)]$ L^{2-}**	**$H_2L^{3pysal}\cdot H_2O$ H_2L**	**$(H_3L^{3pynaph})_2Mo_6O_{19}\cdot 2(H_2O)$ H_3L^+**	**$[MoO_2(H_2L^{3py\text{-}naph})(MeCN)]Mo_6O_{19}\cdot 2(MeCN)$ H^+HL^-**
N1–N2	1.402(4)	1.377(3)	1.362(3)	1.375(15) –
N2–C8	1.315(5)	1.348(3)	1.371(4)	1.337(18) –/=
C8–O2	1.306(4)	1.246(2)	1.222(4)	1.267(12) –/=
C8–N3	1.343(4)	1.357(3)	1.367(3)	1.338(18) –/=
N3–N4	1.369(4)	1.380(3)	1.361(3)	1.368(11) –
Tautomeric form	enol-imino	keto-amino	keto-amino	keto-amino

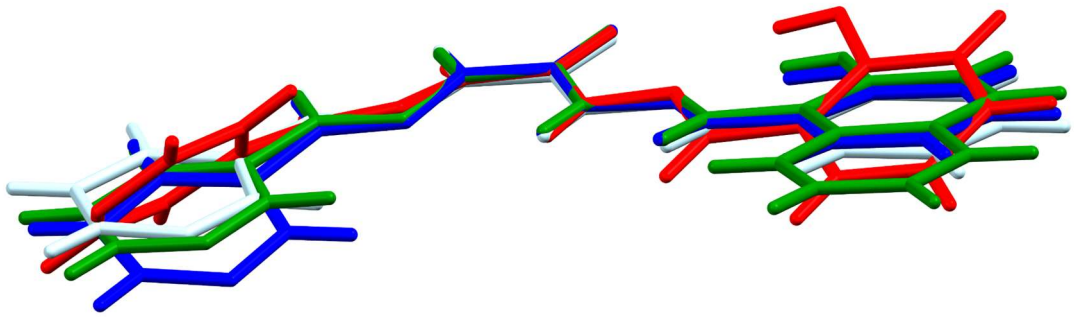

(a)

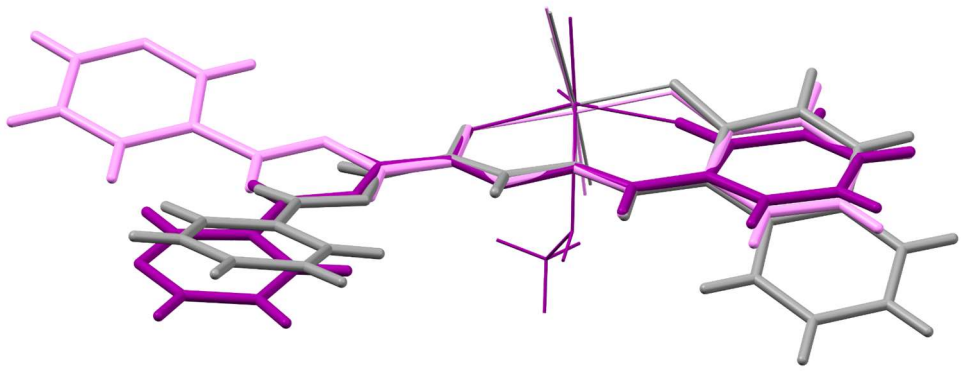

(b)

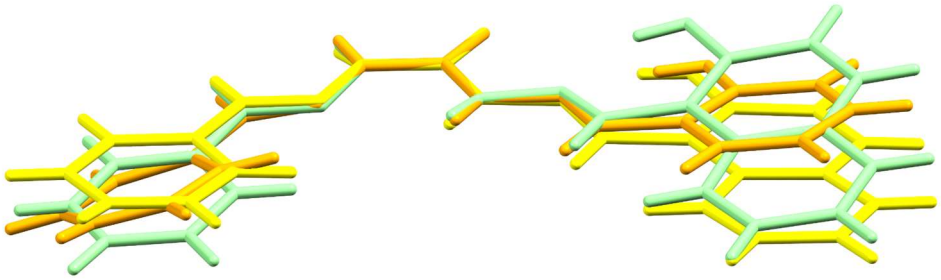

(c)

Figure S30. Overlay of ligand molecule in a) $\mathbf{H_2L^{3pysal}}$ (blue), $\mathbf{H_2L^{3pysal}}\cdot H_2O$ (light blue), $\mathbf{H_2L^{3pynaph}\cdot 0.5CH_3OH}$ (green) and $\mathbf{H_2L^{4pysal}}$ (red); (b) $\mathbf{[MoO_2(L^{3pysal})(CH_3OH)]}$ (purple), $\mathbf{[MoO_2(L^{3pysal})]_2\cdot 2CH_3CN}$ (pink), $\mathbf{[MoO_2(H_2L^{3pynaph})(CH_3CN)]Mo_6O_{19}\cdot 2CH_3CN}$ (gray) and (c) $\mathbf{(H_3L^{4pysal})_2Mo_6O_{19}}$ (orange), $\mathbf{(H_3L^{4pynaph})_2Mo_6O_{19}}$ (yellow), $\mathbf{(H_3L^{3pynaph})_2Mo_6O_{19}\cdot 2H_2O}$ (light green). It can be concluded that the ligand molecule does not significantly deviate from planarity, except in $\mathbf{H_2L^{4pysal}}$, where the ring tilt enables the existence of a supramolecular homosynthon.

Thermal analysis and transformations

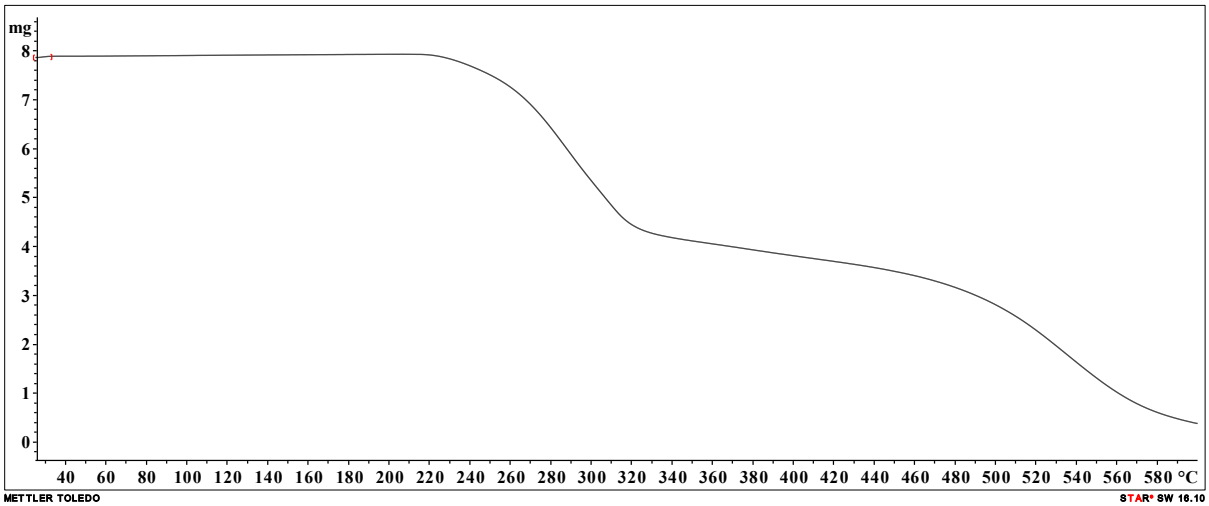

Figure S31. Thermogram of $\mathbf{H_2L^{3pysal}}$.

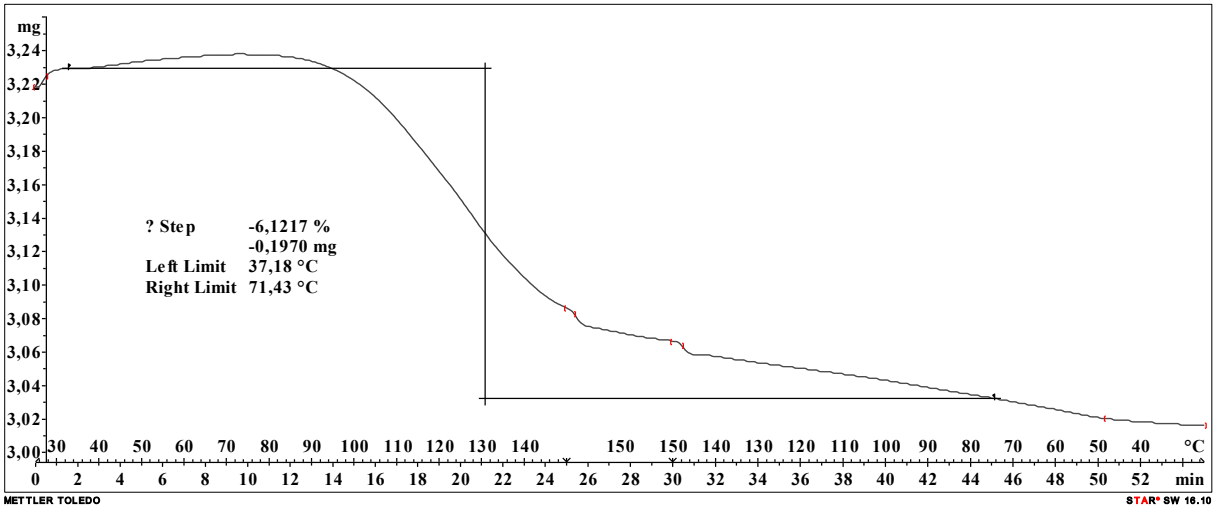

Figure S32. Thermogram of $\mathbf{H_2L^{3pysal}{\cdot}H_2O}$.

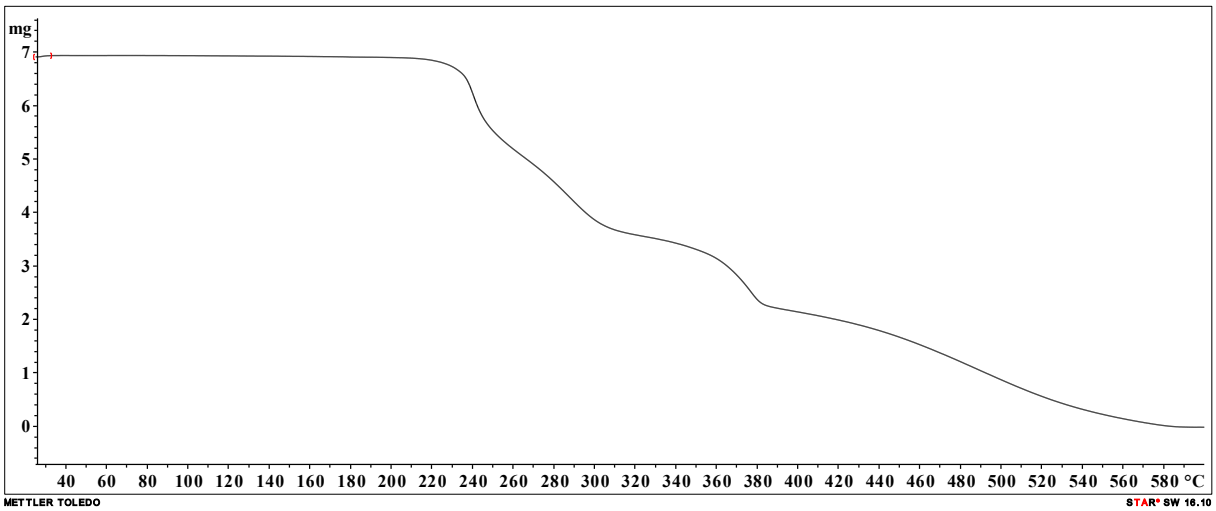

Figure S33. Thermogram of $\mathbf{H_2L^{4pysal}}$.

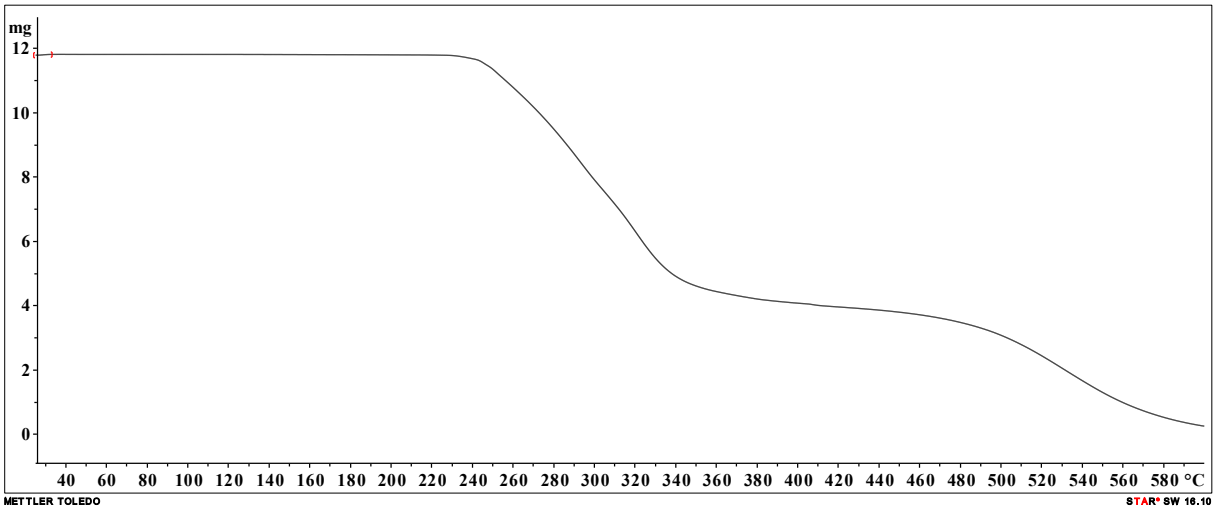

Figure S34. Thermogram of $\mathbf{H_2L^{3pynaph}}$.

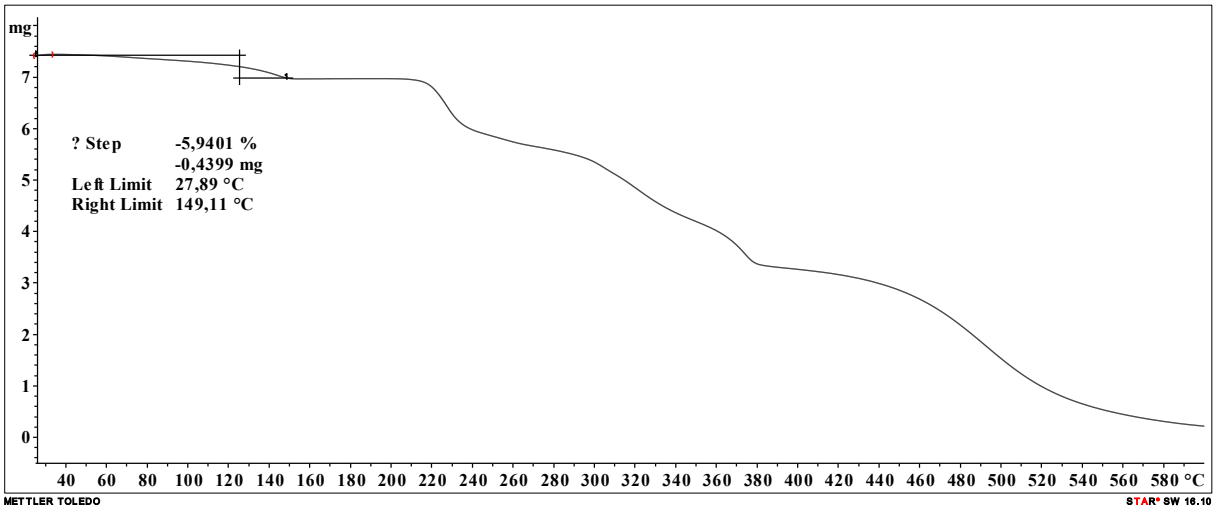

Figure S35. Thermogram of $\mathbf{H_2L^{4pynaph}\cdot H_2O}$.

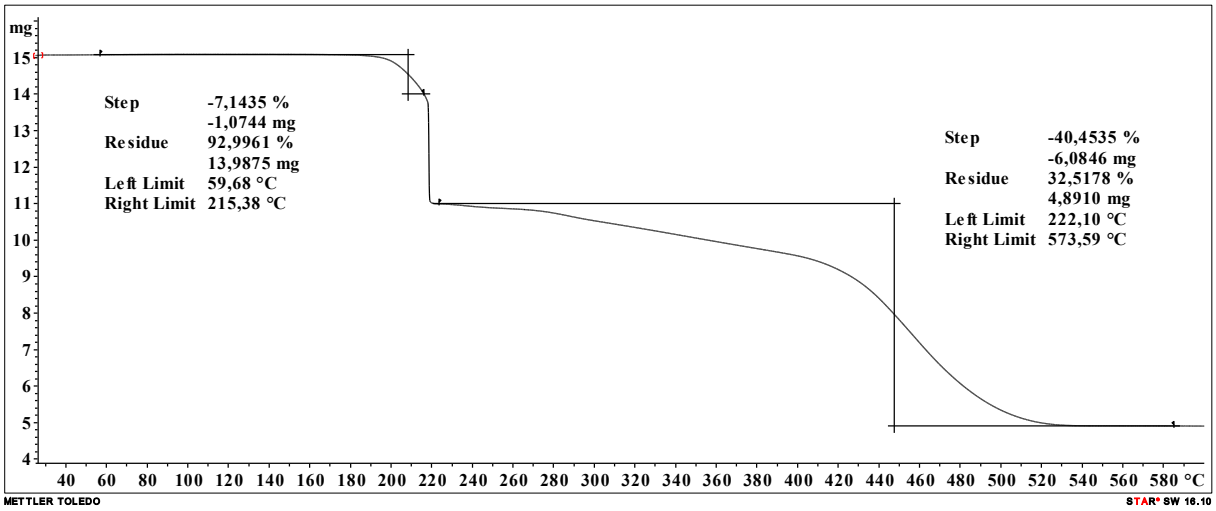

Figure S36. Thermogram of $\mathbf{[MoO_2(L^{3pysal})(CH_3OH)]}$.

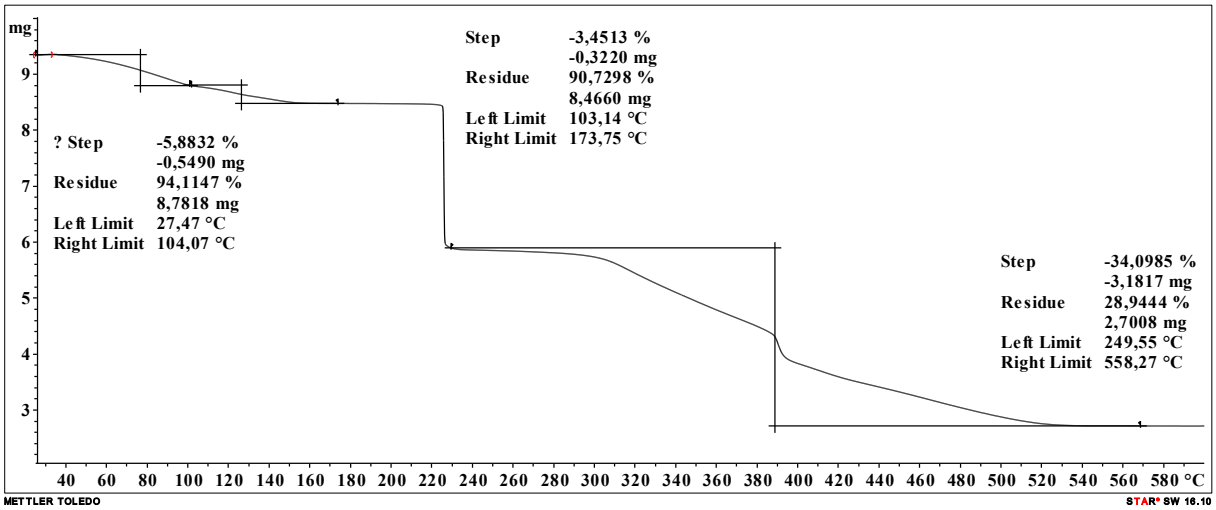

Figure S37. Thermogram of **[$MoO_2(L^{4pysal})(H_2O)]\cdot CH_3OH$**.

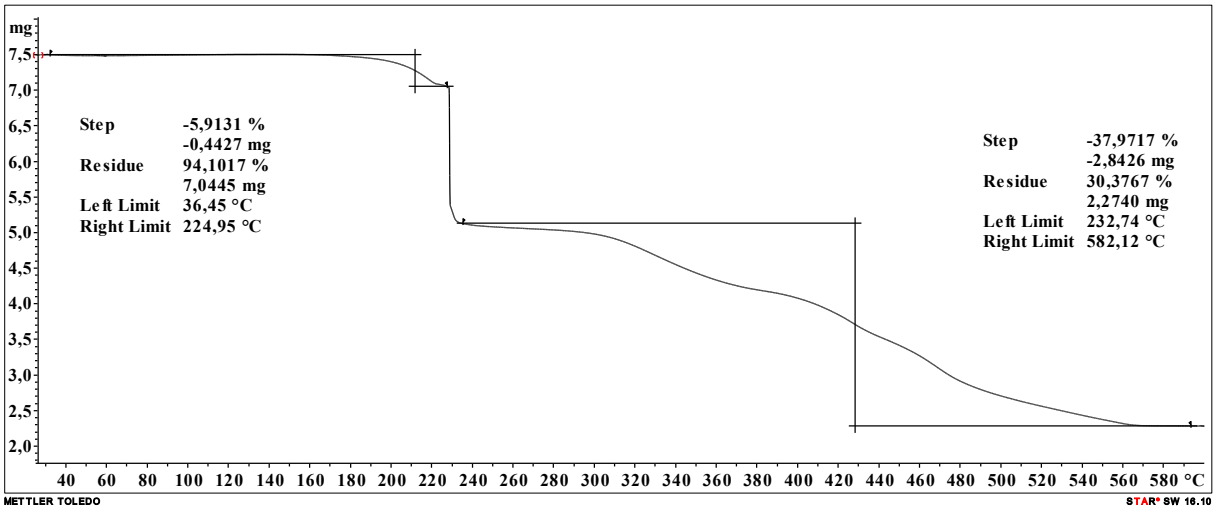

Figure S38. Thermogram of **[$MoO_2(L^{3pynaph})(CH_3OH)$]**.

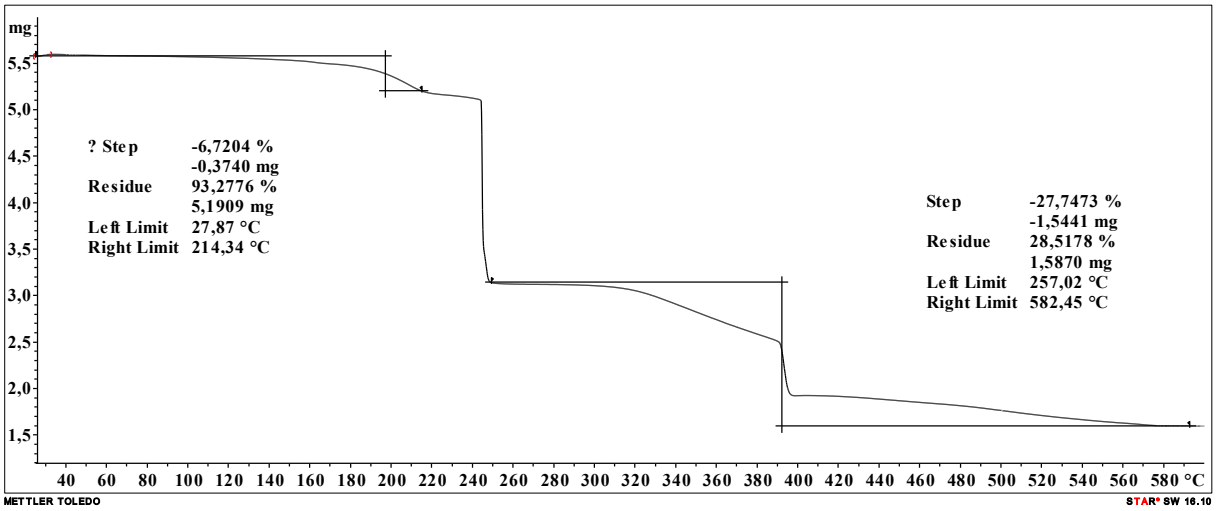

Figure S39. Thermogram of **[$MoO_2(L^{4pynaph})(CH_3OH)$]**

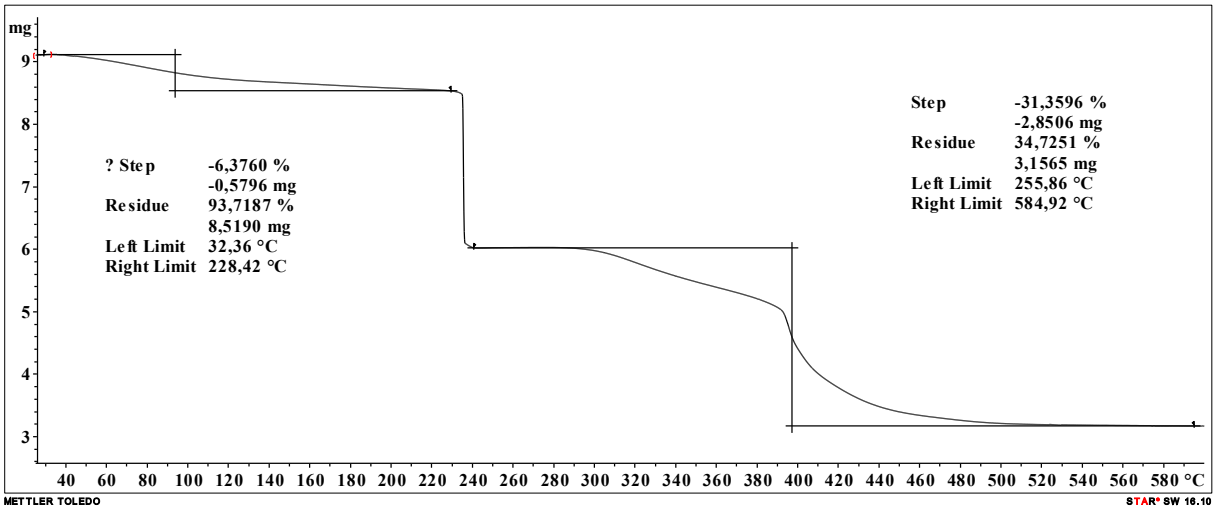

Figure S40. Thermogram of **[$MoO_2(L^{3pysal})]_2 \cdot xCH_3CN$**.

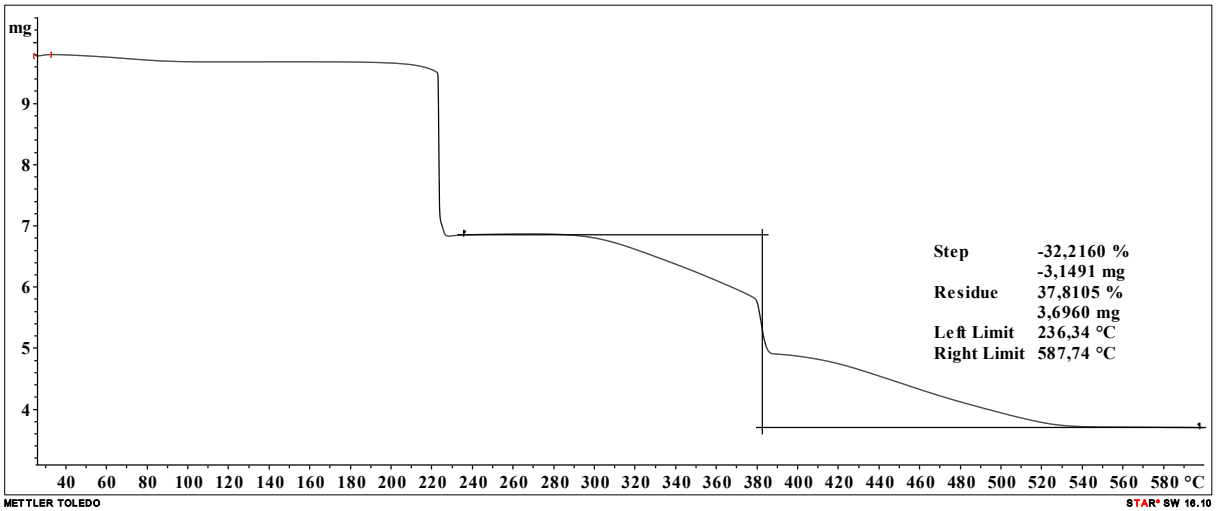

Figure S41. Thermogram of **[$MoO_2(L^{4pysal})]_2$**.

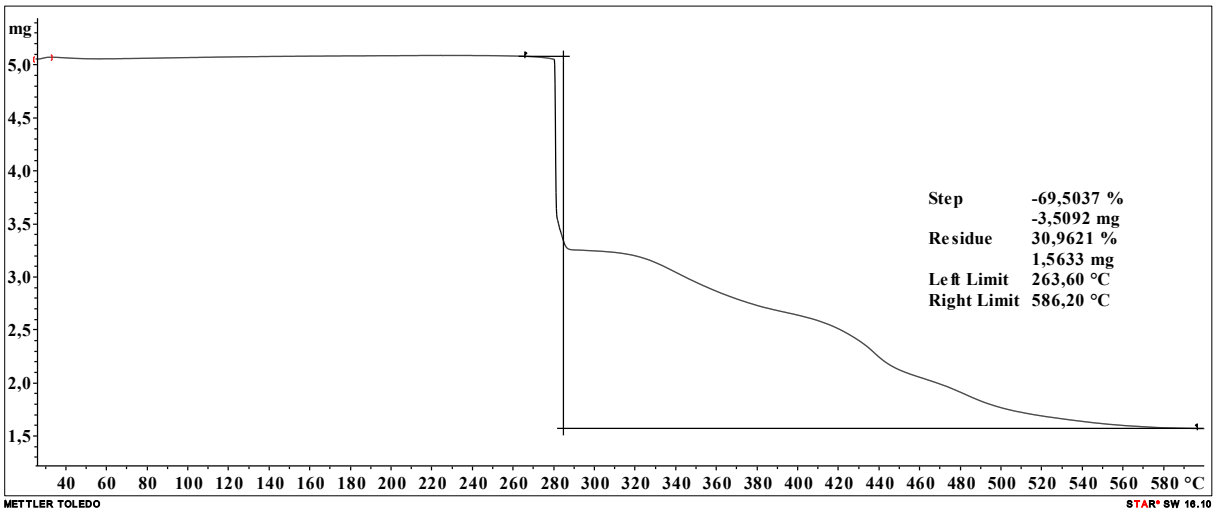

Figure S42. Thermogram of **[$MoO_2(L^{3pynaph})]_2$.**

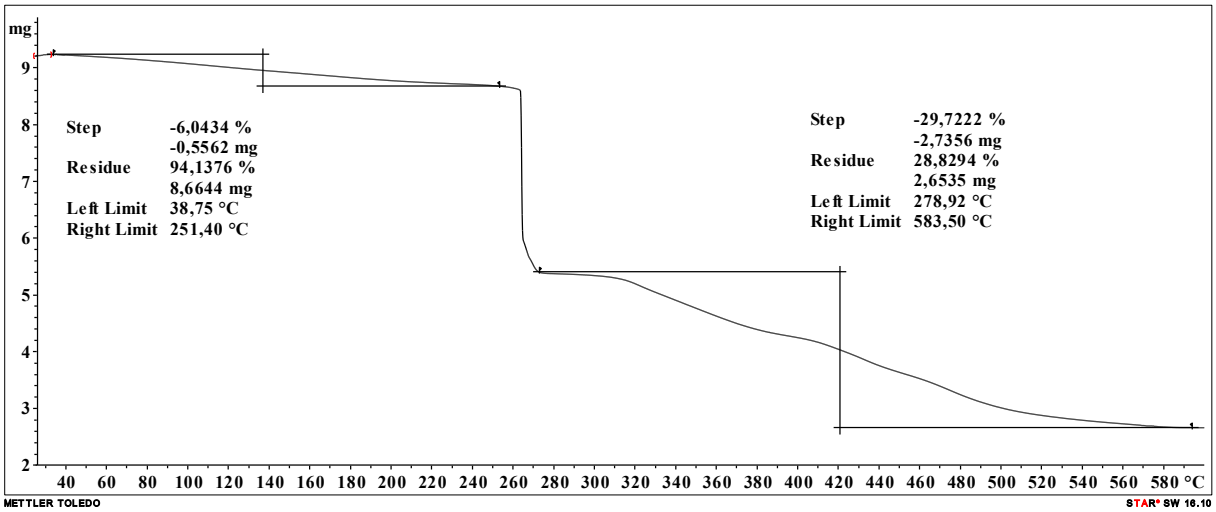

Figure S43. Thermogram of **$[MoO_2(L^{4pynaph})]_n \cdot xnCH_3CN$**.

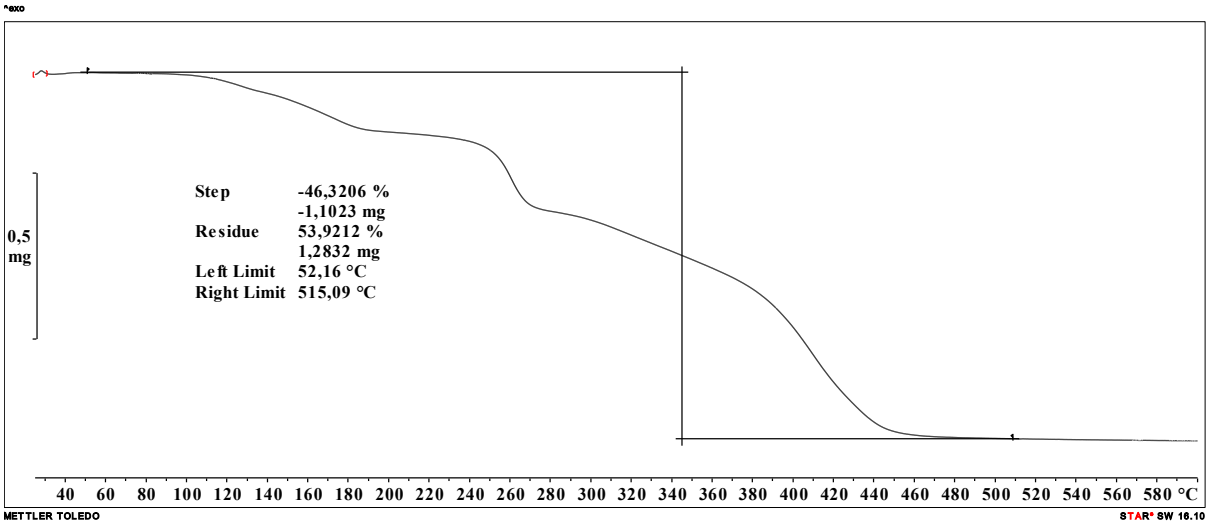

Figure S44. Thermogram of **$(H_3L^{4pysal})_2Mo_6O_{19}$**.

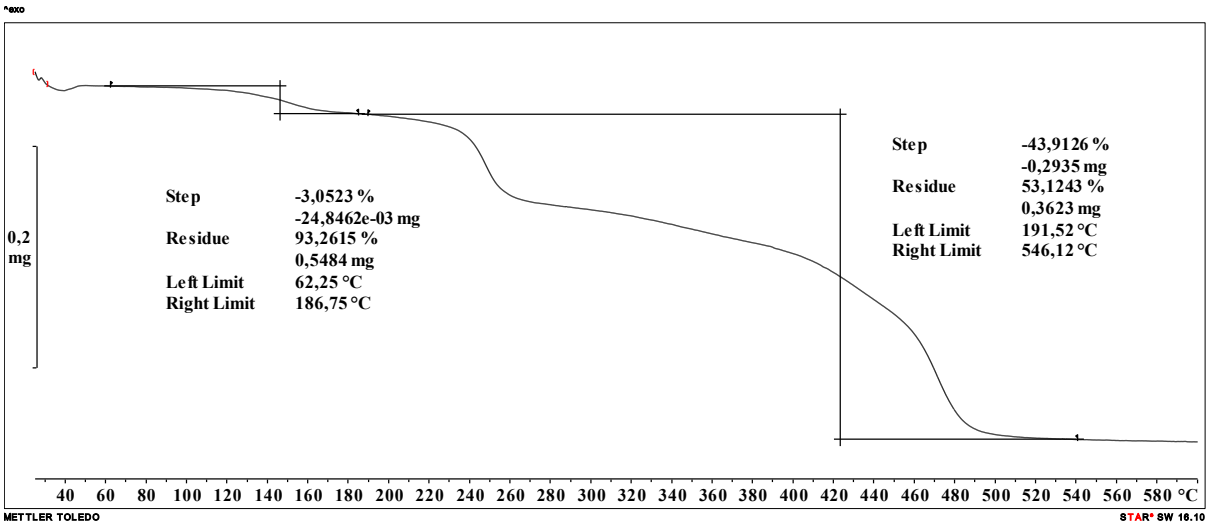

Figure S45. Thermogram of **$(H_3L^{3pynaph})_2Mo_6O_{19} \cdot 2H_2O$**.

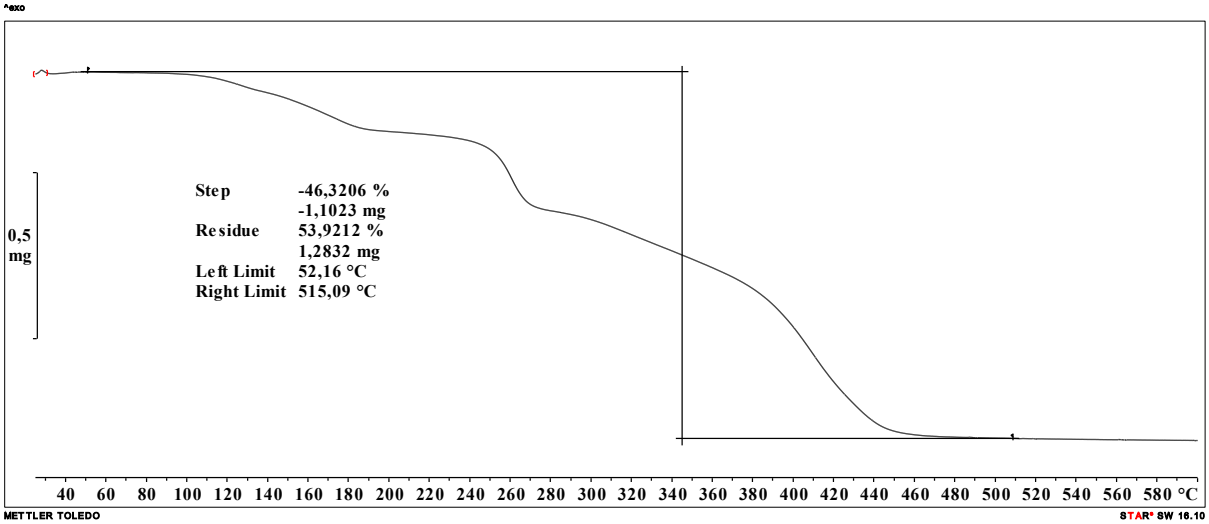

Figure S46. Thermogram of $(H_3L^{4pynaph})_2Mo_6O_{19}$.

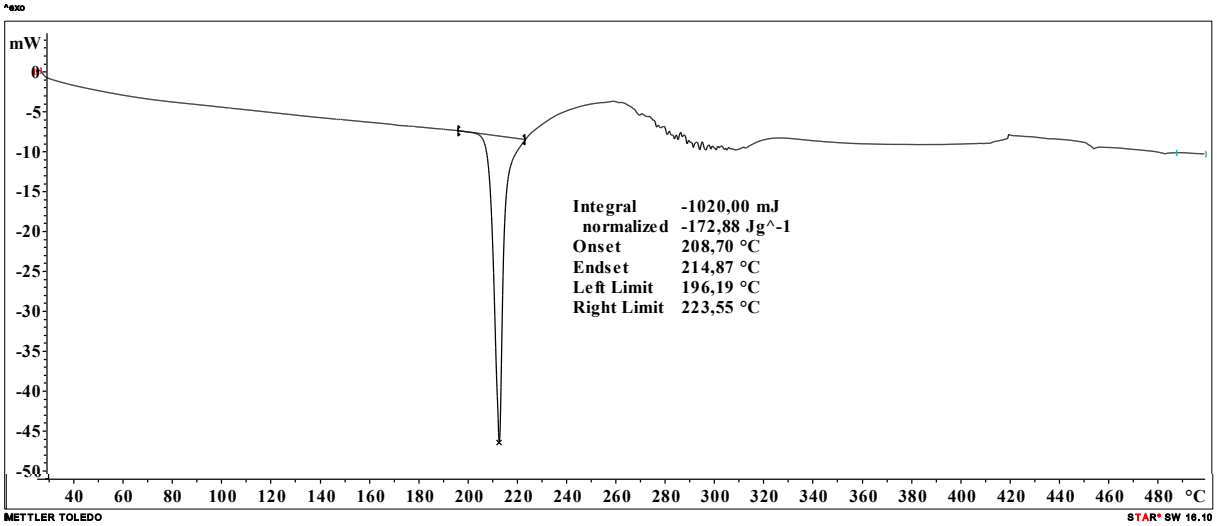

Figure S47. DSC curve of H_2L^{3pysal}.

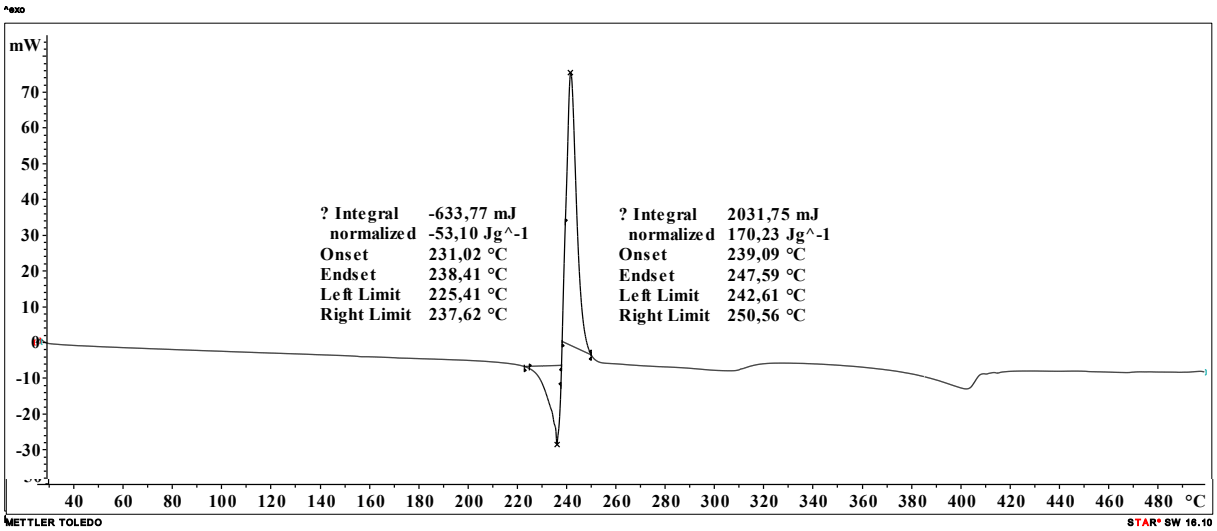

Figure S48. DSC curve of H_2L^{4pysal}.

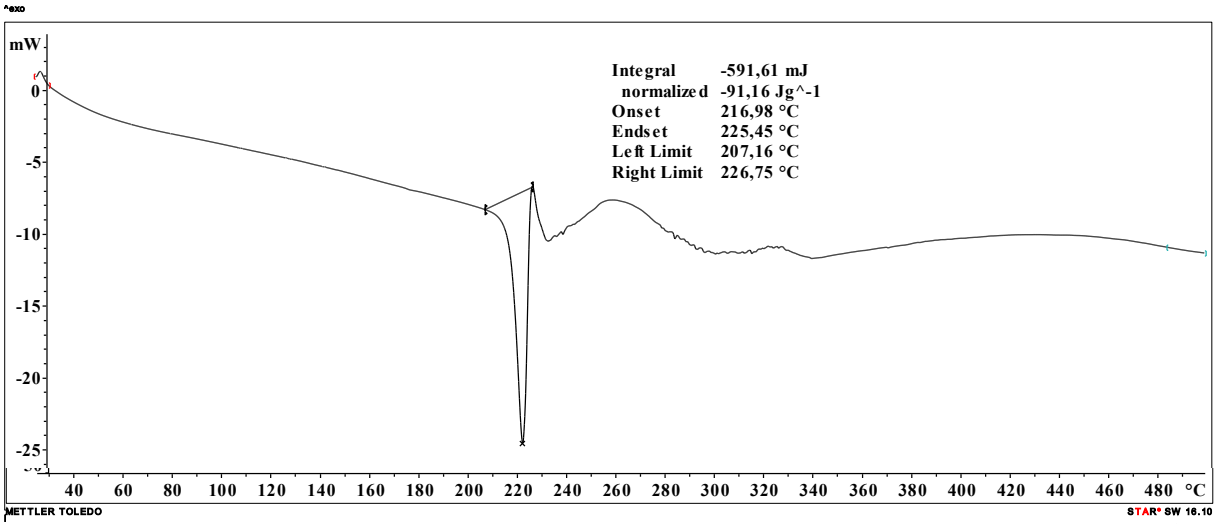

Figure S49. DSC curve of $H_2L^{3pynaph}$.

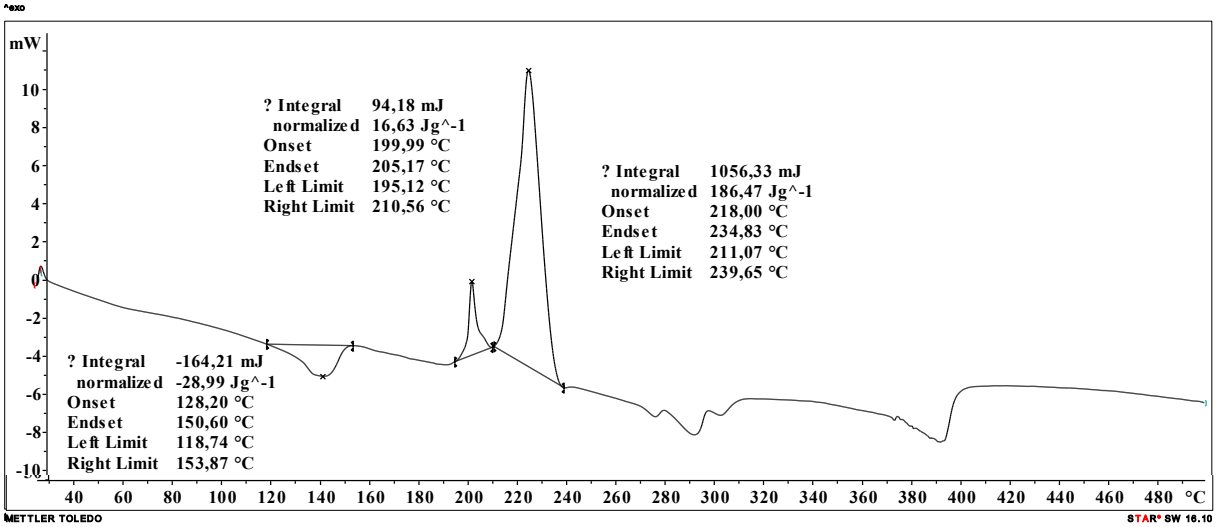

Figure S50. DSC curve of $\mathbf{H_2L^{4pynaph}}$.

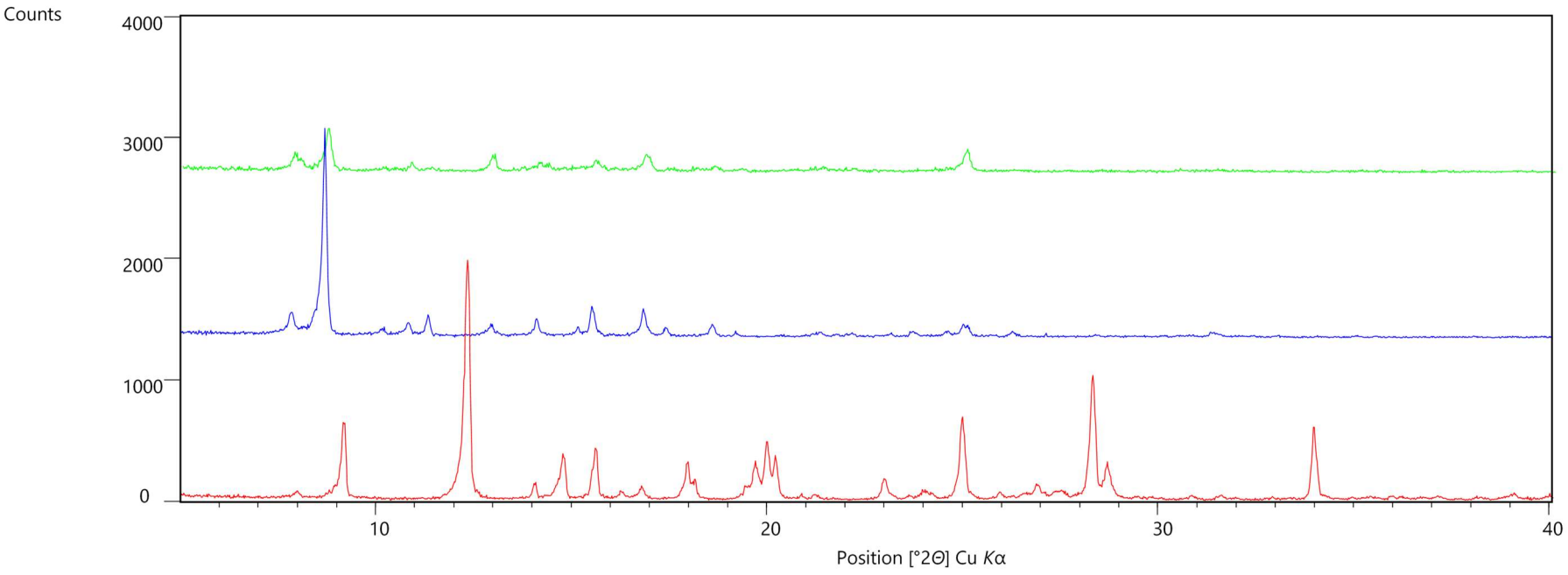

Figure S51. PXRD patterns of [**$MoO_2(L^{3pysal})(CH_3OH)$**] (red), **$[MoO_2(L^{3pysal})]_2$** (blue) and sample obtained by conversion of [**$MoO_2(L^{3pysal})(CH_3OH)$**] in acetonitrile (green).

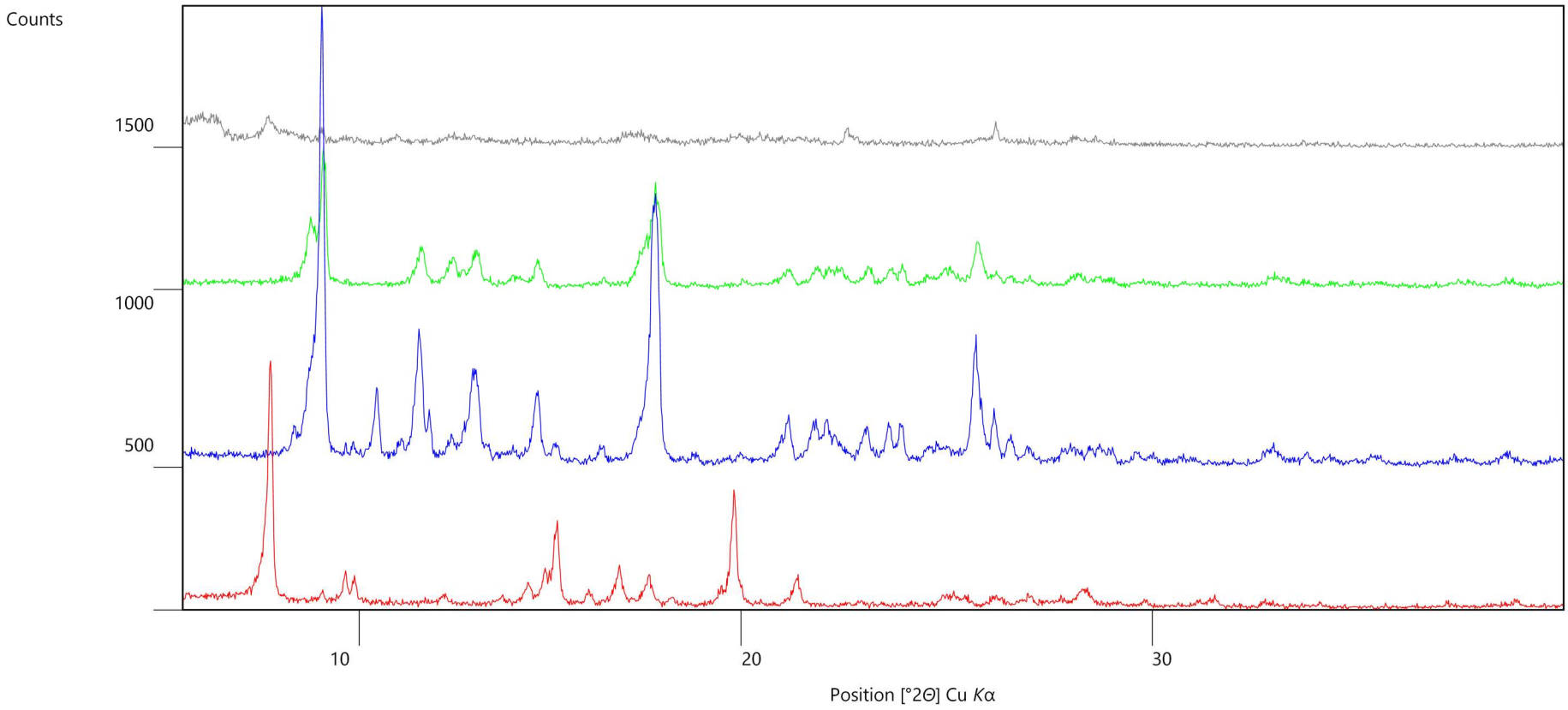

Figure S52. PXRD patterns of **[$MoO_2(L^{4pysal})(H_2O)]\cdot CH_3OH$** (red), **[$MoO_2(L^{4pysal})]_n$** (blue), the sample obtained by conversion of **[$MoO_2(L^{4pysal})(H_2O)]\cdot CH_3OH$** in acetonitrile (green line) and the sample obtained from **[$MoO_2(L^{4pysal})(H_2O)]\cdot CH_3OH$** heated from the ambient temperature up to 170°C (grey).

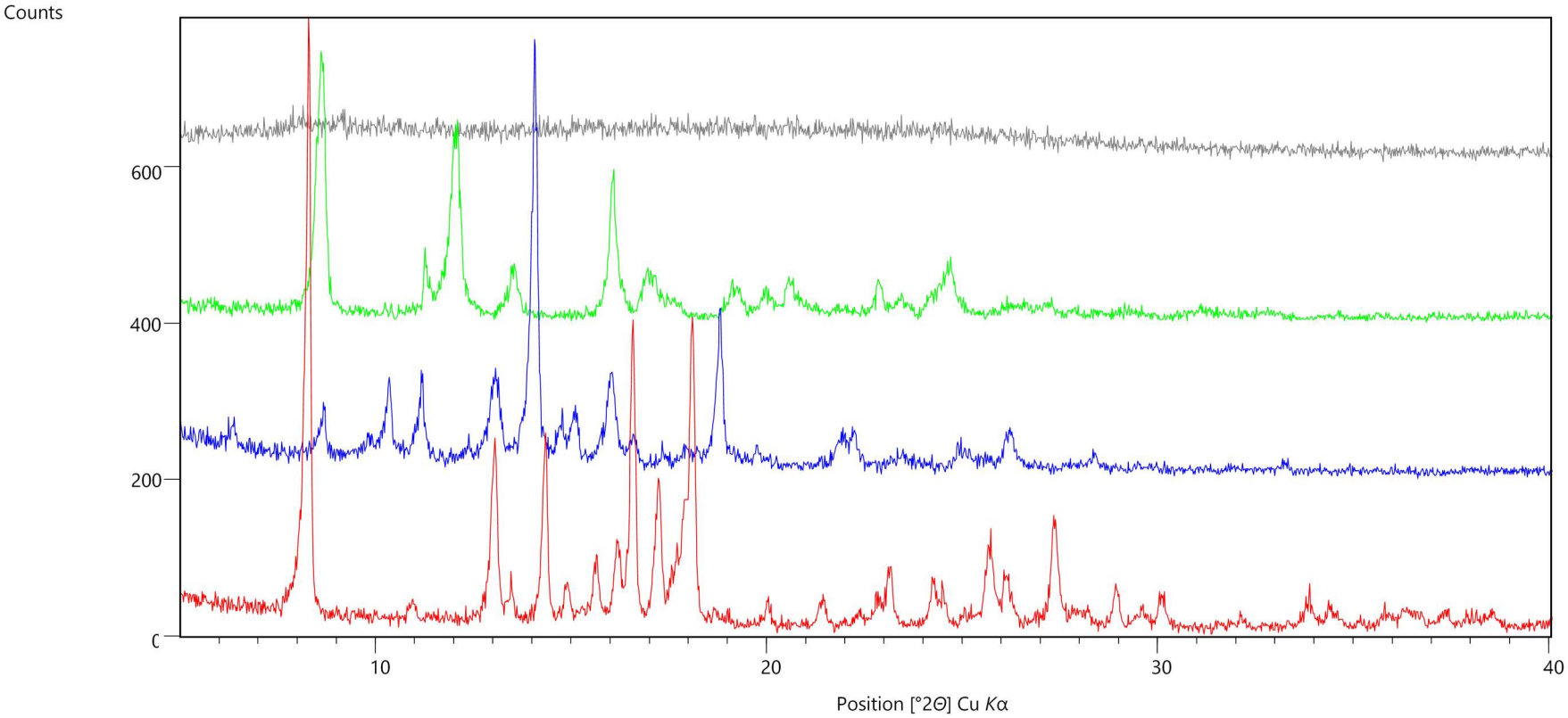

Figure S53. PXRD patterns of **[$MoO_2(L^{3pynaph})(CH_3OH)$]** (red), **[$MoO_2(L^{3pynaph})]_n$** (blue), the sample obtained by conversion of **[$MoO_2(L^{3pynaph})(CH_3OH)$]** in acetonitrile (green line) and the sample obtained from **[$MoO_2(L^{3pynaph})(CH_3OH)$]** heated from the ambient temperature up to 220°C (grey).

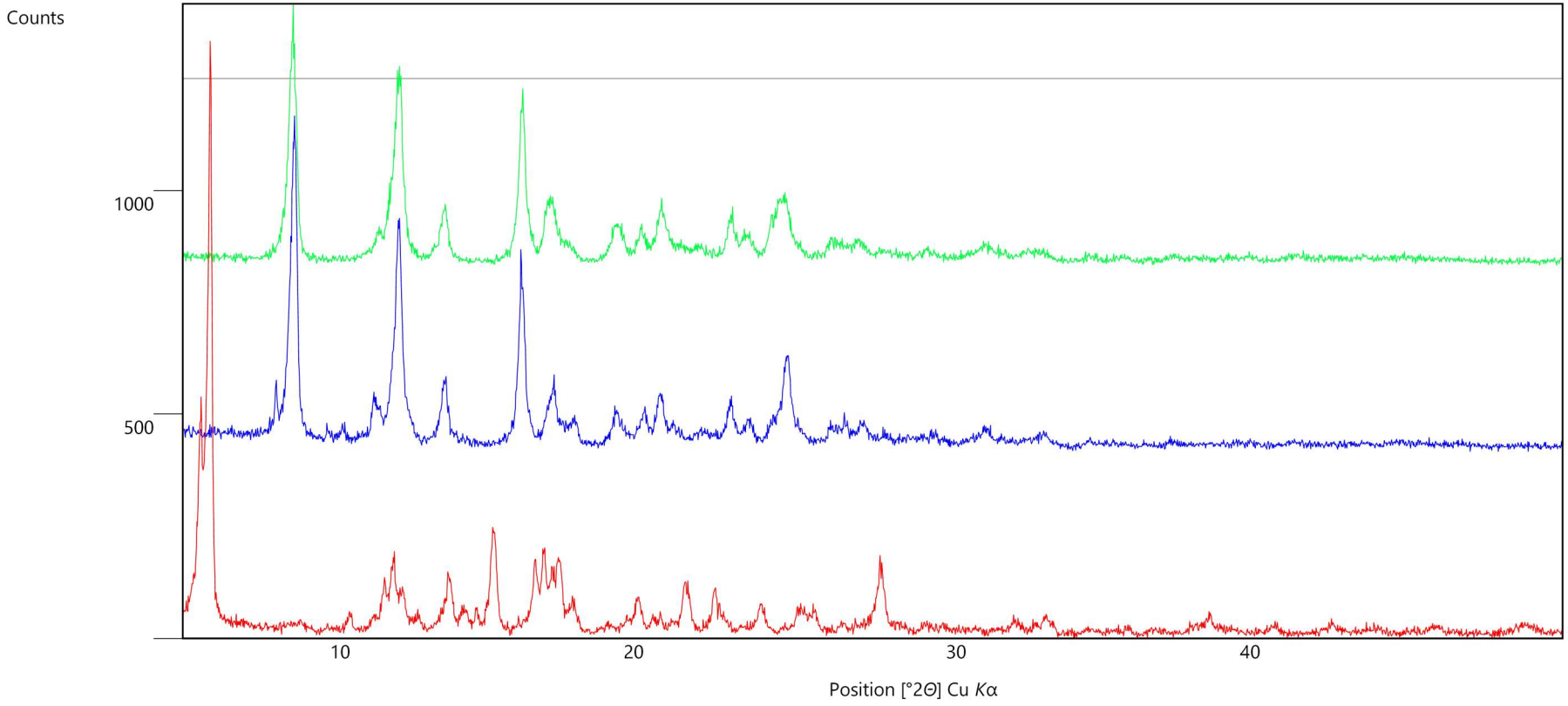

Figure S54. PXRD patterns of **[$MoO_2(L^{4pynaph})(CH_3OH)$]** (red), **[$MoO_2(L^{4pynaph})]_n \cdot xnCH_3CN$** (blue line), the sample obtained by conversion of **[$MoO_2(L^{4pynaph})(CH_3OH)$]** in acetonitrile (green) and the sample obtained from **[$MoO_2(L^{4pynaph})(CH_3OH)$]** heated from the ambient temperature up to 215°C (grey).

FTIR and NMR spectroscopy

Table S17. ^{1}H and ^{13}C chemical shifts for neutral ligands in DMSO–d_6 at 298 K, with atom numbering according to Figures S55 and S56.

	H_2L^{3pysal}		H_2L^{4pysal}		$H_2L^{3pynaph}$		$H_2L^{4pynaph}$	
atom(s)	δ(^{1}H)	δ(^{13}C)	δ(^{1}H)	δ(^{13}C)	δ(^{1}H)	δ(^{13}C)	δ(^{1}H)	δ(^{13}C)
C1		119.5		120.3		128.3		128.3
C2-O1-H1	11.1	157.2	11.2	157.3	12.8	157.8	12.7	157.8
C3-H3	6.9	116.7	6.9	116.7	7.2	119.4	7.2	119.4
C4-H4	7.3	131.1	7.3	131.1	7.9	133.8	7.9	132.4
C5-H5	6.9	119.7	6.9	119.7		132.1		132.0
C6-H6	7.5	129.3	7.6	129.3		132.3		132.2
C7-H7	8.6	146.0	8.6	146.1	9.5	145.0	9.5	145.3
C8		152.3		152.3		152.1		152.0
C9-H9	8.1	139.7	8.0	139.8	8.0	139.5	8.0	139.8
C10		130.8		142.1		130.7		142.0
C11-H11	9.0	148.9	7.8	121.3	9.1	148.9	7.8	121.4
C12-H12	8.3	150.5	8.6	150.2	8.6	150.6	8.7	150.6
C13-H13	7.5	124.2	8.6	150.2	7.5	124.2	8.7	150.6
C14-H14	8.2	134.1	7.8	121.3	8.3	134.2	7.8	121.4
C15-H15					7.9	129.4	7.9	129.4
C16-H16					7.4	123.9	7.4	123.9
C17-H17					7.6	127.9	7.6	128.0
C18-H18					8.2	121.2	8.3	121.2
N2-H2	10.9		11.0		11.2		11.4	
N3-H3	11.1		10.9		11.0		11.0	

Table S18. ^{1}H and ^{13}C chemical shifts for complexes in DMSO–d_6 at 298 K, with atom numbering according to Figures S57 and S58.

	[$MoO_2(L^{3pysal})$]		**[$MoO_2(L^{4pysal})$]**		**[$MoO_2(L^{3pynaph})$]**		**[$MoO_2(L^{4pynaph})$]**	
atom(s)	δ(^{1}H)	δ(^{13}C)	δ(^{1}H)	δ(^{13}C)	δ(^{1}H)	δ(^{13}C)	δ(^{1}H)	δ(^{13}C)
C1		121.8		121.7		113.1		113.0
C2		158.6		158.7		159.0		159.1
C3-H3	6.9	118.5	6.9	118.5	7.2	120.4	7.2	120.4
C4-H4	7.4	133.2	7.4	133.4	8.0	133.9	8.0	134.1
C5-H5	7.1	122.1	7.1	122.2		132.3		132.3
C6-H6	7.6	133.3	7.6	127.9		129.5		129.5
C7-H7	8.6	148.4	8.6	148.9	9.4	144.6	9.4	145.2
C8		164.6		164.5		164.3		164.2
C9-H9	8.1	141.3	8.0	141.5	8.2	141.6	8.1	141.6
C10		130.9		142.3		130.9		142.7
C11-H11	8.8	148.6	7.6	121.0	8.8	148.6	7.7	121.2
C12-H12	8.6	150.5	8.6	150.5	8.6	150.5	8.7	150.1
C13-H13	7.5	124.5	8.6	150.5	7.5	124.5	8.7	150.1
C14-H14	8.1	133.5	7.6	121.0	8.1	133.6	7.7	121.2
C15-H15					7.9	129.3	7.9	129.3
C16-H16					7.5	125.0	7.5	125.1
C17-H17					7.6	128.5	7.6	128.6
C18-H18					8.5	122.2	8.5	122.2
N3-H3	11.5		11.7		11.5		11.7	

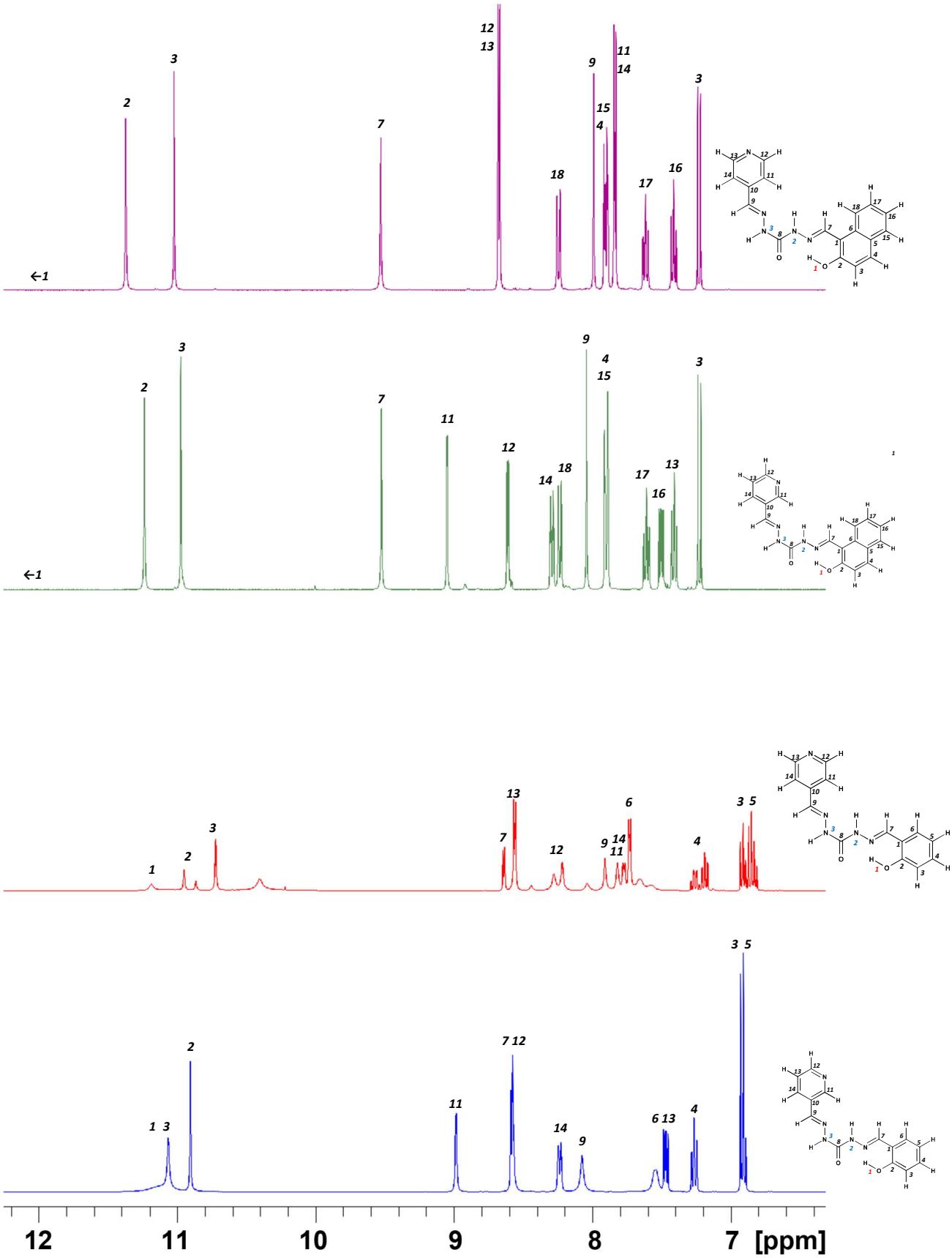

Figure S55. A portion of the ^{1}H NMR spectra of (from bottom to top): $\mathbf{H_2L^{3pysal}}$, $\mathbf{H_2L^{4pysal}}$, $\mathbf{H_2L^{3pynaph}}$ and $\mathbf{H_2L^{4pynaph}}$ in DMSO–d_6 at 298 K.

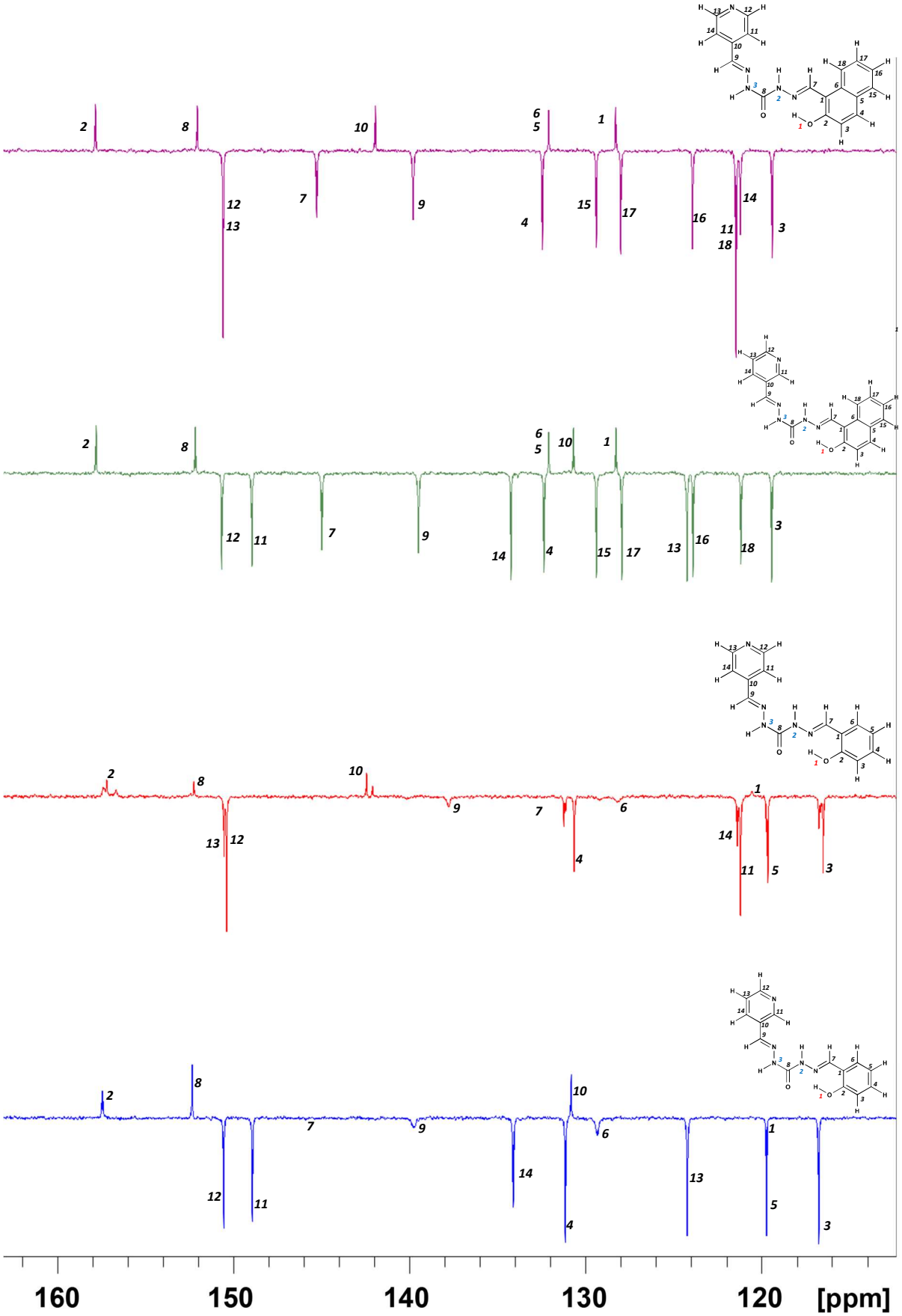

Figure S56. A portion of the DEPTQ ^{13}C NMR spectra of (from bottom to top): $\mathbf{H_2L^{3pysal}}$, $\mathbf{H_2L^{4pysal}}$, $\mathbf{H_2L^{3pynaph}}$ and $\mathbf{H_2L^{4pynaph}}$ in DMSO–d_6 at 298 K.

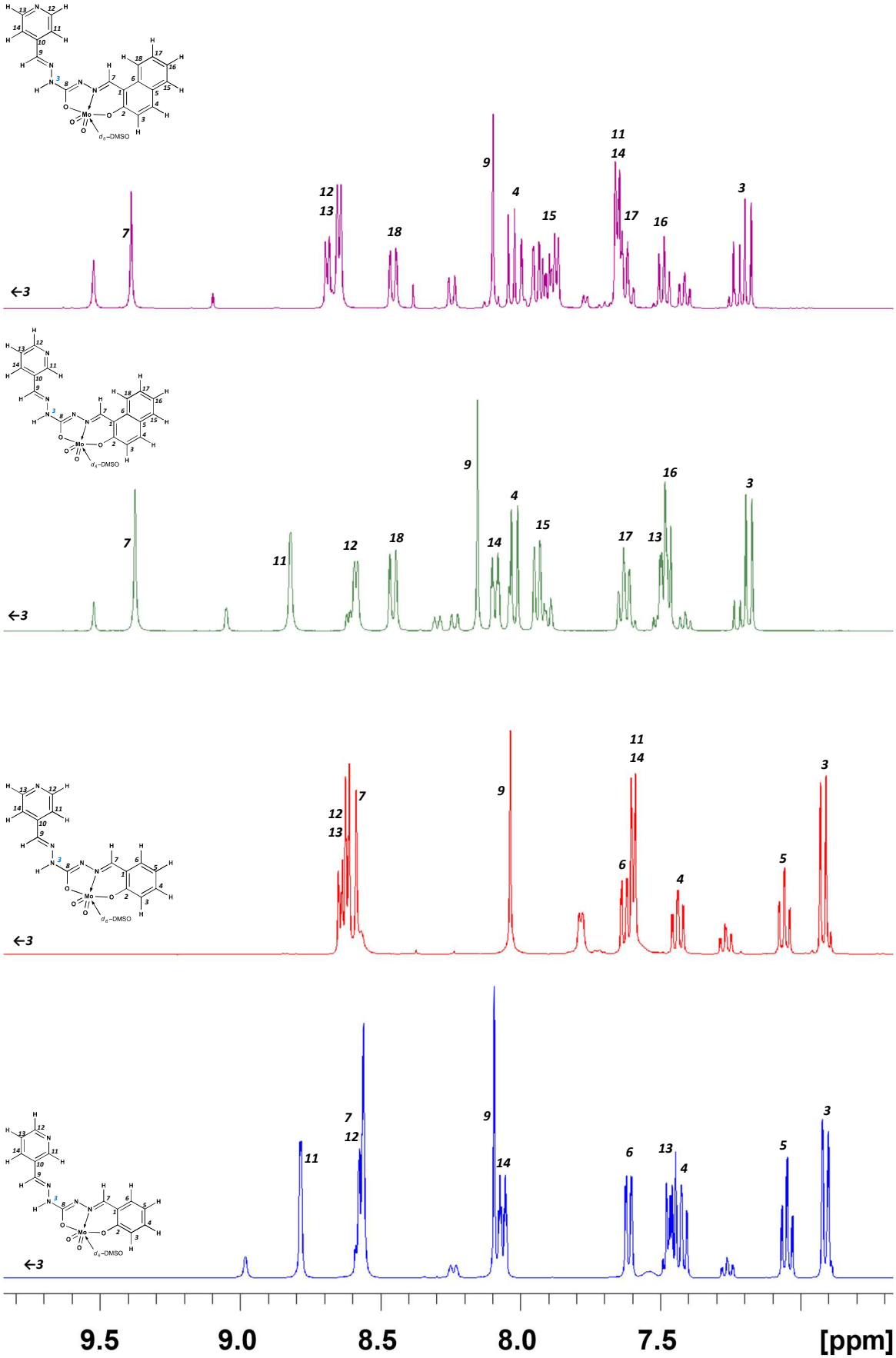

Figure S57. A portion of the ^{1}H NMR spectra of (from bottom to top): [**MoO$_2$(L^{3pysal})**], [**MoO$_2$(L^{4pysal})**], [**MoO$_2$(L^{3pynaph})**] and [**MoO$_2$(L^{4pynaph})**] in DMSO–d_6 at 298 K.

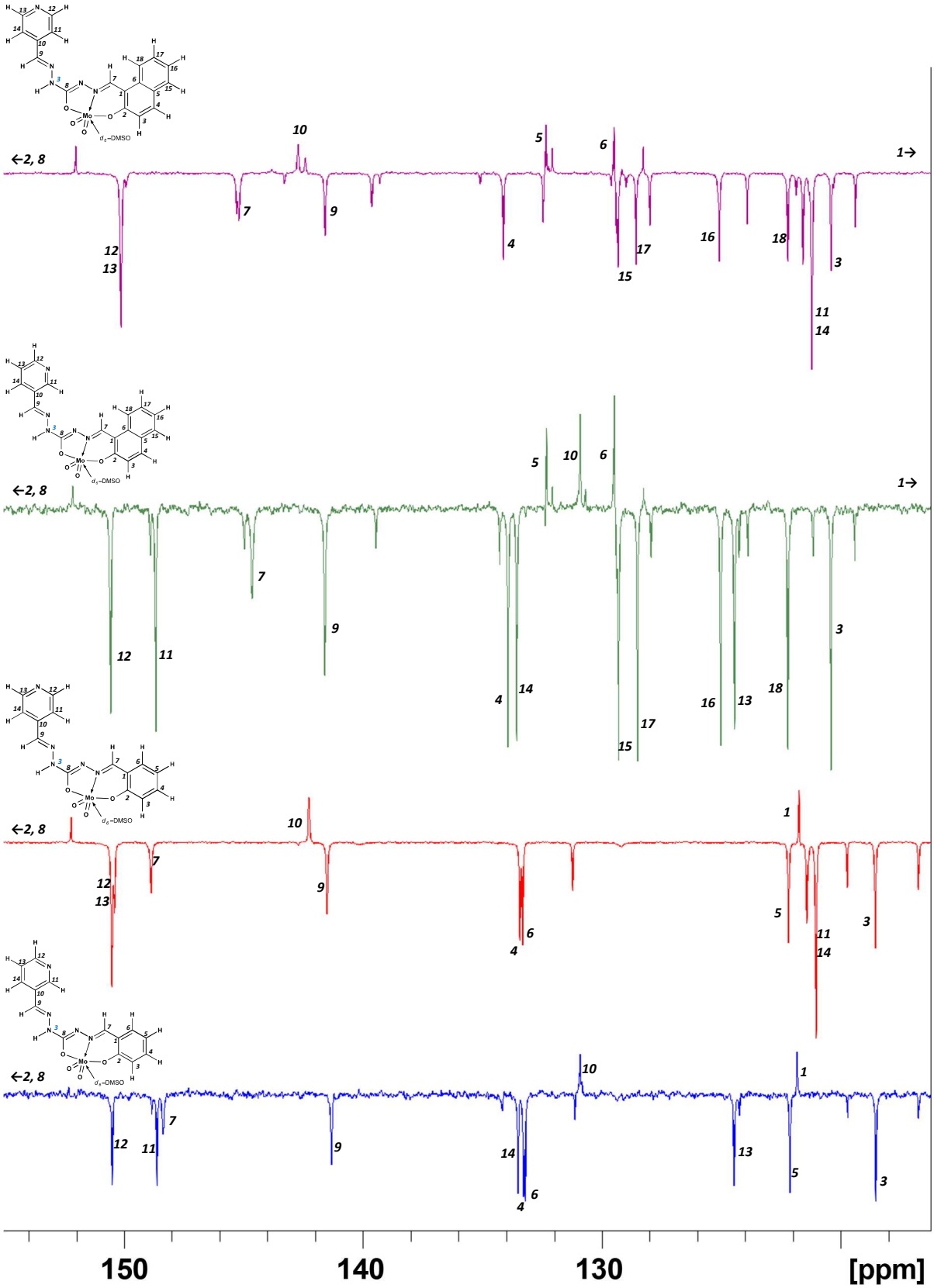

Figure S58. A portion of the DEPTQ ^{13}C NMR spectra of (from bottom to top): [**MoO$_2$(L^{3pysal})**], [**MoO$_2$(L^{4pysal})**], [**MoO$_2$(L^{3pynaph})**] and [**MoO$_2$(L^{4pynaph})**] in DMSO–d_6 at 298 K.

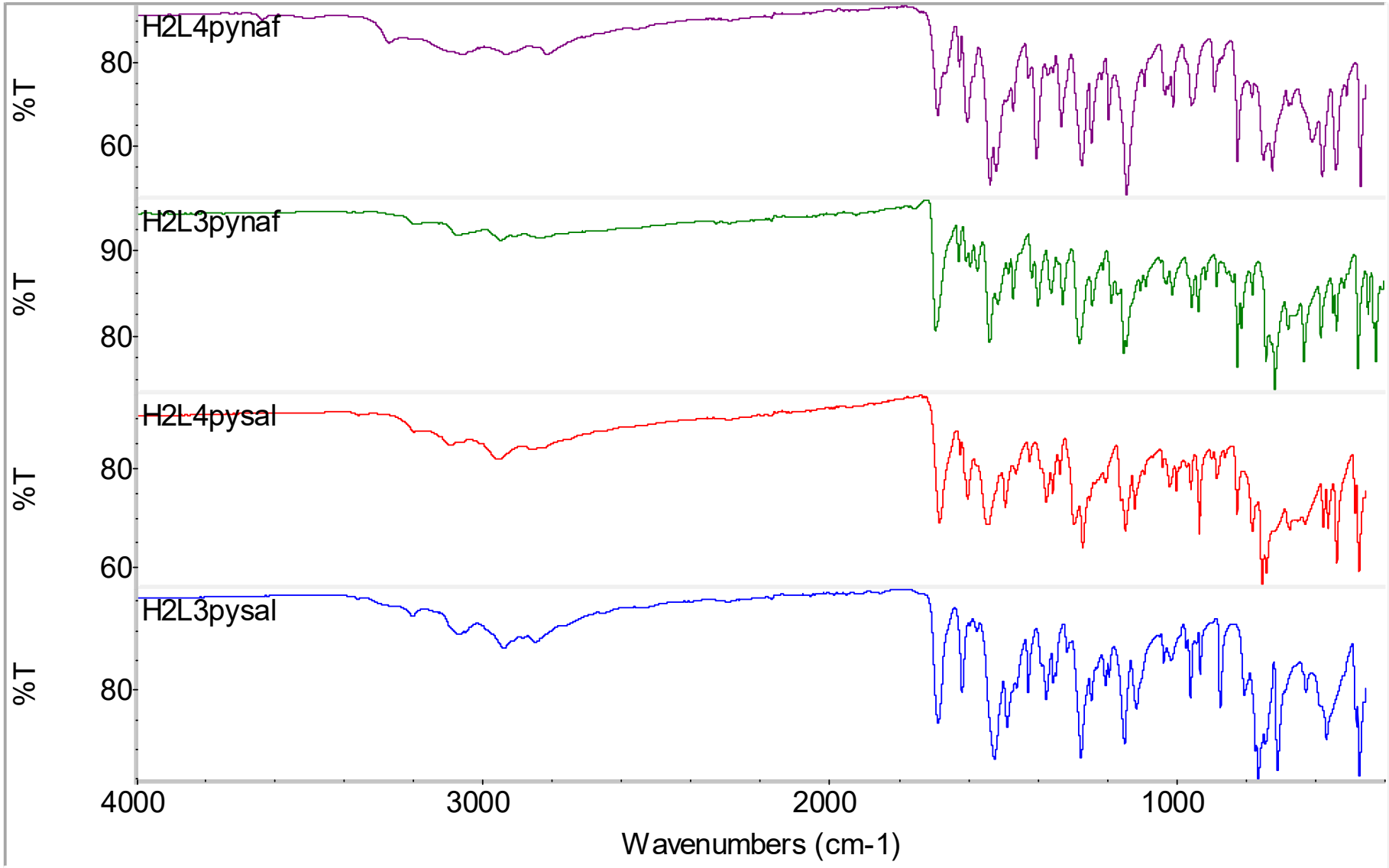

Figure S59. ATR-FTIR spectra of (from bottom to top): $\mathbf{H_2L^{3pysal}}$, $\mathbf{H_2L^{4pysal}}$, $\mathbf{H_2L^{3pynaph}}$ and $\mathbf{H_2L^{4pynaph}}$.

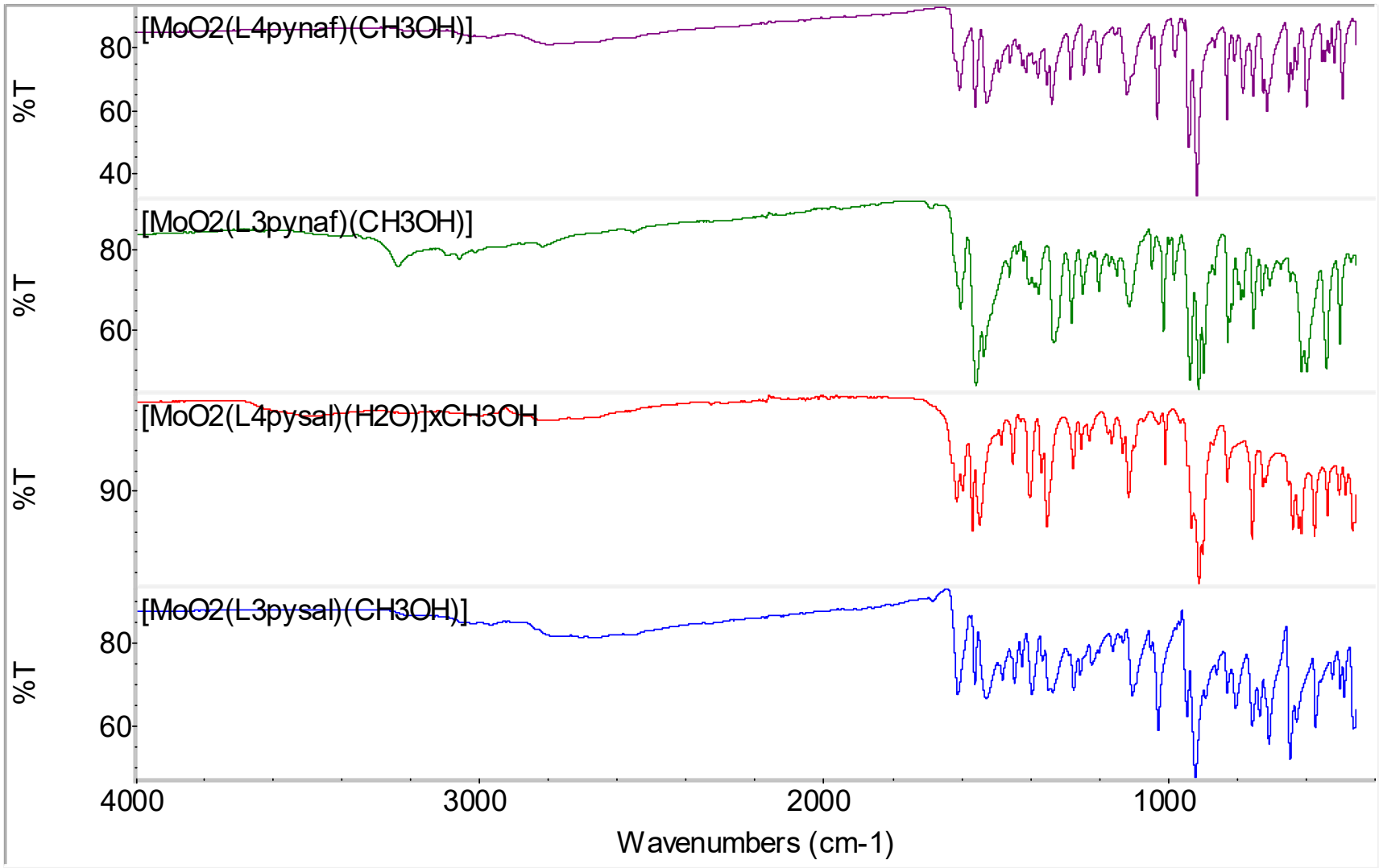

Figure S60. ATR-FTIR spectra of (from bottom to top): [**$MoO_2(L^{3pysal})(CH_3OH)$**], [**$MoO_2(L^{4pysal})(H_2O)]\cdot CH_3OH$**, [**$MoO_2(L^{3pynaph})$ (CH_3OH)**] and [**$MoO_2(L^{4pynaph})(CH_3OH)$**].

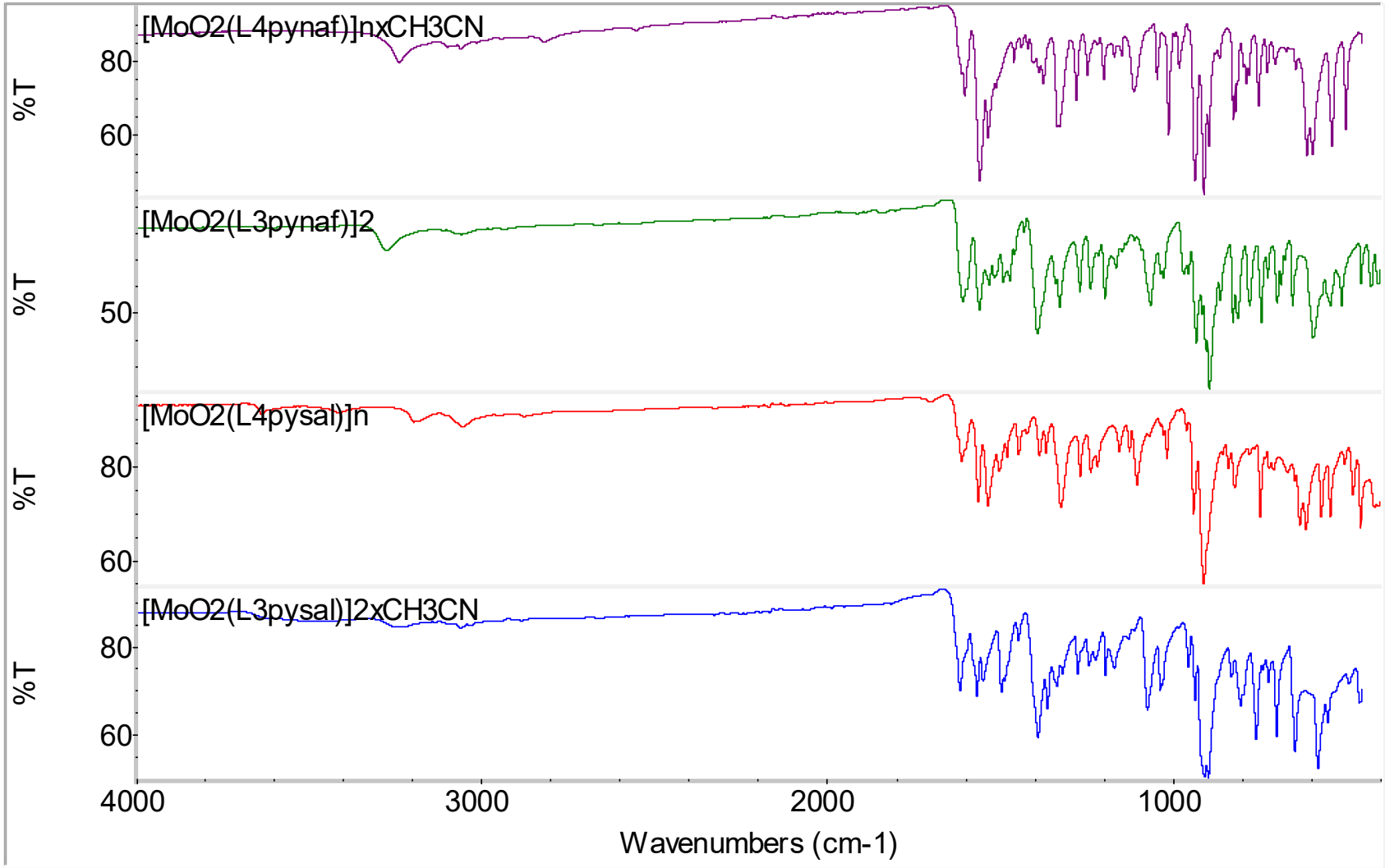

Figure S61. ATR-FTIR spectra of (from bottom to top): **[MoO$_2$(L^{3pysal})]$_2$**, **[MoO$_2$(L^{4pysal})]$_n$**, **[MoO$_2$(L^{3pynaph})]$_2$** and **[MoO$_2$(L^{4pynaph})]$_n$·xnCH$_3$CN**.

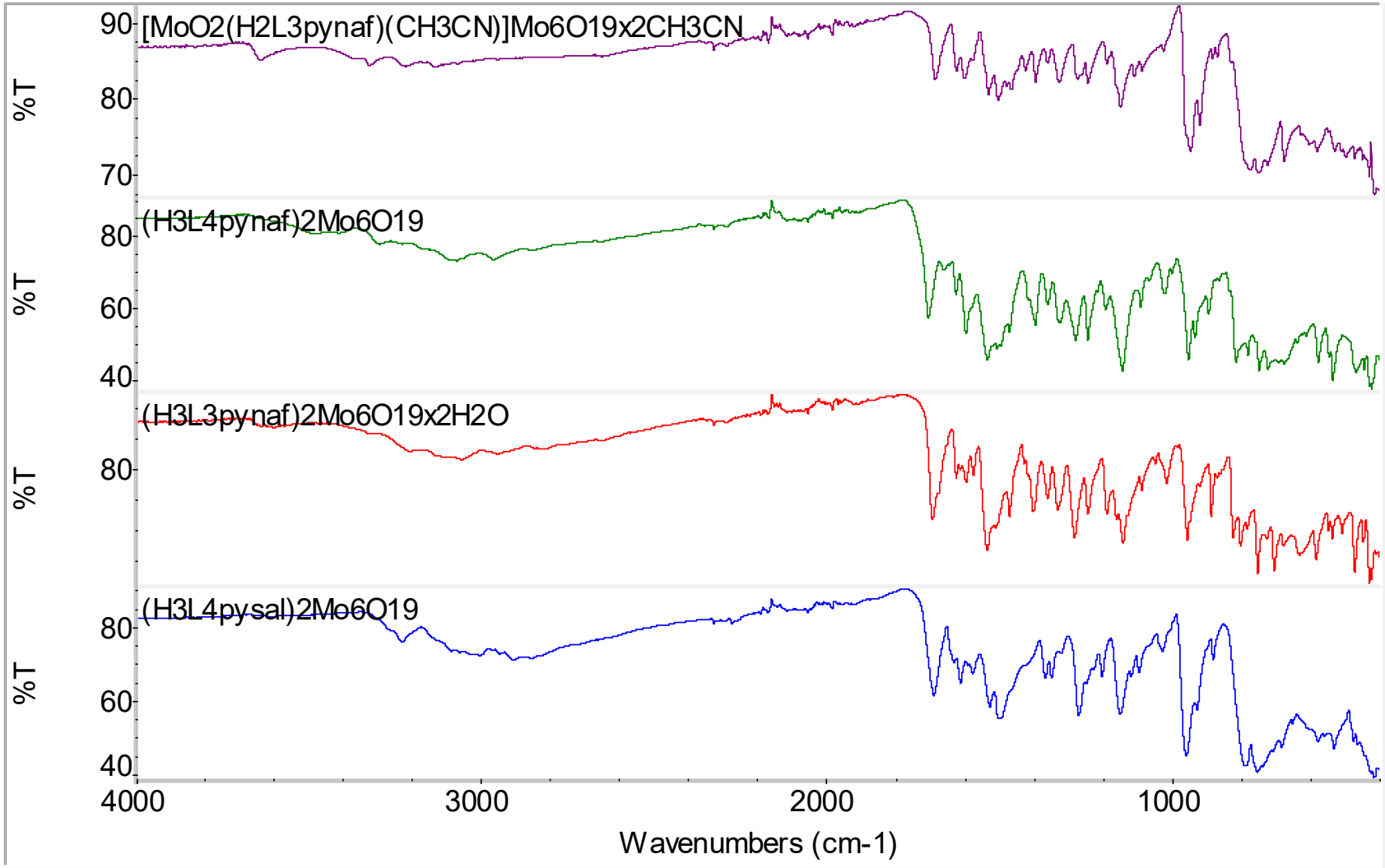

Figure S62. ATR-FTIR spectra of (from bottom to top): **$(H_3L^{4pysal})_2Mo_6O_{19}$**, **$(H_3L^{3pynaph})_2Mo_6O_{19}\cdot 2H_2O$**, **$(H_3L^{4pynaph})_2Mo_6O_{19}$** and **$[MoO_2(H_2L^{3pynaph})(CH_3CN)]Mo_6O_{19}\cdot 2CH_3CN$**.

Experimental data

Physical methods

TG analysis was carried out with a Mettler-Toledo TGA/SDTA851e thermobalance using aluminium crucibles. All experiments were recorded in a dynamic oxygen atmosphere with a flow rate of 100 cm^3 min^{-1}. Heating rates of 10 K min^{-1} were used for all investigations.

DSC analysis was performed using Mettler Toledo DSC823^e instrument. All experiments were recorded in a dynamic nitrogen atmosphere with a flow rate of 100 cm^3 min^{-1}. Heating rates of 10 K min^{-1} were used for all investigations.

Elemental analyses were provided by the Analytical Services Laboratory of the Ruđer Bošković Institute, Zagreb.

FT-IR spectra were recorded on a Perkin Elmer Spectrum Two FTIR Spectrometer using Attenuated Total Reflectance technique (ATR).

NMR spectra were recorded on Bruker Avance III HD 400 spectrometer operating at 400 MHz. Compounds were dissolved in DMSO-d_6 and measured in 5 mm NMR tubes at 298 K with TMS as an internal standard. The sample concentration was 10 mg/mL.

The powder X-ray diffraction data for qualitative phase analysis were collected by the Phillips X'Change powder diffractometer in the Bragg-Brentano geometry using Cu Kα radiation. The sample was contained on a Si sample holder. Patterns were collected in the range of $2\theta = 4–40°$ with the step size of 0.03° and at 0.8 s per step. The data were collected and visualized using the X'Pert programs Suite.

X-ray crystallography. Single crystal diffraction.

High-quality single crystals of the described compounds were grown from the corresponding reaction mixtures. Diffracted intensities were collected on Oxford Diffraction Xcalibur 3 diffractometer using Mo *K*α radiation (λ = 0.71073 Å) using ω-scans. Data were prepared using the CrysAlis[30] program package. A summary of general and crystal data, intensity data collection and final refinement parameters are presented in ESI, Tables S19-S21. The structures were solved with dual space methods using SHELXT.[31] The refinement procedure by full-matrix least-squares methods based on F^2 values against all reflections included anisotropic displacement parameters for all non-H atoms. Hydrogen atoms bound to carbon atoms were placed in geometrically idealized positions and refined by the use of the riding model with $U_{iso} = 1.2U_{eq}$ of the connected carbon atom or as ideal CH_3 groups with $U_{iso} = 1.5U_{eq}$. Hydrogen atoms attached to oxygen atoms and nitrogen atoms (H1(A), H2(A), H3(A) in $\mathbf{H_2L^{3pysal}}$; H1, H2, H3, H3A, H3B in $\mathbf{H_2L^{3pysal}\cdot H_2O}$; H1, H2, H3 in $\mathbf{H_2L^{4pysal}}$; H1(A), H2(A), H3(ABC) in $\mathbf{H_2L^{3pynaph}\cdot 0.5H_2O}$; H1(A), H2(A), H3(ABC) in $\mathbf{H_2L^{3pynaph}\cdot CH_3OH}$; H3, H5 in $\mathbf{[MoO_2(L^{3pysal})(CH_3OH)]}$; H1, H2, H3, H5 in $\mathbf{(H_3L^{4pysal})_2Mo_6O_{19}}$ **and** $\mathbf{(H_3L^{4pynaph})_2Mo_6O_{19}}$, H1, H2, H3, H5, H13(A) in $\mathbf{(H_3L^{3pynaph})_2Mo_6O_{19}\cdot 2H_2O}$) were located in the difference Fourier maps at the final stages of the refinement procedure. Their coordinates were refined freely but with restrained N−H distances of 0.86(2) and O–H distances of 0.82(2) A. Hydrogen atoms not found in difference Fourier maps (H3C in $\mathbf{H_2L^{3pynaph}\cdot 0.5CH_3OH}$, H3 and H3A in $\mathbf{[MoO_2(L^{3pysal})]_2\cdot xCH_3CN}$, H2, H3 and H5 in $\mathbf{[MoO_2(H_2L^{3pynaph})(CH_3CN)]Mo_6O_{19}\cdot 2CH_3CN}$) were placed in geometrically idealized positions and refined by the use of the riding model with $U_{iso} = 1.2U_{eq}$ of the connected heteroatom. All refinements were performed using SHELXL-2013.[32] The SHELX programs operated within the Olex[33] suite. Geometrical calculations and molecular graphics were done with Mercury.[34]

Table S19. General and crystal data, a summary of intensity data collection and structure refinement for **H_2L^{3pysal}, $H_2L^{3pysal}\cdot H_2O$, H_2L^{4pysal}, $H_2L^{3pynaph}\cdot 0.5H_2O$** and **$H_2L^{3pynaph}\cdot 0.5CH_3OH$.**

Identification code	**H_2L^{3pysal}**	**$H_2L^{3pysal}\cdot H_2O$**	**H_2L^{4pysal}**	**$H_2L^{3pynaph}\cdot 0.5H_2O$**	**$H_2L^{3pynaph}\cdot 0.5CH_3OH$**
Empirical formula	$C_{14}H_{13}N_5O_2$	$C_{14}H_{15}N_5O_3$	$C_{14}H_{13}N_5O_2$	$C_{36}H_{32}N_{10}O_5$	$C_{37}H_{34}N_{10}O_5$
M_r	283.29	301.31	283.29	684.71	698.74
T/K	293(2)	293(2)	293(2)	150(2)	293(2)
Crystal system	orthorhombic	monoclinic	triclinic	monoclinic	monoclinic
Space group	$Pca2_1$	$P2_1/c$	P–1	$P2_1/n$	$P2_1/n$
a/Å	20.1878(10)	6.3767(6)	7.7355(5)	8.4843(7)	9.2562(9)
b/Å	6.1088(3)	7.7407(7)	9.1187(5)	12.7276(8)	12.8021(9)
c/Å	23.5694(13)	30.099(3)	9.7039(5)	31.583(2)	30.334(3)
α/°	90	90	93.758(5)	90	90
β/°	90	93.079(8)	93.790(5)	92.519(7)	95.858(9)
γ/°	90	90	92.877(5)	90	90
V/Å^3	2906.7(3)	1483.5(2)	680.50(7)	3407.2(4)	3575.8(6)
Z	8	4	2	4	4
ρ_{calc}/g cm^{-3}	1.295	1.349	1.383	1.335	1.298
μ/mm^{-1}	0.091	0.099	0.098	0.093	0.09
F(000)	1184	632	296	1432	1464
Crystal size/mm^3	0.5 × 0.4 × 0.1	0.1 × 0.1 × 0.05	0.4 × 0.1 × 0.1	0.5 × 0.25 × 0.2	0.5 × 0.2 × 0.15
Radiation	Mo $K\alpha$ (λ = 0.71073 Å)				
2Θ range/°	8.532 to 54.000	8.586 to 65.678	8.440 to 65.838	8.228 to 54.000	8.538 to 54.000
Index ranges	$-25 \le h \le 25$ $-7 \le k \le 7$ $-30 \le l \le 29$	$-9 \le h \le 9$ $-11 \le k \le 11$ $-44 \le l \le 41$	$-11 \le h \le 11$ $-13 \le k \le 13$ $-14 \le l \le 13$	$-10 \le h \le 10$ $-15 \le k \le 16$ $-40 \le l \le 40$	$-11 \le h \le 10$ $-16 \le k \le 9$ $-28 \le l \le 38$
Reflections collected	6167	5029	4700	7417	7770
Independent reflections	3959 [R_{int} = 0.0711, R_{sigma} = 0.1029]	1845 [R_{int} = 0.0824, R_{sigma} = 0.1285]	2221 [R_{int} = 0.0540, R_{sigma} = 0.0580]	3776 [R_{int} = 0.0928, R_{sigma} = 0.1820]	2442[R_{int} = 0.0773, R_{sigma} = 0.1541]
Data/restraints/ parameters	6167/2/398	5029/5/214	4700/0/199	7417/9/484	7770/6/494
g_1, g_2 in w^a	0.0288, 0	0.0249, 0	0.0626, 0.0121	0.0254, 0	0.0562, 0
Goodness–of–fit on F^2, S^b	1.018	0.968	1.012	0.966	0.915

Final R and wR^c values [$I \geq 2\sigma(I)$]	R_1 = 0.0638, wR_2 = 0.0880	R_1 = 0.0716, wR_2 = 0.0967	R_1 = 0.0625, wR_2 = 0.1273	R_1 = 0.0654, wR_2 = 0.0964	R_1 = 0.0789, wR_2 = 0.1524
Final R and wR^c values [all data]	R_1 = 0.1194, wR_2 = 0.1016	R_1 = 0.216, wR_2 = 0.132	R_1 = 0.1506, wR_2 = 0.1634	R_1 = 0.1462, wR_2 = 0.1219	R_1 = 0.2451, wR_2 = 0.2161
Largest diff. peak/hole / e Å^{-3}	0.109/–0.106	0.145/–0.176	0.142/–0.199	0.335/–0.25	0.267/–0.219

[a] $w = 1/[\sigma^2(F_o^2) + (g_1P)^2 + g_2P]$ where $P = (F_o^2 + 2F_c^2)/3$

[b] $S = \{\Sigma[w(F_o^2 - F_c^2)^2]/(N_r - N_p)\}^{1/2}$ where N_r = number of independent reflections, N_p = number of refined parameters.

[c] $R = \Sigma||F_o| - |F_c||/ \Sigma|F_o|$; $wR = \{\Sigma[w(F_o^2 - F_c^2)^2]/\Sigma[w(F_o^2)^2]\}^{1/2}$

Table S20. General and crystal data, a summary of intensity data collection and structure refinement for **$[MoO_2(L^{3pysal})(MeOH)]$, $[MoO_2(L^{3pysal})]_2 \cdot 2CH_3CN$** and **$[MoO_2(H_2L^{3pynaph})(CH_3CN)]Mo_6O_{19} \cdot 2CH_3CN$.**

Identification code	**$[MoO_2(L^{3pysal})(MeOH)]$**	**$[MoO_2(L^{3pysal})]_2 \cdot 2CH_3CN$**	**$[MoO_2(H_2L^{3pynaph})(CH_3CN)]Mo_6O_{19} \cdot 2CH_3CN$**
Empirical formula	$C_{15}H_{15}MoN_5O_5$	$C_{32}H_{28}Mo_2N_{12}O_8$	C24 H24 Mo7 N8 O23
M_r	441.26	900.54	1464.09
T/K	293(2)	293(2)	150(2)
Crystal system	monoclinic	monoclinic	monoclinic
Space group	$P2_1/n$	$P2_1$	C2/c
a/Å	7.7443(3)	11.3525(9)	45.012(7)
b/Å	19.3301(6)	13.6312(8)	11.4125(5)
c/Å	11.3770(3)	12.5586(8)	21.787(4)
α/°	90	90	90
β/°	91.632(3)	116.102(9)	134.52(3)
γ/°	90	90	90
V/Å^3	1702.42(10)	1745.2(2)	7980(3)
Z	4	2	8
ρ_{calc}/g cm^{-3}	1.722	1.714	2.437
μ/mm^{-1}	0.809	0.789	2.225
F(000)	888	904	5616
Crystal size/mm^3	0.2 × 0.1 × 0.05	0.1 × 0.1 × 0.05	0.2 × 0.1 × 0.05
Radiation	Mo $K\alpha$ (λ = 0.71073 Å)		
2Θ range/°	6.282 to 55.992	6.460 to 65.898	8.061 to 49.424
Index ranges	$-10 \le h \le 10$ $-25 \le k \le 25$ $-15 \le l \le 15$	$-15 \le h \le 17$ $-20 \le k \le 19$ $-19 \le l \le 18$	$-52 \le h \le 52$ $-13 \le k \le 13$ $-25 \le l \le 25$
Reflections collected	4100	10637	6786
Independent reflections	2583[R_{int} = 0.1073, R_{sigma} = 0.0727]	5239 [R_{int} = 0.1097, R_{sigma} = 0.2347]	4672[R_{int} = 0.2144, R_{sigma} = 0.0948]
Data/restraints/ parameters	4100/1/239	10637/1/489	6786/0/566
g_1, g_2 in w^a	0.0346, 0	0.0117, 0	0.035, 48.3992
Goodness–of–fit on F^2, S^b	0.994	0.954	1.103

Final R and wR^c values [$I \geq 2\sigma(I)$]	R_1 = 0.0458, wR_2 = 0.0846	R_1 = 0.0793, wR_2 = 0.0857	R_1 = 0.0717, wR_2 = 0.1088
Final R and wR^c values [all data]	R_1 = 0.0920, wR_2 = 0.0983	R_1 = 0.1846, wR_2 = 0.1123	R_1 = 0.1178, wR_2 = 0.1216
Largest diff. peak/hole / e Å^{-3}	0.727/–0.585	1.065/–1.202	1.08/–0.975

[a] $w = 1/[\sigma^2(F_o^2) + (g_1P)^2 + g_2P]$ where $P = (F_o^2 + 2F_c^2)/3$

[b] $S = \{\Sigma[w(F_o^2 - F_c^2)^2]/(N_r - N_p)\}^{1/2}$ where N_r = number of independent reflections, N_p = number of refined parameters.

[c] $R = \Sigma||F_o| - |F_c||/ \Sigma|F_o|$; $wR = \{\Sigma[w(F_o^2 - F_c^2)^2]/\Sigma[w(F_o^2)^2]\}^{1/2}$

Table S21. General and crystal data, a summary of intensity data collection and structure refinement for **$(H_3L^{4pysal})_2Mo_6O_{19}$, $(H_3L^{3pynaph})_2Mo_6O_{19}\cdot 2H_2O$** and **$(H_3L^{4pynaph})_2Mo_6O_{19}$.**

Identification code	**$(H_3L^{4pysal})_2Mo_6O_{19}$**	**$(H_3L^{3pynaph})_2Mo_6O_{19}\cdot 2H_2O$**	**$(H_3L^{4pynaph})_2Mo_6O_{19}$**
Empirical formula	$C_{28}H_{28}Mo_6N_{10}O_{23}$	$C_{36}H_{36}Mo_6N_{10}O_{25}$	$C_{36}H_{32}Mo_6N_{10}O_{23}$
M_r	1448.24	1584.39	1548.35
T/K	293(2)	293(2)	293(2)
Crystal system	monoclinic	monoclinic	monoclinic
Space group	$P2_1/n$	$P2_1/c$	$P2_1/c$
a/Å	9.1525(5)	9.7786(3)	9.3887(3)
b/Å	17.7564(7)	16.9721(4)	17.2816(5)
c/Å	13.2831(9)	14.4712(4)	14.7114(6)
α/°	90	90	90
β/°	106.419(7)	104.582(3)	105.236(4)
γ/°	90	90	90
V/Å^3	2070.7(2)	2324.33(11)	2303.05(14)
Z	2	2	2
ρ_{calc}/g cm^{-3}	2.323	2.264	2.233
μ/mm^{-1}	1.862	1.673	1.683
F(000)	1404	1548	1508
Crystal size/mm^3	0.2 × 0.12 × 0.05	0.31 × 0.22 × 0.15	0.1 × 0.1 × 0.05
Radiation	Mo $K\alpha$ (λ = 0.71073 Å)		
2Θ range/°	8.170 to 65.934	8.396 to 65.538	8.386 to 65.940
Index ranges	$-13 \le h \le 12$ $-26 \le k \le 26$ $-20 \le l \le 20$	$-14 \le h \le 9$ $-22 \le k \le 24$ $-13 \le l \le 21$	$-14 \le h \le 14$ $-26 \le k \le 25$ $-21 \le l \le 21$
Reflections collected	6769	7627	7902
Independent reflections	5095 [R_{int} = 0.0345, R_{sigma} = 0.0556]	6156 [R_{int} = 0.0275, R_{sigma} = 0.0456]	5336 [R_{int} = 0.0854, R_{sigma} = 0.0772]
Data/restraints/ parameters	6769/1/316	7627/6/366	7902/4/352
g_1, g_2 in w^a	0.0276, 0.6332	0.029, 0.9346	0.0355, 0.6409
Goodness–of–fit on F^2, S^b	1.056	1.032	1.042

Final R and wR^c values [$I \geq 2\sigma(I)$]	R_1 = 0.0393, wR_2 = 0.0737	R_1 = 0.0319, wR_2 = 0.0661	R_1 = 0.0476, wR_2 = 0.0852
Final R and wR^c values [all data]	R_1 = 0.0629, wR_2 = 0.0839	R_1 = 0.0468, wR_2 = 0.0729	R_1 = 0.092, wR_2 = 0.1005
Largest diff. peak/hole / e Å^{-3}	0.923/–0.726	0.701/–0.648	0.842/–0.949

[a] $w = 1/[\sigma^2(F_o^2) + (g_1P)^2 + g_2P]$ where $P = (F_o^2 + 2F_c^2)/3$

[b] $S = \{\Sigma[w(F_o^2 - F_c^2)^2]/(N_r - N_p)\}^{1/2}$ where N_r = number of independent reflections, N_p = number of refined parameters.

[c] $R = \Sigma||F_o| - |F_c||/ \Sigma|F_o|$; $wR = \{\Sigma[w(F_o^2 - F_c^2)^2]/\Sigma[w(F_o^2)^2]\}^{1/2}$

References

30 Rigaku Oxford Diffraction (2018). CrysAlisPro. Version 1.171.39.46e. Rigaku Oxford Diffraction, The Woodlands, Texas, USA.

31 G. M. Sheldrick, *Acta Cryst.*, 2015, **A71**, 3.

32 G. M. Sheldrick, *Acta Cryst.*, 2015, **C71**, 3.

33 O. V. Dolomanov, L. J. Bourhis, R. J. Gildea, J. A. K. Howard and H. Puschmann, *J. Appl. Cryst.*, 2009, 42, 339-341.

34 C. R. Groom, I. J. Bruno, M. P. Lightfoot and S. C. Ward, *Acta Cryst.*, 2016, **B72**, 171.